photonics

MDPI

Review

Review of Optical Fiber Sensors: Principles, Classifications and Applications in Emerging Technologies

Denzel A. Rodriguez-Ramirez [1], Jose R. Martinez-Angulo [1,*], Jose D. Filoteo-Razo [1], Juan C. Elizondo-Leal [1], Alan Diaz-Manriquez [1], Daniel Jauregui-Vazquez [2], Jesus P. Lauterio-Cruz [3] and Vicente P. Saldivar-Alonso [1]

[1] Facultad de Ingeniería y Ciencias, Universidad Autónoma de Tamaulipas, Centro Universitario Victoria, Ciudad Victoria 87149, Tamaulipas, Mexico; a2243018003@alumnos.uat.edu.mx (D.A.R.-R.); darazo@uat.edu.mx (J.D.F.-R.); jcaelizondo@docentes.uat.edu.mx (J.C.E.-L.); amanriquez@docentes.uat.edu.mx (A.D.-M.); vpsaldiv@docentes.uat.edu.mx (V.P.S.-A.)
[2] Centro de Investigación Científica y de Educación Superior de Ensenada (CICESE), División de Física Aplicada-Departamento de Óptica, Carretera Ensenada-Tijuana, No. 3918, Zona Playitas, Ensenada 22860, Baja California, Mexico; djauregui@cicese.mx
[3] Departamento de Investigación en Física, Universidad de Sonora, Blvd. Luis Encinas y Rosales, Hermosillo 83000, Sonora, Mexico; pablo.lauterio@unison.mx
* Correspondence: jrangulo@docentes.uat.edu.mx

Abstract

Optical fiber sensors (OFSs) have emerged as essential tools in the monitoring of physical, chemical, and bio-medical parameters in harsh situations due to their high sensitivity, electromagnetic interference (EMI) immunity, and long-term stability. However, the current literature contains scattered information in most reviews regarding individual sensing technologies or domains. This study provides a structured exploratory review in a novel inter-family analysis of both intrinsic and extrinsic configurations by analyzing more than 23,000 publications between 2019 and 2025 in five key domains: industry, medicine and biomedicine, environmental chemistry, civil/structural engineering, and aerospace. The analysis aims to critically discuss how functional principles/parameters and methods of interrogation affect the applicability of different OFS categories. The results reveal leading trends in the use of techniques like the use of fiber Bragg gratings (FBG) and distributed sensing in high-accuracy conditions or the rising role of extrinsic sensors in selective chemical situations and point out new approaches in areas like Artificial Intelligence (AI)- or Internet of Things (IoT)-integrated sensors. Further, this synthesis not only connects pieces of knowledge but also defines the technological barriers in terms of calibration cost and standardization: this provides strategic insight regarding future research and the scalability of industry deployment.

Keywords: optical fiber sensors; intrinsic sensors; extrinsic sensors; multidisciplinary applications

Check for updates

Received: 31 October 2025
Revised: 3 December 2025
Accepted: 5 December 2025
Published: 31 December 2025

Copyright: © 2025 by the authors. Licensee MDPI, Basel, Switzerland. This article is an open access article distributed under the terms and conditions of the Creative Commons Attribution (CC BY) license.

1. Introduction

Accurate, safe, and efficient measurement of physical and chemical variables is a cornerstone for technological advancement in fields such as precision agriculture [1], food processing [2], and biomedical monitoring [3]. In this context, optical fiber sensor (OFS) technology has established itself as one of the most promising and versatile technologies in recent years due to specific characteristics such as sensitivity [4], robustness [5,6], EMI immunity [7], small size, and potential for remote and distributed detection [8].

Since the 1970s [5,8], the development and application of OFS technology have undergone substantial advancements. These advances include diversification in sensor structures, materials, and sensing mechanisms [9]. The areas of application have also expanded to include medicine [10], the aerospace industry [11], civil engineering [12], and environmental chemistry [13].

Classifying OFSs as intrinsic and extrinsic schemes has been a key point in their technological development [5]. Intrinsic sensors use fiber as both a transmission medium and a sensing element, enabling detection of parameters through changes in their internal optical properties, such as refractive index, intensity, phase, or wavelength [5]. These properties have led to various research projects aimed at exploiting their advantages over other sensors, such as electronic sensors [5,14], and has given OFSs the ability to be used for detecting vibrations, deformations, or temperature changes in hostile environments [15], including geological hazard detection [16]. Among the most prominent architectures of this type are fiber Bragg gratings (FBG) [17], and sensors based on Raman scattering [18,19], Brillouin scattering [14,20], and certain interferometers like Mach–Zehnder [5,21], Sagnac [17], and Michelson [6,22].

Conversely, extrinsic sensors use optical fiber only as a signal guide, with phenomena that modify the light's properties occurring outside the fiber [5]. This allows for greater flexibility in designing measurement points and is often used in industrial processes [23]. Typical architectures include variations of Fabry–Perot interferometers [24,25]. This distinction between sensor schemes influences not only the design and material selection but also the construction, data collection, and calibration strategies for the final sensor [5,8,23].

Given the continuous progress in scientific publications related to OFSs and the fragmentation of knowledge in specialized reviews by application or sensor type, there is a need for a structured exploration review that compares both usage schemes. The primary objective of this work is to provide an updated and structured overview of the operating principles, emerging technologies, and dominant applications of OFSs, from basic concepts and various classifications to the most common OFS configurations for measuring different parameters. In addition, discussions and comparisons are presented throughout the work, addressing the most significant points of the relevant works of other authors. Likewise, the areas of applications of OFSs are categorized into five main fields: (1) industrial, (2) medicine and biomedicine, (3) environmental chemistry, (4) civil engineering or structural analysis, and (5) aerospace. These categories were not chosen randomly but derived from a detailed review of the use cases described by the authors of the analyzed articles. During classification, each study was assigned to an application field based on the orientation explicitly presented in its content, particularly in the abstract, introduction, or stated objectives, ensuring consistency in theme and minimizing subjective judgment.

2. Methodology

The compilation of works is carried out through a thorough and structured exploratory review of scientific literature, focusing on the applications of OFSs. This is achieved using the TAK (Title, Abstract, Keywords) methodology [26,27], which is widely employed in academic reviews. This approach allows for the identification of relevant works through cross-analysis of titles, summaries, and keywords. Three major scientific databases were used, each employing multiple search strings for different application areas, primarily covering the years 2019–2025. The selection of these sources was based on their technical relevance, editorial credibility, and ability to provide multidisciplinary coverage. Together, they offer a balanced, high-quality collection that minimizes irrelevant entries and facilitates a structured review across both theoretical and practical domains.

It is essential to highlight that, unlike approaches that depend only on keyword searches or citation metrics, this method combines the analysis of titles, abstracts, and keywords. Such integration provides a more accurate understanding of the thematic focus of articles and reduces the chance of missing relevant works that might otherwise be excluded due to variations in terminology or indexing [28,29]. Additionally, compared to bibliometric or purely narrative review methods, TAK provides broader and more balanced coverage by combining a thematic filter with a structured classification system, enabling consistent comparisons of both theoretical reviews and experimental studies [28,29]. Furthermore, different methodological guidelines highlight that traditional approaches, which focus only on keywords or citations, often lack the rigor and thoroughness needed to ensure review reliability [30,31].

To complement this methodological framework, the articles selected through the TAK-based research were also subjected to detailed quantitative and visual analysis. This analysis includes various data visualizations, such as annual publication trends by discipline, sensor typology distributions, and thematic relevance per application area, to provide a broad overview of the field's evolution and priorities.

3. Historical Analysis of the Development of OFSs

The history of OFSs begins in the second half of the 20th century, and its evolution has been closely linked to technological advances in optical communications. The first significant record dates back to 1967 with the invention of the "fotonic sensor" (FS), patented under US number 03327584, and recognized in the literature as the first sensor of its kind [32,33]. This device used a bifurcated fiber, where one part of the beam illuminated a surface and the other part received the reflected light (Figure 1). In this way, it was possible to measure the relative position between the sensor (fiber tip) and the reflective surface with high precision, laying the foundation for the future development of what would become extrinsic OFSs.

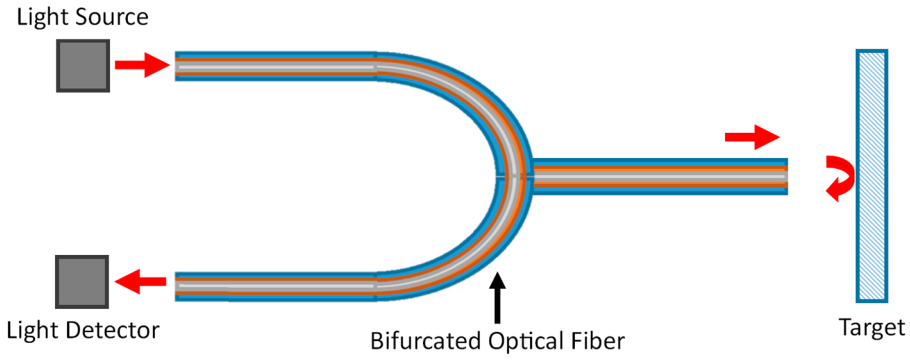

Figure 1. Schematic representation of FS, illustrating how the bifurcated optical fiber guides light toward a reflective target to determine its position relative to the fiber tip.

The simplicity and effectiveness of the FS were not only vital for demonstrating the feasibility of non-contact sensing with light but also laid the foundation for decades of research into proximity and vibration sensors, many of which still use similar principles today [33].

The 1970s marked a key transition with the development of interferometric techniques within the fiber core, enabling the emergence of intrinsic OFSs [34,35]. The most notable advances included dual-path interferometers such as MZI and MI interferometers implemented in fiber, which offered unprecedented sensitivity. These systems could detect phase changes on the order of microradians in the optical signal, making them highly valuable tools for measuring physical parameters such as vibrations, strain, pressure, and temperature [34,36,37].

Another key moment in the development of OFSs was the idea of distributed sensing, a technology that started in the 1980s and allowed the measurement of a physical variable along the fiber at different points [38,39]. This feature greatly expanded the sensing uses of optical fibers, making it possible to monitor large structures like pipelines, tunnels, bridges, or power lines. At the same time, multiplexing systems were also introduced, enabling multiple sensors to be integrated into a single fiber network, which improved efficiency and lowered the cost of monitoring multiple variables [32,37,39,40].

Throughout these first two decades of evolution, the technological foundations supporting the development of OFSs were firmly established. These include the distinction between extrinsic and intrinsic sensors, the implementation of interferometric techniques, and the advancement of distributed sensing and multiplexing capabilities. As optical telecommunications made significant improvements in fibers, laser light sources, and photonic devices, it is clear that scientists successfully leveraged these advancements and adapted them to the sensing field, fostering a technological synergy that continues today.

Understanding this historical landscape not only emphasizes the technical milestones that marked the emergence of OFSs but also offers insight into the conceptual evolution that transformed them from laboratory experiments into versatile and commercially viable technologies. The path started by the FS in 1967 laid the foundation for a discipline that has expanded year by year alongside global optical technologies, and that now plays a leading role in intelligent monitoring, biomedical diagnostics, and many other scientific advancements of the 21st century.

Figure 2 illustrates the temporal evolution of scientific publications related to OFS applications across five major disciplinary areas. The data show a sustained growth during the past three decades, with a pronounced increase between 2010 and 2024. The record of publications for the year 2025 was truncated until the month of July, when all the queries were compiled. To obtain the dataset, the "All Databases" option of Web of Science was used, applying the keyword string "optical fiber sensors applications [discipline]", where *discipline* was replaced with *industry*, *environmental chemistry*, *medicine/biomedicine*, *civil engineering/structural analysis*, and *aerospace*. Each search was performed under the "All Collections" setting and using the "Topic" field (searches title, abstract, and indexing). The annual publication counts from each query were exported as Excel files and subsequently combined to construct the final plot.

In the last fifteen years, the development of OFSs has seen unprecedented growth, characterized by both technological diversification and practical validation across multiple fields. One of the most notable aspects of this period is the shift from laboratory prototypes to real-world applications. While in the past OFSs were often limited to experimental setups, recent years have seen their adoption in field applications such as industrial monitoring of turbines and pipelines [41], biomedical sensing during surgical procedures [22], and large-scale deployment in smart infrastructures like tunnels and bridges [15]. The availability of distributed sensing architectures based on Rayleigh, Raman, and Brillouin scattering has been crucial to this transition, allowing continuous monitoring along kilometers of fiber with centimeter-level resolution [5].

Another key factor has been the integration of OFSs with advanced materials and functional coatings, such as nanocomposites, metal oxides, and graphene layers, which have significantly improved selectivity, chemical stability, and resilience in harsh environments. These innovations have allowed OFSs to address issues such as biofouling in environmental monitoring [42], long-term drift in biomedical applications [43], and high-temperature degradation in aerospace systems [44]. The emphasis on coatings and packaging underscores how the last decade has shifted research from purely optical principles to multidisciplinary solutions that ensure long-term durability and reliability [9].

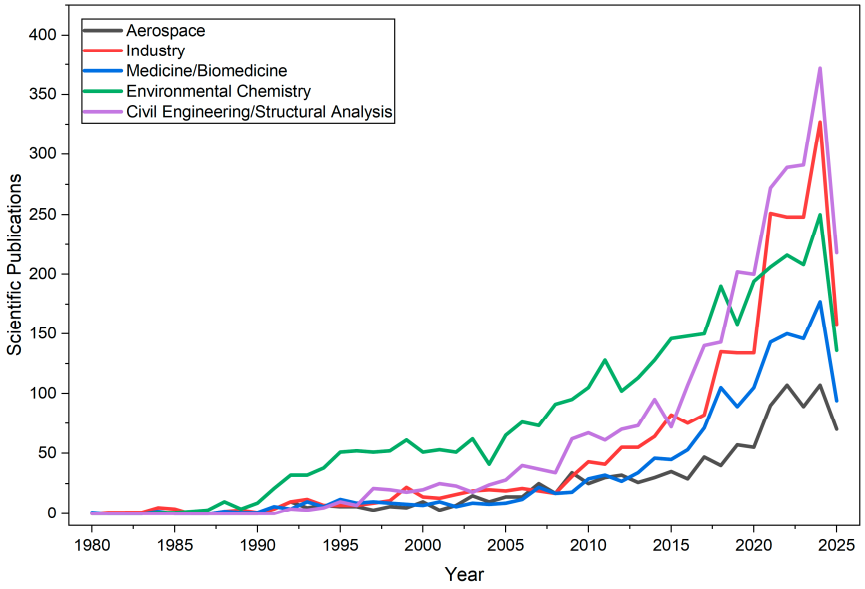

Figure 2. Temporal evolution of scientific publications related to OFSs, indexed in the Web of Science database, illustrating the growth of research activity across major application domains from the early 1980s to July 2025.

The comparison with traditional sensors has also intensified during this period. In civil and aerospace engineering, OFSs have demonstrated superior multiplexing capacity and EMI immunity compared to strain gauges, accelerometers, or eddy-current devices [16]. Similarly, in medicine, OFSs have moved beyond in vitro validation to clinical trials, proving their feasibility in applications such as catheter-based pressure monitoring, tissue ablation guidance, and wearable biosensors [25]. These advances highlight how OFSs are not only alternatives but, in many cases, disruptive technologies that redefine sensing strategies in critical fields [45].

Despite their progress, practical challenges remain, including cost, calibration protocols, and service life. The need for specialized interrogators and protective coatings continues to raise the cost of large-scale deployment [46], though prices are gradually decreasing as manufacturing and integration techniques mature [47]. Calibration in field conditions, especially in dynamic and hostile environments, has required adaptive algorithms and hybrid validation methods [10]. Regarding service life, the last 15 years have brought solutions such as radiation-hardened fibers for aerospace [48], metal-coated fibers for industrial machinery [49], and anti-fouling treatments for environmental sensors [50], ensuring improved long-term stability compared to earlier generations.

Overall, the last decade and a half marks a period of consolidation in which OFSs have evolved from niche laboratory devices into established technologies with multidisciplinary influence. The trend shown in Figure 2 illustrates not only exponential academic interest but also the strategic importance of OFSs in global technological progress. From the invention of the FS in 1967 to today's distributed, multifunctional, and clinically validated architectures, the discipline has grown into one of the main pillars of intelligent monitoring and next-generation sensing solutions [51].

4. Fundamentals and Classification of OFSs

4.1. Optical Fiber and Principle of Operation of an OFS

The general structure of an optical fiber is shown in Figure 3; this structure is for a silica or plastic-based thread that carries a beam of light. The core, cladding, and outer coating are the three concentric layers that make up the general structure of an optical fiber. The core is the thin central cylindrical layer that carries light from one end to the

other. This core is covered by a cladding with a refractive index n lower than that of the core, and the light is trapped inside due to the difference in refractive index between the core and the cladding. The outermost plastic layer, the outer coating, surrounds both layers further, shielding the fiber from physical harm and reducing light dispersion losses due to microbends [20,52,53].

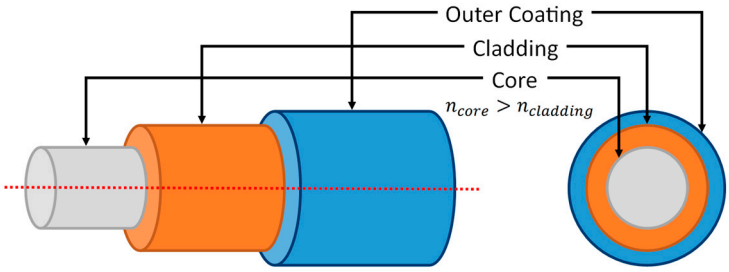

Figure 3. Schematic representation of the basic structure of an optical fiber, highlighting the core, cladding, and protective outer coating, with the refractive-index condition required for total internal reflection and guided light propagation.

In addition to its basic structure, optical fiber can be classified according to its propagation mode, which directly influences its performance as a sensing medium [21]. In this field, two main types can be distinguished: single-mode fiber (SMF) and multimode fiber (MMF), to which are added hybrid configurations explicitly designed for specific sensing applications, such as SMS (Single-Mode–Multimode–Single-Mode) composite fibers, each type with its modal distribution of the optical signal.

Single-mode fiber (SMF) has a very small core (8–10 μm), which allows the propagation of a single light mode. It exhibits low dispersion and provides high precision in optical signal measurement, making it suitable for high-resolution sensing and accurate determination of optical parameters [15,54–56].

Multimode fiber (MMF) has a larger core (50–62.5 μm), enabling the simultaneous propagation of multiple light modes. This feature facilitates coupling and allows higher light power capture, although with lower resolution. MMFs are typically used in short-range systems, in sensors requiring robust coupling, and in applications where greater light capture is needed [4,19,21,23,41,57].

Finally, hybrid SMS (Singlemode–Multimode–Singlemode) fibers represent a combined configuration in which multiple modes are excited in the multimode fiber and subsequently coupled back into the single-mode fiber. This type of fiber is employed in specific multimodal sensing applications and advanced experimental designs [21,58,59].

Figure 4 shows an area between fibers called “interface”, which corresponds to the transition point between the SMF and the MMF, where an abrupt change in the refractive index profile occurs together with the change in core diameter. At this interface, the refractive index shifts suddenly from the SMF core value n_1 to the MMF core value n_2, generating multiple-mode excitation in the multimode fiber. Conversely, at the second interface, the index drops back from n_2 to n_1 as the modes propagated in the MMF are coupled again into the single-mode output fiber.

The choice of fiber type depends on the sensor’s physical operating principle, as well as the requirements for resolution, range, sensitivity, and the installation environment. Therefore, understanding the dynamics of light propagation in each type of fiber is crucial for designing efficient and reliable optical sensing systems.

Another relevant dimension in classifying optical fibers is the type of fiber, encompassing the material used to manufacture it and its internal structure. The mechanical, chemical, and optical properties of the fiber directly influence its sensitivity, operating

range, and suitability for various applications. In this field, although no standard classification is mentioned in the literature, three broad categories are generally identified, as shown in Table 1.

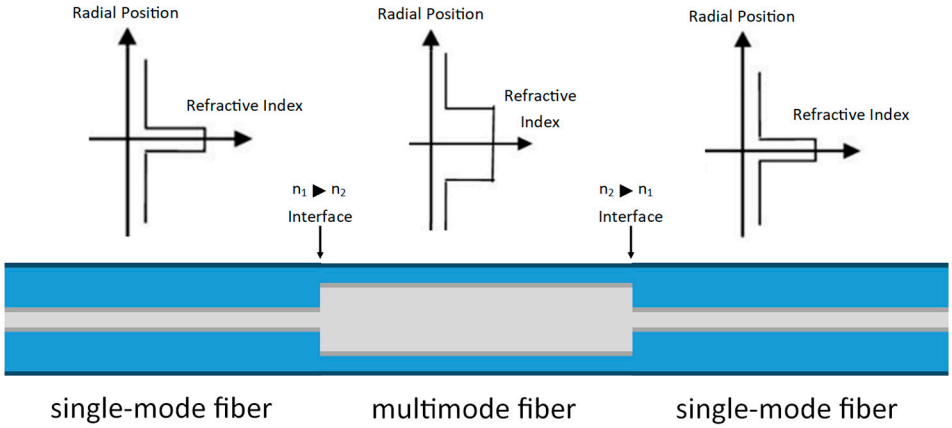

Figure 4. Schematic representation of hybrid SMS (Single-Mode–Multimode–Single-Mode) fiber structure, illustrating the refractive-index profiles and the interfaces where modal transitions occur as light propagates through the composite configuration.

Table 1. Types of optical fiber according to their manufacturing material and internal structure.

Fiber Type	Main Properties	Typical Applications	Ref
Silica Optical Fibers (OF)	Standard silica fiber. Low attenuation, high thermal stability, compatible with telecommunications systems	Commercial and industrial use, monitoring in demanding environments.	[6,57]
Polymer Optical Fibers (POF)	Greater flexibility, lower cost, and larger core diameter. Higher optical losses compared to silica fibers	Short-range applications, physiological monitoring, and detection in environments requiring high maneuverability	[58,60,61]
Special Optical Fibers (PCF, hollow-core, doped, microstructured, coated)	Complex designs such as photonic crystal fibers (PCF), hollow-core, doped, or microstructured fibers. Functional coatings (polydimethylsiloxane, polyimide, graphene). Enabled advanced property manipulation (dispersion, birefringence, sensitivity to gases or liquids)	Specialized sensing, chemical and environmental detection, high-sensitivity applications in extreme conditions	PCF [5,6,21,62–64], hollow-core fibers [24,65–67], doped fibers [7,68], microstructured fibers [8,9,23,69,70]

OFS devices typically use an optical fiber, a light source, a sensor element, and a light detector such as a spectrometer or an optical detection unit. This system works together to detect, transmit, and often also transform physical information from the environment for visualization and analysis (Figure 5) [5,6,22,50]. Its operating principle is based on the interaction of an optical signal, typically laser light or from a light-emitting diode (LED), with an external physical or chemical variable. This generates a measurable change in the property of the light signal, such as intensity, phase, frequency, or polarization [5,12,22]. This modification in the light beam is then analyzed by an optical spectrum analyzer (OSA) or another optical detection module, allowing for continuous or spot monitoring of the magnitude of interest.

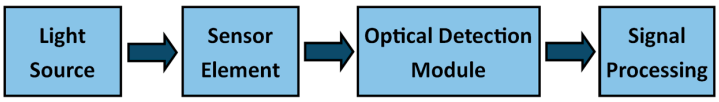

Figure 5. General operational scheme of an OFS, illustrating the sequential stages comprising the light source, the sensing element, the optical detection module, and the subsequent signal-processing unit.

Optical fiber, when implemented in monitoring systems, offers unique advantages over other types of sensors, including EMI immunity [5], high precision [71], high flexibility [72], resistance to extreme conditions [6], and the capacity for distributed monitoring [73]. These properties have driven its adoption as a platform for sensing in harsh environments where other types of sensors may fail or be impractical to install and maintain [6,16,19].

4.2. Classification of OFSs: Intrinsic Sensors vs. Extrinsic Sensors

The evolution of the technological diversity of OFSs over the years has led to the development of multiple classification schemes, which respond to various technical, physical, and operational criteria [74]. This variety of approaches not only reflects the versatility of technology but also allows OFSs to be adapted to specific environments and needs. Figure 6 shows and summarizes these classification dimensions to provide a structured view of the OFSs ecosystem.

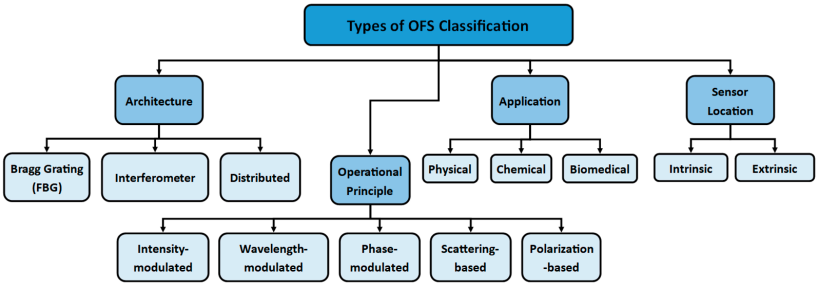

Figure 6. Sketch of the general taxonomy of OFS based on four categories: architecture, operational principle, application domain, and sensor location.

According to the literature, OFSs can be categorized based on different characteristics [74]; for example, they can be classified according to their application or measurement architecture [5,23]. Taking into account their application, OFSs can be grouped according to the type of parameters they are designed to measure, dividing them into three groups: physical (pressure, temperature) [20,22,71], chemical (pH, ammonia, humidity) [21,41,71], and biomedical (oxygen, carbon dioxide, proteins) [8,22,57,75].

On the other hand, regarding architecture, OFSs are classified into three groups: FBG [10,65,76], interferometric [10,76], and distributed [11,68]. FBGs are created by exposing a section of the optical fiber core to a periodic pattern of ultraviolet light (UV), which results in a permanent alteration of the core's refractive index. The reflected wavelength exhibits high sensitivity to variations in pressure and temperature [10,15,43]. Interferometric sensors, on the other hand, are phase-modulated sensors that measure the interference of light in an optical fiber. The most popular types of interferometers include: Mach-Zehnder [17,58], Sagnac [12,17], Michelson [6,8], and Fabry-Perot [54,58]. Distributed sensors, on the other hand, have a configuration that allows them to detect changes in the light signal at multiple points, enabling distributed measurement along the optical fiber [11,68].

In addition to the principle or physical design of the sensor, OFSs can also be classified by the physical principle that modulates the optical signal, i.e., the mechanism by which the external quantity affects the propagated light [5,74]. In this regard, five broad categories can be identified:

- **Intensity-modulated sensors:** The quantity to be measured causes a variation in the intensity of the transmitted or reflected light [17,58].
- **Wavelength-modulated sensors:** These use structures such as FBGs that alter the reflected wavelength as the external stimulus changes [7,16,23].
- **Phase-modulated sensors:** These use optical interferometry to identify phase transformations of the signal [5,8,14].
- **Dispersion-based sensors:** These are based on phenomena such as Raman, Brillouin, or Rayleigh scattering, whereby an interaction between light and fiber generates a backscattering spectrum that varies depending on temperature or deformation [11,43,68].
- **Polarization-based sensors**: These detect changes in the polarization of light induced by mechanical stress, magnetic fields, or thermal fields [5,6,12].

In addition to the criteria explained above, a more fundamental classification, based on the OFSs literature, is based on the location of the sensing phenomenon with respect to the fiber [23,24,58]. In this context, according to the literature, OFSs can be divided into two groups: intrinsic and extrinsic sensors, as shown in Figure 7 [5,12,23,24,58].

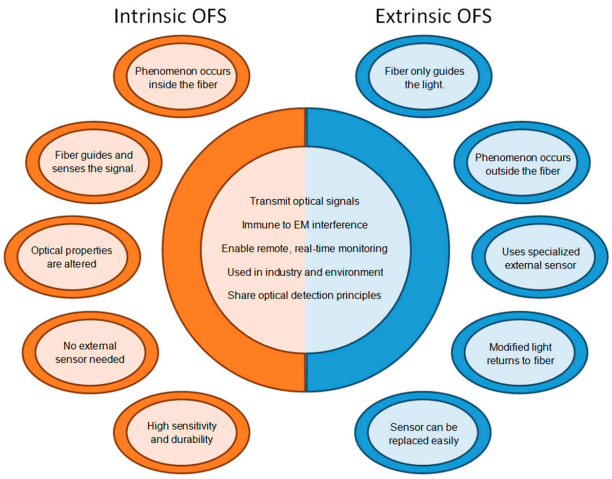

Figure 7. Comparative overview of intrinsic and extrinsic OFSs, highlighting their respective sensing mechanisms, operational characteristics, and shared advantages.

- **Intrinsic sensors:** The physical phenomenon to be measured occurs within the optical fiber itself. In other words, the fiber acts as both a light guide and a sensitive medium (Figure 8a). The optical properties of the fiber (such as refractive index, propagation mode, or dispersion) are directly altered by the external variable to be measured [7,12,23,58,77].

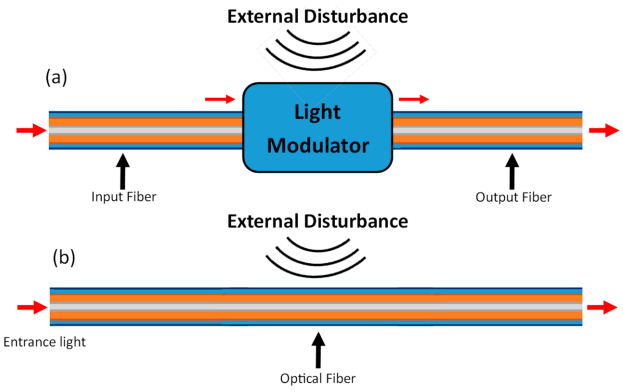

Figure 8. Schematic comparison between (**a**) an extrinsic OFS, in which an external modulation element alters the guided light, and (**b**) an intrinsic OFS, where the perturbation directly affects the optical properties of the fiber itself.

- **Extrinsic sensors:** The fiber is used solely as a means of transporting the optical signal to an external sensor element, where interaction with the physical quantity occurs. Subsequently, the modified light is recaptured by the fiber and sent to the detection system (Figure 8b) [7,12,23,24,58,77].

5. Intrinsic and Extrinsic OFS Architectures

5.1. Intrinsic: Sensors Based on Fiber Bragg Grating (FBGs)

A sensor based on FBG features a periodic modulation of the refractive index within the optical fiber's core, typically created by exposing the fiber to ultraviolet radiation [5,14,20,22,65,78]. This modified fiber functions as a spectral filter, as illustrated in Figure 9, reflecting a specific wavelength of incoming light known as the Bragg wavelength (λ_B). This reflected wavelength depends on the grating period and the effective refractive index of the core, both of which can be affected by mechanical deformation, temperature variations, or stress. The reflected Bragg wavelength (λ_B) is described by Equation (1) [5–7,16,17,58,79]:

$$\lambda_B = 2 * n_{eff} * \Lambda, \quad (1)$$

where n_{eff} is the effective refractive index of the fiber core, and Λ is the grating period. The grating period is affected by variations in deformation, and the effective refractive index is influenced by temperature changes.

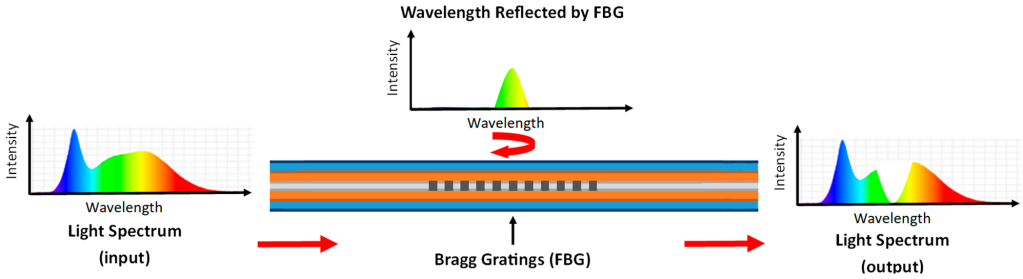

Figure 9. Schematic of a typical FBG–based sensing structure, showing the broadband input spectrum, the selective reflection of the Bragg wavelength, and the resulting transmitted output spectrum after interaction with the periodic grating.

To measure a physical parameter with an FBG sensor, it is essential to isolate the effects of temperature from those of deformation in the fiber. Using a reference grating provides a practical and straightforward approach [5,8,14,20,54]. FBG sensors require a component called a demodulator, or interrogator, which extracts information about the measurand from the light signals emitted by the sensor heads. Because the information is encoded in the Bragg wavelength, interrogators must detect shifts in this wavelength and deliver data related to the measurand [5–7,54,58,80,81].

The ability of FBGs to operate as passive and compact units makes them ideal for harsh environments or applications requiring minimal intrusion. They also provide several advantages, such as easy multiplexing over a single fiber line (using wavelength) [20,22–24,57] and EMI immunity [5,14,20,22,23,65].

5.2. Interferometers

Optical interferometers operate on the principle of wave superposition, where two or more optical beams follow different paths and then recombine [5,12,22,24]. The phase difference that develops between them depends on changes caused by the variable being measured, allowing for precise measurements [5,12,22,24,58,65,75]. There are several types of interferometers.

5.2.1. Intrinsic and Extrinsic: Fabry-Perot Interferometer

Fabry-Perot interferometer sensors (FPIs) operate by measuring light wave interference between two mirrors within the fiber, one of which is partially transparent. By adjusting the distance between the mirrors, the sensor can be fine-tuned to a specific wavelength, enabling precise measurement of physical parameters such as deformation, temperature, and pressure [5,12,22,24,82]. The FPI configuration is among the simplest and most extensively studied in the development of compact OFSs [12,19,22,58,65,75].

With variations in their structure, FPI sensors are divided into two groups: intrinsic (IFPI) and extrinsic (EFPI) [6,24,58]. For IFPI, the Fabry-Perot cavity forms between two reflectors (mirrors) aligned within the optical fiber, as shown in Figure 10a. This can be accomplished through methods such as femtosecond laser micromachining, fusion splicing, using two FBGs in series, chemical etching, or creating an air bubble inside the fiber [6,24,54,58]. In its simplest form, when the cavity uses low-reflectivity mirrors, it can be modeled as a two-wave IFPI interferometer [6,8,24,54,58]. In such cases, the reflection spectrum is mainly determined by the phase difference (δ_{FP}) between the waves reflected by the two mirrors, as described by Equation (2) [24,58].

$$\delta_{FP} = \frac{4\pi * n_{eff} * L_{FP}}{\lambda}, \quad (2)$$

where n_{eff}, (L_{FP}) and λ represent the effective refractive index of the cavity material, the physical length of the cavity, and the wavelength of the incident light, respectively. When an external disturbance occurs, such as a change in deformation, temperature, or other parameters, both the cavity length and the effective refractive index can change, leading to a shift in the phase difference [5,12,22,24].

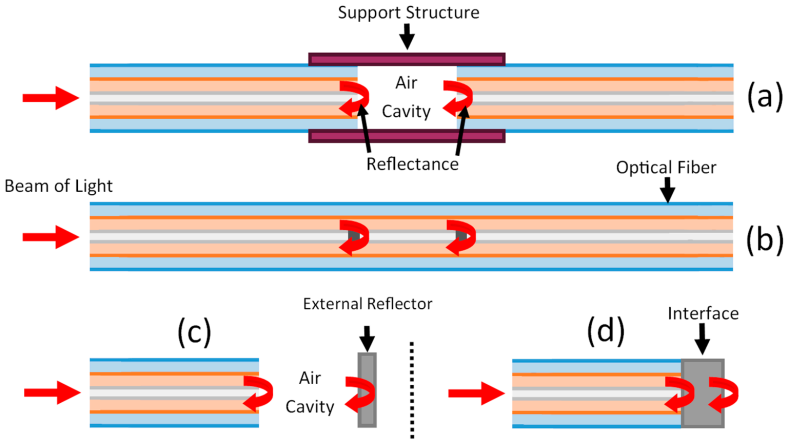

Figure 10. Schematic of various FPI interferometer sensor configurations: (**a**) IFPI with a solid cavity. (**b**) EFPI with an air cavity supported by a tube. (**c**) EFPI with an external free-space reflector and air cavity. (**d**) EFPI with a film deposited on the end face of the optical fiber without an air cavity.

In contrast, for EFPI, the Fabry-Perot cavity is formed between the tip of the fiber with its cleaved end and an external reflector, with the air between them serving as the cavity medium, without requiring any microfabrication process. Instead, a tube or support structure holds both fibers (Figure 10b) [6,24,54,58,83]. Since the first reflector of an EFPI sensor is typically the interface between the fiber's end face and the air, accounting for less than 4%, the multiple light trips can be approximated as a single round trip within the cavity. Consequently, a two-beam interference model can describe a low-finesse EFPI device. In this case, total reflection (I) can be expressed by Equation (3) [24,58]:

$$I = I_1 + I_2 + 2\sqrt{I_1 I_2} * cos(\varphi + \varphi_0), \quad (3)$$

where I_1 and I_2 are the intensities of light reflected at the fiber-air interface and the external reflector, respectively; φ_0 is the additional phase introduced by the second reflector, and φ is the round-trip phase delay caused by the Fabry-Perot cavity, as defined in [24,58].

$$\varphi = \frac{4\pi * n * L_{FP}}{\lambda}, \tag{4}$$

where n denotes the refractive index of the cavity medium, which is considered constant for air with $n = 1$, L_{FP} is the physical length of the Fabry-Perot cavity, meaning the distance between the two reflectors, and λ represents the wavelength of light.

Alternatively, for the EFPI structure, a separate mirror positioned at a certain distance from the end of the input fiber can serve as an external reflector [24,54,58], with the fiber and mirror fixed to different structures to form the Fabry-Perot cavity (Figure 10c). Alternatively, a thin film of the material of interest can be deposited on the cleaved end of an optical fiber to create the EFPI [24,54,58], where the interface between the fiber and the material acts as the first reflector and the interface between the material and the environment functions as the second reflector (Figure 10d).

The FPI configuration can be used for both physical and mechanical detection, as well as for chemical and biological sensing, by encoding the measurand of interest according to changes in the refractive index of the medium within its cavity [8,10,43,54,76].

5.2.2. Intrinsic: Mach-Zehnder Interferometer

Mach-Zehnder interferometer (MZI) sensors are widely used in various multiparametric detection applications due to their inherent design. In this setup, the phase shift between two light beams is measured, one beam exposed to the environment and the other serving as a reference [84]. Although the physical lengths of the sensor and reference arms are identical, differences in the optical path length produce interference. For parameter measurement, the sensor arm is exposed to the environment, while the reference arm remains isolated [42,85–89], as shown in Figure 11. Any change in the surrounding parameters induces a phase difference, resulting in a measurable interference pattern. This phase difference of the MZI interferometer (ϕ) is described by Equation (5) [42,89]:

$$\phi = \frac{2\pi}{\lambda}\left|n_{eff1} * L_1 - n_{eff2} * L_2\right| + \phi_0, \tag{5}$$

where n_{eff1} and n_{eff2} are the effective refractive indices of the two optical paths, L_1 and L_2 are the transmission lengths of the two optical paths, λ is the wavelength of light, and ϕ_0 is the initial phase.

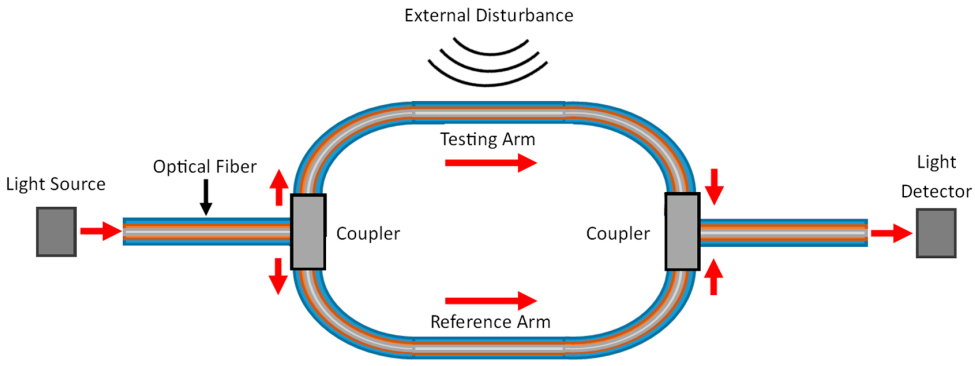

Figure 11. Schematic configuration of an MZI sensor, showing the division of light into a testing arm and a reference arm via optical couplers and the subsequent recombination used to detect phase variations induced by external disturbances.

5.2.3. Intrinsic: Michelson Interferometer

Michelson interferometer (MI) is another type of intrinsic interferometer very similar to MZIs, following the same principle of two light beams in two fiber optic arms, with the difference that, in the MI, each beam is reflected at the end of each arm [5,51,90–92]. The measurand (the physical quantity to be measured) modifies the phase of the signal beam, while the reference beam remains in a constant environment. The signal and reference beams end in mirrors and are reflected along the same path to recombine in the same coupler used (Figure 12) [5,51,90,91,93–96].

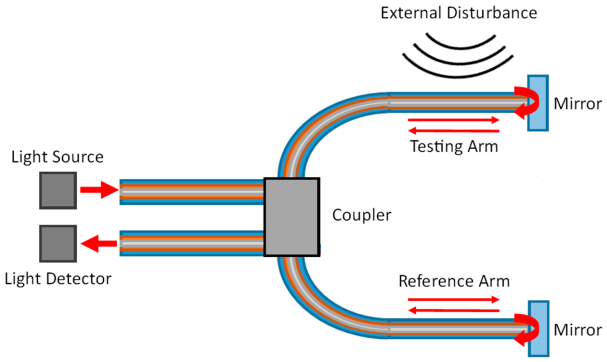

Figure 12. Schematic configuration of an MI sensor, showing the splitting of light into testing and reference arms, its reflection by mirrors, and the recombination at the coupler used to detect phase variations produced by external disturbances.

5.2.4. Intrinsic Sagnac Interferometer

The intrinsic Sagnac interferometer (SI) sensor is built with a simple setup, usually using just one optical fiber in a loop. In this setup, a light beam enters the coupler and splits into two coherent beams. These beams travel in opposite directions (clockwise and counter-clockwise) and have different polarization states, forming a closed optical loop that recombines in the coupler after completing the loop in the fiber, then sends the light to the detector (Figure 13) [5,17,42,86]. Although the two beams follow the same optical length, because they are altered at different times, the propagation loop changes, creating a difference in the optical path between them, which leads to measurable interference [17,42,51,86,93,94].

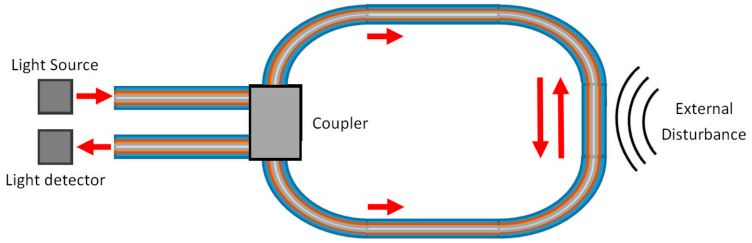

Figure 13. Schematic configuration of an SI sensor, where counter-propagating light waves travel along a looped fiber path and experience phase shifts induced by external disturbances, which are subsequently detected after recombination at the optical coupler.

5.3. Intrinsic: Distributed Sensors Based on Dispersion

The distributed optical fiber sensor (DOFS) architecture enables information to be collected using just a single optical fiber along its entire length, functioning as a continuous sensor. Unlike earlier setups, where measurements are taken at specific points on the fiber, distributed sensors are an innovative technology for large-scale monitoring [12,20,68,97–101].

This intrinsic architecture of DOFS measures by analyzing backscattered light. This occurs when a light pulse with an original wavelength (called the Rayleigh linear component) interacts with microscopic imperfections or physical effects within

the fiber core, where most of the light travels. Simultaneously, a small fraction is backscattered (Figure 11) [12,97,99]. This creates displaced light beams that contain components with wavelengths above and below the original signal, known as non-linear Raman and Brillouin components. These components offer information about the local properties of the fiber and disturbances like temperature or deformation. However, the accuracy of these measurements declines as the distance from the fiber increases, due to optical signal attenuation, low signal-to-noise, and hardware limitations of the optical interrogator [97,99,101].

Rayleigh scattering results from the interaction of incident light with fluctuations in the refractive index of the fiber core, mainly at the molecular level, and it is characterized by having the same frequency as the incident light [97,100,101]. Brillouin scattering, on the other hand, occurs when incident light interacts with acoustic modes in the medium, which are generated by the propagation of light in the fiber. Measuring the Brillouin frequency shift relative to the incident light allows for the estimation of parameters such as temperature or strain and supports distributed detection over long-range fibers [100,101]. On the other hand, Raman scattering is a consequence of the interaction between light and molecular vibrations within the medium, involving an energy exchange between light and matter. This type of scattering has a higher power threshold than Brillouin scattering and is also used in distributed sensing systems [99–101].

Figure 14 illustrates the operating principle of a DOFS, where a light source emits pulses that travel along the fiber, while a detector measures the backscattered light. At the bottom, the spectrum displays the three main types of dispersion: Rayleigh, Brillouin, and Raman. In the center, a dominant peak corresponding to Rayleigh scattering is observed, centered at the operating wavelength $\lambda_0 = 1550$ nanometers (nm), which indicates backscattering without a frequency shift. This scattering does not exhibit a significant frequency shift relative to the incident light and occurs within a narrow band of approximately 88 picometers (pm). On either side of the Rayleigh peak are the Brillouin components with an approximate shift of $\Delta vb \sim 35$ megahertz (MHz) relative to λ_0. The bandwidth of these components is indicated as Gb, and the total spectral separation is about $\Delta v_0 \sim 11$ gigahertz (GHz). The Brillouin components respond to changes in temperature (T) and mechanical strain (ε), enabling distributed sensing of these variables. In the farthest regions of the spectrum, Raman components appear on both the anti-Stokes side (shorter wavelength and higher frequency than λ_0) and the Stokes side (longer wavelength and lower frequency than λ_0). The frequency of the Raman components shifts by terahertz (THz) to approximately 206 THz (anti-Stokes) and 180 THz (Stokes), and their intensity is closely related to temperature T.

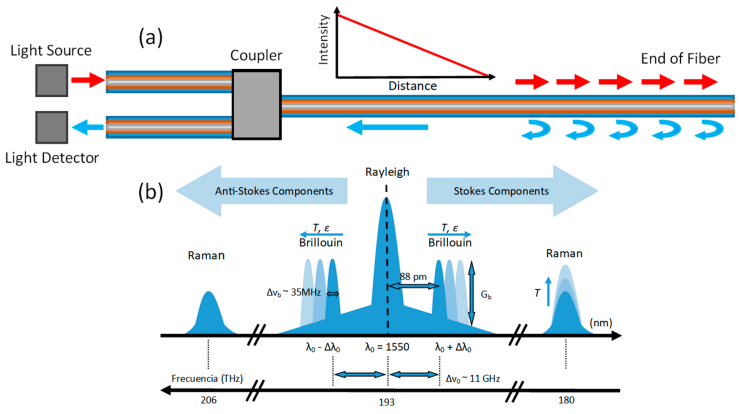

Figure 14. (**a**) Schematic representation of a DOFS, illustrating the emission, backscattering, and return path of the optical signal along the fiber length. (**b**) Spectral distribution of Rayleigh, Raman, and Brillouin scattering components under 1.55 µm excitation, highlighting the corresponding Stokes and anti-Stokes shifts (adapted from [102]).

The theoretical basis for light scattering in fibers was proposed by Froggatt and Moore, demonstrating that backscattered light from permittivity is a deterministic function of distance along the fiber [103,104]. Demonstrating that, for an optical fiber, as for any waveguide, the electric field ($E(z)$), where z is the location of the fiber, obeys the homogeneous wave equation adjusted by the dispersion term (Equation (6)) [68,98,100,101]:

$$\frac{\partial^2 E(z)}{\partial z^2} - g^2 \left[1 + \frac{\Delta\varepsilon(z)}{\varepsilon}\right] E(z) = 0, \quad (6)$$

where g is the complex propagation constant, the term $\frac{\Delta\varepsilon}{\varepsilon}$ contains the dispersion phenomena that occur in the fiber, which are responsible for local reflections at each location in the fiber, ε is the dielectric permittivity of the fiber, and $\Delta\varepsilon(z)$ contributes to local reflections that are a function of both wavelength and space.

The complex propagation constant is expressed as Equation (7) [98,100,101]:

$$g = \propto + j\beta, \quad (7)$$

where the real part $\propto$ represents the one-way losses of the fiber, and the imaginary part β is the wave number.

6. Applications by Technological Area

In recent years, OFSs have been used across a wide range of scientific, industrial, and technological fields, thanks to advantageous characteristics such as high sensitivity, EMI immunity, multiplexing ability, and the capacity to operate in extreme environments [5,6,9,10,12,16].

6.1. OFSs in Industry

In the industrial sector, OFSs have proven to be essential devices for measuring physical parameters in challenging environments. Both intrinsic and extrinsic sensors have been adopted, each with specific advantages depending on environmental conditions and the type of variable to be measured [23,41,65,74,105].

The literature clearly shows the dominance of intrinsic sensors, especially those based on FBG and interferometers (Table 2). The most common configurations include FBGs used for detecting temperature and mechanical deformation in industrial components such as pipes, turbines, and electrochemical cells. Notably, FBGs distributed along a single fiber enable multipoint monitoring, allowing for the detection of anomalies or structural fatigue in critical installations [106–108]. The use of Fabry-Perot and Michelson interferometers for measuring pressure and temperature has also been documented [91,109]. Conversely, extrinsic sensors (Table 3) are employed in specific applications requiring more localized or specialized interactions, such as inspecting electrochromic devices (EC) [110] or materials with complex geometries [111–113].

Regarding the fiber material, the most commonly used are silica SMFs with coatings tailored to industrial needs: from polyamide coatings for high temperatures [108] to metal coatings for machinery applications [91,106,107,114]. It is also common to use fibers with special coatings and encapsulated structures that enable them to operate in environments with high humidity or exposure to chemical compounds [115–118].

Along with their benefits, the industrial use of OFSs still encounters major technical and economic hurdles. One common problem is cost, since advanced designs like photonic crystal fibers or sapphire-based fibers significantly increase fabrication costs and restrict their use compared to traditional electronic sensors [41,51]. Even in more standardized technologies like FBGs, the requirement for specialized interrogation systems and encap-

sulation methods suited to harsh environments continues to be a financial obstacle for large-scale deployment [21,49].

Another critical aspect is field calibration, which becomes a complex task in real industrial environments. The response of optical fibers can be influenced by temperature changes, mechanical stress, or chemical exposure, requiring in situ recalibration protocols that are not always compatible with continuous operation demands [24,76]. Some strategies suggest hybrid calibration models that combine laboratory references with adaptive algorithms to enhance the sensor's stability over time [93].

The service life of OFSs also plays a key role in their competitiveness. Although silica fibers provide high thermal and mechanical stability, extended exposure to radiation, high humidity, or corrosive agents causes gradual degradation of sensitivity and signal-to-noise ratio [6].

Coatings made from polymers or metals can reduce these effects, but they increase manufacturing complexity and sometimes lessen the sensor's flexibility [51]. In high-temperature settings, crystal fibers such as sapphire or neodymium-doped aluminum have proven to significantly extend the operating lifespan, although their fragility and cost are still limiting factors [41].

Finally, issues related to integration and maintenance also impact industrial adoption. Unlike traditional sensors, OFSs often require interrogation units and optical alignment that must be periodically checked to ensure reliable operation [21]. This increases the need for trained personnel and restricts their use in environments where access is limited [76]. Despite these challenges, the literature emphasizes that the long-term benefits, such as distributed measurement, EMI immunity, and multifunctionality, outweigh the drawbacks, indicating that the current barriers are temporary and will diminish as manufacturing techniques advance [49,51].

Table 2. Intrinsic OFSs in industry.

Architecture	Application	Fiber Type	Features	Ref.
FBG + IFPI in a single fiber	Measurement of internal pressure and temperature in lithium-ion batteries	Silica SMF with polymer section	- FPI sensitivity: −11.2 nm/bar, 920 pm/°C - FBG sensitivity: 8.3 pm/°C - Resolution: ±0.4 mbar, ±0.5 °C - Response time: 1.7 s to 3.1 s - Operation tested up to 40 °C - Pressure range recorded: up to ±4.5 bar	[108]
Modal interferometry by curvature in the shape of a globe	Measurement of refractive index and temperature in aqueous solutions of acetic acid	Silica SMF and a silica capillary tube secured with a polytetrafluoroethylene tube	- Refractive index sensitivity: up to 170.66 nm/RIU - Temperature sensitivity: −119.2 pm/°C (in the range 29–43 °C) - Resolution: 0.0000303 RIU and 0.57 °C	[109]
Multiple architectures: - IFPI - FBG - Rayleigh scattering DOFS	Measurement of temperature and deformation within industrial metal structures	Aluminum-coated silica SMF, stainless steel, or metal capillary	- High temperature-resistant FBG, engraved with a femtosecond laser—IFPI encapsulated in a steel tube with an internal mirror - Integrated sensors without compromising the mechanical properties of the component	[107]
Distributed sensor based on Rayleigh scattering	Detection of Delamination damage	Silica SMF	- Spectral strain sensitivity: ~1 με resolution - Spatial resolution: millimeter-scale - Enables detection of strain mutation peaks caused by delamination - Capable of localizing damage with <3 mm error	[106]
FBG	Monitoring of optical transmittance in EC	Silica MMF	- Wavelength used: 810 nm LED - Detects temperature, but does not correlate well with optical transmittance	[110]
FBG	Measurement of mechanical deformation in structures	Silica SMF	- Measured deformation range: up to 2 mm/m - Sensitivity: ~1.2 nm per 0.2% - Accuracy: relative error of 0.04%	[119]
Distributed reflectometer sensor	Detection of water leaks in underground systems	Plastic MMF	- Leak location accuracy: ±10 cm - System range: up to 100 m - Response time: in real time	[120]
MI	Temperature measurement in high-temperature environments	Silica SMF Optional coating with gold film to improve reflectivity.	- Temperature range: 100–900 °C - Sensitivity: 80 pm/°C (100–450 °C), 109 pm/°C (450–900 °C) - Thermal stability up to 900 °C - Reflected sensor with increased reflectivity of 16 dB when gold is applied	[91]
FBG	High-resolution liquid level measurement	Plastic MMF with a polymethylmethacrylate core	- Measurement range: 7.2 cm - Resolution: 0.5 mm - Sensitivity: 17.4 pm/mm - No direct contact with the liquid required	[118]
Distributed sensor based on Rayleigh scattering	Measurement of surface temperature of cylindrical cells in Li-ion batteries 21700	Silica SMF	- Spatial resolution: 3 mm - Measurement range: from 25 °C to 82 °C. - Sensitivity: 1.55 GHz/°C (requires prior calibration) - Accuracy: ±0.2 °C	[121]
FBG	Deformation in carbon fiber composite materials	Silica SMF	- Sensitivity to deformation: ~1.2 pm/ με - Measurement of deformations up to ~2000 με - Accuracy: on the order of ±10 με - Multiplexing capability	[122]

Table 2. *Cont.*

Architecture	Application	Fiber Type	Features	Ref.
FBG	Deformation and temperature monitoring in smart structures and composite materials	Silica SMF with acrylate coating	- The sensor can simultaneously measure deformation and temperature. - No exact values are given for sensitivity or temperature range, but the high fidelity of response after the insertion process is highlighted.	[117]
FBG	Simultaneous measurement of temperature and deformation	Erbium-doped silica SMF	- Temperature resolution: ±0.1 °C - Strain resolution: ±0.85 $\mu\varepsilon$ - Sensitivities: 9.29 pm/$\mu\varepsilon$ and 11.29 pm/°C - Spectral operating range: around 1550 nm	[116]
Distributed sensor based on Rayleigh scattering	Distributed magnetic field measurement	Silica SMF with germanium-doped core and nickel-acrylate composite coating	- Sensitivity: 22.85 MHz/mT - Measurement range: 3 mT to 245 mT - Spatial resolution: 20 cm - Measured deformation change: up to 36.4 $\mu\varepsilon$ - High linearity ($R^2 > 0.99$) - Remote detection capability and resistant to extreme environments	[115]
Distributed sensor based on Rayleigh scattering	Distributed temperature monitoring in continuous emulsion polymerization tubular reactors	Silica SMF	- Distributed thermal detection with a spatial resolution of 2.6 mm - Temperature range: inferred up to ~100 °C, although no upper limit is specified. - No process intrusion or direct contact with the fluid is required	[123]
FBG	Measurement of mechanical vibrations (frequency and acceleration)	Silica SMF coated with silver film	- Operating frequency: 100 Hz to 800 Hz; resonance at ~1900 Hz - Acceleration sensitivity: up to 38.79 mV/g - Axial strain sensitivity: −2.57 pm/$\mu\varepsilon$, −1.6 pm/$\mu\varepsilon$ - Frequency range: up to 10,000 Hz - Signal-to-noise ratio: 55.1 dB at 1900 Hz	[114]

Table 3. Extrinsic OFSs in industry.

Architecture	Application	Fiber Type	Features	Ref
1. Transmittance with fibers on both sides of the device 2. Fiber-to-fiber measurement crossing the device 3. Lateral transmittance through the edge	Monitoring of optical transmittance in EC devices	Silica SMF	- Wavelength used: 810 nm LED - 1. Signal sensitive to the angle of incident light - 2. Clear signal, but dependent on the alignment of fibers - 3. Good correlation with reference transmittance, robust for manufacturing	[110]
Sensor based on ultraviolet-visible absorption spectroscopy	Monitoring of ammonia in the air inside poultry farms	Plastic MMF	- Detection limit: 0.33 ppm - Linear range: 0.33 to 8 ppm - Response time: 5–10 min - Proven selectivity against interference (carbon dioxide, humidity, temperature)	[113]
EFPI integrated with microelectromechanical systems	Vibration/acceleration measurement in high-temperature environments	Gold-coated silica SMF	- Axial sensitivity: ~2.48 nm/g (at 20 °C), higher at elevated temperatures - Thermal stability: maximum phase drift of 0.0109 rad in 110 min at 400 °C - Thermal range: tested from 20 °C to 400 °C - Non-linearity error: 1.88% at 300 °C	[112]
Backscatter reflection-based sensor	Pressure measurement to detect mechanical filter blockages in hydraulic systems	Plastic MMF	- Measurement range: 0–35 kPa - Sensitivity: 0.285 mm/kPa - System repeatability: ±0.0038 mm - Near-linear response up to 35 kPa	[111]

Overall, the industrial deployment of OFSs shows a clear shift toward intrinsic configurations, especially FBG- and interferometer-based systems, because of their high precision and capacity to support distributed, multipoint measurements. Extrinsic sensors remain important in specialized applications that require localized interactions or compatibility with complex device geometries. In both categories, the choice of fiber coatings and encapsulation methods reflects a move toward materials designed for harsh conditions, balancing sensitivity with durability. Despite ongoing challenges related to fabrication costs, field calibration, and long-term stability, the literature suggests a steady shift from laboratory demonstrations to scalable industrial integration, driven by the need for reliable monitoring solutions in increasingly demanding environments.

6.2. OFSs in Medicine and Biomedicine

In recent years, in the fields of medicine and biomedicine, the use of OFS has appeared as a means for tracking physiological and biochemical parameters. These OFS are used in medical procedures and surgeries, generally [17,22,57,75].

The tendencies are visible in these applications, favouring two types of intrinsic sensors as are summarised in Table 4, most commonly those exploiting Bragg gratings, including interferometric ones. Here, intrinsic sensors are of prime importance within smart catheters, temperature observation in ablated tissues, muscle vibration measurement, and real-time physiological observation [17,22,43]. It is worth highlighting the utilization of FBG sensors applied for temperature and strain observation in medical applications due to the strong, predictable reflectance spectrum and the ability to be implanted in tissues or built into wearable devices [14,22].

On the other hand, the use of extrinsic sensors has proved beneficial in cases where the coupling of the variable of interest with the fiber takes place outside the core region of the fiber itself (Table 5). This includes EFPI sensors used in endovascular applications for pressure measurements, and scintillating detectors used in brachytherapy procedures for radiation treatment measurements. This kind of sensor design enables the use of external cavities and sensitive materials, thus adding towards increased versatility, especially in cases demanding high resolution with medical devices [10,22,54]. Silica SMF are the most used types of fibers, although many examples involve plastic MMF in extrinsic sensors, most preferably due to flexibility and low-cost factors. Functional coatings including refractive index-sensing films and those used for biomarker detection have become common in FBG setups, adding towards an increased biological sensing potential [14,58].

It is apparent from the recent available literature that the level of interest in the use of OFSs in the field of biomedicine has increasingly moved from in vitro proof-of-principle measurements to in vivo validations, proving that OFSs have applications beyond the lab feasibility stage and can function exceedingly well within a medical setting and clinical trials. Various reviews have highlighted the effectiveness of FBG and FPI integration with minimally invasive surgical tools and catheters, where measurements related to intracranial and intravascular pressure, thermal ablation, and tissue deformation tests were performed within living organisms [22,58]. Such medical validations establish the fact that OFSs not only compete with electronic sensors but can be superior because of their EMI immunity within MR environments [68].

Despite these benefits, the transition from research-to-innovation-based translations to mainstream clinical use is currently hampered by some challenges. First, the cost is a key concern, considering the increased costs due to the use of interrogation technologies and the loss of the cost advantage of standard biosensors [10,25]. Moreover, calibrating these devices in a real clinical environment is a complex process due to physiological complexities, including temperature variations, motion of tissues, and fluid dynamics, which create noise levels requiring recalibration [14].

A further consideration is related to service life and biocompatibility. Over a period of exposure to bio-fluids, degradation of optical coatings can occur, leading to a reduction in sensitivity, biofouling effects on the surface of the fiber, and ultimately influencing the reliability of the sensors [43,60]. To mitigate these effects, progress has been made in developing biocompatible coatings of polymeric and graphene materials with improved robustness and the ability of fibers to identify specific bio-markers [14]. However, maintaining a balance is a challenge.

The use of OFSs in wearable devices and rehab instruments is already past the prototyping stage, with clinical tests underway for tracking respiration, joint motion, and cardiac activity. Such devices exploit the non-invasive, continuous tracking offered by OFSs. But such instruments have limitations related to cost, fragility, and recalibration requirements for longer-term use [10,17,43].

It is emphasized in the literature that the progress of OFSs in the field of medicine demands an interdisciplinary approach by engineers, clinicians, and regulatory agencies. Even though some OFSs have already received approval from the Food and Drug Administration (FDA) for use in physical measurements such as pressure [22], biochemical sensing, including glucose and protein targets, is currently only researched in lab-scale and pilot-scale settings due to issues with calibration, biofouling, and the need for clinical validation [14,25]. However, advances in distributed sensing approaches and Ruthenium-based electrochemical sensing methods hold much promise [25,68].

Table 4. Intrinsic OFSs in Medicine and Biomedicine.

Architecture	Application	Fiber Type	Features	Ref.
MZI	Detection of acetone in human breath as a biomarker for diabetes mellitus	Silica SMF coated with a polydimethylsiloxane film	- Concentration range: 0–332 ppm - Detection limit: 1.5 ppm - Sensitivity: up to 0.0147 ppm^{-1} - Operating temperature: ≈25 °C	[124]
Sensor based on intensity modulation	Detection of acetone in human breath as a biomarker for diabetes mellitus	Silica SMF thinned by thermal process without coating	- Measurement range: 0–500 ppm - Detection limit: 5.56 ppm - Operating temperature: ≈25 °C	[125]
IFPI	Monitoring of tissue refractive index during radiotherapy sessions	Silica SMF with external coating of nanocrystalline diamond film	- Adjustable sensitivity range through design variations - High spatial and temporal resolution - Interferometric modulation dependent on refractive index	[126]
FBG	Thermal analysis of perfusion cooling in porcine liver tissue during and after laser ablation	Silica SMF encapsulated within a stainless steel guiding needle	- Monitored temperature range: up to 100 °C - Thermal resolution: 0.1 °C - Minimally invasive instrumentation - In vitro experimental validation with perfused and non-perfused porcine liver	[127]
IFPI	Gas pressure measurement	Silica SMF	- Maximum sensitivity: 2.526 nm/kPa - Pressure range: 200–300 kPa - Cavity formed with epoxy resin to enhance sensitivity and response	[128]
FBG	Monitoring of brain deformations induced by pressure waves during impacts	Silica SMF mounted on a flexible silicone substrate	- Strain range: up to ~4% - Temporal resolution: 650 kHz - Millimetric spatial accuracy - Sensor response time: ~1.5 µs	[129]
MZI	Detection of acetone in gaseous phase	Silica SMF with a stripped fiber section coated with a thin layer of indium oxide	- Application of PLS regression (Projection to Latent Structures) for spectral response modeling - Sensitivity: up to 1 ppm - Interrogation in the visible spectral range (~630 nm) - Good fit between experimental data and model: $R^2 > 0.98$	[89]
FBG	Simultaneous measurement of temperature and relative humidity in confined environments	Silica SMF with partial coating of SFT (sensitive functional tube) material	- Humidity sensitivity: ~1.007 pm/%RH in the range 11–97% RH - Thermal sensitivity: ~10.18 pm/°C in the range 20–80 °C - Compact dimensions (external diameter < 1 mm)	[130]

In the biomedical field, the dominant trend favors intrinsic FBG- and interferometer-based sensors, which allow for precise, minimally invasive monitoring of physiological variables and can be easily integrated into surgical tools or wearable devices. Extrinsic configurations complement these advances in specialized roles, such as pressure monitoring or radiation dosimetry, where external cavities and scintillating materials provide additional versatility. A clear shift is observed from in vitro validations to in vivo applications, emphasizing the clinical potential of OFSs beyond laboratory settings. Meanwhile, research highlights ongoing challenges, including high interrogation costs, calibration in dynamic biological environments, and ensuring long-term biocompatibility, but the overall path points steadily toward clinical translation and routine medical use.

Table 5. Extrinsic OFSs in Medicine and Biomedicine.

Architecture	Application	Fiber Type	Features	Ref.
Bending sensor based on curvature-induced attenuation	Estimation of the knee flexion/extension angle during walking	Plastic MMF coated with a heat-shrink tube	- Need for a neural network to model temporal dynamics - Minimum root mean square error (RMSE): 3.41° (IQR: 2.50–5.19°) - Sampling frequency: 1800 Hz	[131]
EFPI	Pressure monitoring during endovascular surgical procedures	Silica SMF with an interferometric thin film on the fiber core end face	- Pressure sensitivity: 0.4646 nm/kPa - Measurement range: up to 200 kPa - Resolution: 0.1 kPa - Sensor diameter: 125 µm (compatible with vascular guidewires)	[132]
Optical sensor based on scintillation radiation detection	Dose measurement in low-dose-rate brachytherapy	Plastic MMF with a core doped with scintillating material, coated with reflective material	- High spatial resolution for dose distribution detection - Reproducible response under varying orientation and distance conditions - Passive sensor, no need for an electrical power supply - Good performance within a water phantom, simulating human tissue	[133]
EFPI	Wide field photoacoustic microscopy for monitoring acoustic signals induced by laser pulses	Silica SMF with a cavity formed by a thin polymer film	- Lateral resolution: ~6.3 µm - Field of view: 3.3 × 3.3 mm^2 - Penetration depth: ~1 mm - High-speed interrogation with an acquisition rate of 1.6 kHz per channel - Sensitivity to acoustic signals	[134]

6.3. OFSs in Environmental Chemistry

OFSs have found wide acceptance in chemistry for gas and liquid analysis, and for measurements of physicochemical parameters of the environment [13,135]. A review of the literature shows a wide variability of design and functional materials according to the demand for sensitivity and selectivity.

Intrinsic sensors dominate in interferometric and scattering setups (Table 6). Such setups are used for gas sensing of substances such as ethanol and dimethyl sulfoxide, as

well as metal ions Hg^{2+} and Pb^{2+}, due to the high sensitivity, low detection thresholds, and ability to work with functional materials such as polyaniline layers, metallic nanoparticles, metal oxide, and printed nanostructures [98,136].

On the other hand, extrinsic sensors can be better fitted into applications with modularity requirements, design versatility, and integration with other external materials, which cannot be readily included within the fiber core itself (Table 7). The use of POFs [135], metallic layers such as gold nanostars and palladium layers, polymeric layers, and evanescent field-based sensors has already been explained [13,72,135,137]. Their performance is excellent with regard to the measurement of volatile organic substances, inflammable gases, and traces of heavy metals present in a liquid [13,72].

A new direction is the use of nanocomposites and hybrid functional structures, which enhance the optical properties of the sensor and enable increased levels of sensitivity, stability, and selectivity [13,72,135,136]. This reflects a new direction for OFSs in promoting green technologies for environmental monitoring and the detection of priority pollutants.

Regarding environmental measurements, the transition of lab-scale designs into reality shows limitations for each specific medium. For example, in evanescent field sensors and other surface-based sensors, the sensing region is always close to, or actually at, the fiber–medium interface, which makes it necessary to access or reduce the cladding thickness in order to allow for optical interaction. This makes it prone to fouling and biofouling effects (non-specific adsorption of biomolecules, organic layers, or biofilms), introducing baseline drift and loss of selectivity. This also demands stable surface functionalization and protection against the mentioned effects in the mechanical design of the sensor itself. Literature shows that surface sensing using evanescent light depends on the analyte's proximity to the core and often involves cladding removal, affecting robustness and field stability [13].

For interferometric setups designed for volatile organic compound detection, the reviews indicate remarkably sensitive detection thresholds in the ppb–ppm range whenever thin-film materials such as polydimethylsiloxane and zeolites were used. However, some issues concerning the respective setups' selectivity, ability to demodulate spectra, and temperature, pressure, and humidity dependence still exist in most cases. The majority of these interferometric setups were only able to function within a centralized setting due to a lack of a means for distributed monitoring [42].

Humidity effects can also produce strong errors due to the impact of humidity interference. The swelling process in a polymer coating will make the change non-linear with a low response rate, making calibration a challenge, especially for a broad range of relative humidity values. Experimental evidence shows that a graphene oxide coating has a strong sensing capability with a rapid response compared with a "water-swelling" polymer [50].

As regards cost and complexity of the interrogator, the interferometric methods provide a much better sensitivity; however, these methods may be prone to a temperature effect and need a temperature compensation system, thereby complicating the acquisition cost and complexity. In contrast, reflective methods with a micromirror design can be cost-effective, but these methods mostly tend to be intensity-based and may be prone to pathlength variations in the optical measurements and can only be used for a single-point measurement [136].

The service life of OFSs largely depends on the material choice. Group IV metal oxide coatings (HfO_2, ZrO_2, TiO_2) demonstrate high chemical stability and resistance to corrosion, while also being more cost-effective than polymer films. As a result, they are promising options for long-term humidity and gas sensing in harsh environments. However, careful control of coating thickness and microstructure is necessary to prevent drift and fatigue during repeated exposure cycles [50].

Taken together, these observations suggest prioritizing: (i) anti-fouling surfaces or inorganic protective coatings for evanescent-field sensors; (ii) thermal compensation and robust demodulation in interferometric schemes; (iii) range-specific calibration strategies for humidity-affected coatings; and (iv) material and coating choices aligned with the expected lifetime and cost-effectiveness of environmental monitoring systems [13,42,50].

Table 6. Intrinsic OFSs in Environmental Chemistry.

Architecture	Application	Fiber Type	Features	Ref.
Distributed sensor based on Raman scattering	Temperature measurement in high-temperature environments for environmental monitoring	Graded-index silica MMF with a germanium-doped silica core. Two variants: one with gold coating and another with polyimide coating	- System operating temperature range: −270 °C to 700 °C, depending on coating - Gold coating withstands up to 700 °C, polyimide up to 300 °C - Attenuation with gold: 14.8 dB/km at 850 nm, 13.4 dB/km at 1300 nm - Attenuation with polyimide: 2.58 dB/km at 850 nm, 0.73 dB/km at 1300 nm - Typical thermal resolution: <0.3 °C	[138]
MI	Detection of chemical compounds in liquids at low concentrations and reduced volumes	Silica SMF with a microcavity, forming two reflective arms within the fiber itself	- Minimum required volume: <50 nL - Concentration detection limit: <0.005% (v/v) - High spectral resolution due to the use of a ring cavity laser - Reusable and regenerable sensor	[95]
IFPI	pH measurement in aqueous solutions	Silica SMF with a sensitive film of titanium dioxide and palladium applied via sol-gel method	- pH range: 1.0 to 7.0 - Response time: ~7 s - Sensitivity: up to 30 $\mu\varepsilon$ at pH 1.0, and ~6 $\mu\varepsilon$ at pH 7.0 - Minimum detectable strain resolution: 64 nε - Operating temperature: ambient	[139]
Distributed sensor based on Rayleigh scattering	Monitoring of mooring lines in floating wind turbines	Plastic SMF with a polymethylmethacrylate resin core	- Total fiber length: up to 12 m - Damage event localization resolution: ~50 cm - Standard deviation <3.5% across 30 consecutive reliability tests - Compatible with large curvatures due to the mechanical properties of the POF	[140]

Table 7. Extrinsic OFSs in Environmental Chemistry.

Architecture	Application	Fiber Type	Features	Ref.
Sensor based on intensity modulation through evanescent interaction	Detection of ethanol at low concentrations, with application in environmental monitoring	Silica SMF coated with $Bi_2Fe_4O_9$ nanoparticles and biomass-derived biochar	- Concentration range: 0–250 ppm - Cost-effective and eco-friendly sensor due to the use of biomass-derived materials - Maximum sensitivity at 250 ppm of ethanol with a significant optical signal change - Operation in the visible range ~600 nm	[141]
Sensor based on intensity modulation via evanescent interaction	Detection of dimethyl sulfoxide in liquid solutions, relevant for environmental and water quality monitoring	Silica SMF with a central stripped section coated with a functional layer of polymer/MXene TiO_2	- Detection range: up to 10% v/v - Response time: 5 s; recovery time: 8 s - Estimated detection limit: <1% v/v - Potential for miniaturization and low cost	[142]
Sensor based on intensity modulation and spectral shift via localized surface plasmon resonance	Detection of changes in the refractive index of liquids, applicable in environmental monitoring and chemical analysis in solutions	Silica SMF with a region coated with a layer of gold nanostars	- Detection limit: changes of 0.001 in refractive index - Resonance peak tunable in the visible–NIR range (~730 nm) - High reproducibility and spectral stability - Evaluated in water/glycerol mixtures to test optical index response	[137]
EFPI	Detection of Pb^{2+} ions in aqueous solutions	Silica SMF with a coating of sodium alginate hydrogel ionically imprinted with Pb^{2+}	- Sensitivity: 1.78475 nm/(mg/L) in the range 0–2.5 mg/L - Evaluated temperature range: 12–42 °C with low thermal sensitivity (0.07223 nm/°C) - Selectivity: high against other ions (Cu^{2+}, Cr^{3+}, Mn^{2+}, Fe^{3+}, Zn^{2+}) - Linearity: 0.9	[143]
Sensor based on intensity modulation via evanescent interaction	Detection of a wide range of organic solvents and volatile chemical compounds	Combination of silica SMF and MMF	- Intensity changes of up to 40% in the presence of solvents such as acetone and methanol - Fast response time: ~10 s - Good repeatability: variation < 5% after multiple cycles	[144]
Sensor based on localized surface plasmon resonance	Detection of mercury ions (Hg^{2+}) in aqueous solution	Plastic MMF with tip treated by chemical etching and subsequent functionalization with gold nanoparticles and glutaric acid	- Detection limit (LOD): 0.03 µM of Hg^{2+} - Linear detection range: 0.03–1.0 µM - Maximum spectral response at ~530 nm - High selectivity against other metal ions - Response time: ~1 min - Portable, cost-effective, and low-power sensor	[145]
EFPI	pH detection in aqueous solutions	Silica SMF coated with a uniform layer of polyaniline	- Measured pH range: 4 to 10 - Sensitivity: up to ~145 pm/pH - High linearity ($R^2 > 0.995$) - Response time: 5 s - Good repeatability, variations under 2% - Detection limit: ~0.02 pH units	[146]

OFSs show a clear trend toward hybrid and nanocomposite designs that improve sensitivity, chemical selectivity, and robustness for pollutant detection. Intrinsic interferometric and scattering setups dominate where ultra-low detection limits are needed, while extrinsic architectures with plastic fibers and functional coatings offer modular and cost-effective solutions for large-scale monitoring. Despite ongoing challenges like humidity interference, surface fouling, and calibration stability, the literature shows steady progress toward reliable, field-ready systems. These advancements position OFSs as key enablers of next-generation environmental monitoring technologies aligned with sustainability and early-warning detection needs.

6.4. OFSs in Civil Engineering and Structural Analysis

In such fields, OFSs have played an important role in detecting strain, cracks, and displacement in infrastructures such as tunnels, bridges, concrete linings, and historical buildings, especially in intrinsic OFS employing backscattering architectures (Table 8) [18–20].

DOFSs, well-known for such capabilities as mapping data at high spatial resolution all the way along the fiber length, offer great applicability in early detection and measurement of concrete cracks and ground displacements. The applicability can be identified through the success of DOFS applications in submerged tunnels and in lab experiments using concrete cover coatings under loading [12,15,16,19,147]. The distributed nature of these devices allows analysis from micro-strain to local failure mechanisms at high resolution in millimeters, dependent on the installation process or the detection technology employed (Rayleigh, Brillouin, or Raman).

The use of extrinsic-type sensor usage is limited (Table 9), but some studies have explored the role of surface roughness in sensor output in structural monitoring applications [148].

Regarding fiber type, silica SMF is used because of its low fiber attenuation and compatibility with distributed scattering methods. Installation arrangements and corresponding coatings (polymeric or metal) vary according to the final application, with cables or fibers reinforced in concrete often used to effectively transfer strains from the structure to the sensor [15,148].

One of the main benefits of OFSs regards the fact that they can operate as distributed sensors. These characteristics make OFSs superior to traditional sensors such as electrical strain gauges, linear variable differential transformers, or vibrating wires, which offer data merely at discrete points and at high densities in order to detect local events [19]. The economic and operational issues related to the installation of thousands of conventional sensors in large-scale facilities make OFSs, especially DOFSs, highly competitive because they can offer data on large-scale structures through merely one fiber line [15].

Comparison studies using conventional sensors reveal that although inclinometers, extensometers, and accelerometers have long-established application history, these devices tend to cause service interruptions during installation, display low-level automation, and offer limited spatial resolution. Visual observation and 3D laser scanning offer complementary data, but these methods tend to be time-consuming and expensive, hence not suitable or practical in real-time and large-scale structural health monitoring. In comparison, DOFS devices using the Rayleigh, Brillouin, or Raman scattering principle can offer non-interruptive long-term stable measurement capabilities [15,19].

Despite these benefits, there are several challenges that exist in terms of cost, calibration, and lifespan. The upfront cost of interrogators and the installation cost of fiber cables is much higher than conventional sensing technologies; however, the cost per unit is reducing with increased usage. There are several challenges in the process of calibration due to the reliance of fiber-strain transfer characteristics on certain adhesives, coatings, and installation procedures, which affect the measurement signal when not treated effectively [15]. For service lifespan, silica SMF cables ensure robustness against environmental factors but require protective coatings or cables to counter adverse environmental influences such as water seepage or heavy loads in buried or underwater infrastructures [5,12].

In terms of maintenance and standardization, OFSs, unlike electronic sensors, require both interrogation devices and alignment procedures, which need trained staff. Further, there exist no global standards regarding OFS calibration and installation, thus hindering large-scale deployment in Structural Health Monitoring missions [15]. However, based on current literature assessments, the long-run advantages of OFS technology, including multiplexing, non-intrusiveness, and compatibility with smart infrastructures,

overcome current challenges in advancing them as alternatives in the state-of-the-art in monitoring technology [16,20].

In the area of structural monitoring, OFSs can offer an effective and scalable solution to overcome the spatial constraints and operational limitations of conventional sensors. They can offer real-time, distributed, and automated data acquisition; all these aspects are critical in advanced infrastructures where accurate and early damage assessment and maintenance are absolutely essential. In the future, there shall be scopes to make installation cost-effective, make calibration easier, and develop standard operational procedures to make them widespread in civil engineering as conventional monitoring tools [15,19].

In structural and civil engineering, the use of OFSs is solidifying around distributed and FBG-based systems, which allow for precise, continuous monitoring of large structures like bridges, tunnels, and dams. These systems offer vital data on strain, vibration, and thermal effects, aiding preventive maintenance and helping to extend the service life. Extrinsic configurations remain useful in situations where adaptability to complex shapes or localized measurements is necessary. Despite challenges related to installation costs, field calibration, and long-term durability under changing environmental conditions, the overall trend points toward a shift to integrated smart infrastructures where OFSs serve as key parts of structural health monitoring systems.

Table 8. Intrinsic OFSs in Civil Engineering and Structural Analysis.

Architecture	Application	Fiber Type	Features	Ref.
Distributed sensor based on Brillouin and Rayleigh scattering	Structural monitoring of strain in joints of submerged tunnels	Silica SMF	- Detected strain range: up to 4000 $\mu\varepsilon$ (microstrain) - Measurement resolution: 1.5 $\mu\varepsilon$ - Maximum covered length: up to 1 km per segment - Spatial accuracy: ~1 m	[147]
Distributed sensor based on Brillouin and Rayleigh scattering	Study of local failure mechanisms in hard rock tunnel linings	Silica SMF	- Detected strain range: up to 12,000 $\mu\varepsilon$ (microstrain) - Measurement resolution: 10 $\mu\varepsilon$ (Brillouin) and 1 $\mu\varepsilon$ (Rayleigh) - Spatial resolution: 10 cm (Rayleigh) and 50 cm (Brillouin) - Monitored length: up to 30 m	[149]
IFPI	Monitoring of structural displacements in heritage building elements	Silica SMF	- Measurement range: up to 10 mm of linear displacement - Resolution: 1–2 μm - Strain sensitivity: determined by Bragg wavelength shift (~1.2 pm/$\mu\varepsilon$) - Discrete installation, suitable for historical monuments	[150]
Distributed sensor based on Rayleigh scattering	Simultaneous monitoring of ground displacements and water pressure	Silica SMF mounted on a geotechnical tube with a deformable structure	- Displacement measurement range: up to 40 mm ($\pm$20 mm) - Displacement resolution: 0.5 mm - Hydraulic system accuracy: $\pm$2.5 kPa - Rayleigh sensor spatial resolution: 1.3 mm	[151]
Distributed sensor based on Rayleigh scattering	Real-time monitoring of fouling formation in tubular reactors	Silica SMF helically wound around the reactor	- Fouling detection range: detects deposits on the order of 0.1 mm - Spatial resolution: ~0.65 mm - Capability to identify specific fouling initiation zones - Measurement at 2-min intervals	[49]
Distributed sensor based on Raman scattering	Measurement of transient seepage flows and heat transfer in saturated soil	Silica MMF with acrylate coating	- Spatial resolution: 0.25 m - Temporal resolution: 15 s - Thermal accuracy: $\pm$0.1 °C - Total sensor length: 15 m (spirally wound over the area of interest)	[152]

Table 9. Extrinsic OFSs in Civil Engineering and Structural Analysis.

Architecture	Application	Fiber Type	Features	Ref.
Sensor based on surface plasmon resonance (SPR)	Experimental evaluation of the influence of surface roughness	Silica SMF with an aluminum film	- Modified fiber length: ~4 mm - Evaluation for surface roughness between 0.45 μm and 2.4 μm (Ra) - Spectral range: 400–900 nm - Maximum sensitivity: peak shifts > 20 nm with changes in the refractive index of the medium	[153]

6.5. OFSs in Aerospace Engineering

In the field of aerospace technology and aerial vehicles, OFSs are widely used for evaluating integrity during flight and detecting high-precision dynamic events. In addition, because they are lightweight, multiplexable, and stable in extreme environments, they can easily be incorporated for use in aircraft, space construction, and high-pressure environments [11,154,155].

In this area, the main type of sensor used is intrinsic (Tables 10 and 11), and FBG, MZI, and the distributed sensor layout are the most popular ones in use. FBG stands out because

of its ability to detect strain, temperatures, and impacts in composite aircraft components such as aircraft fuselage panels, wings, and other important aircraft components [11,155]. New designs in these sensing components involve the use of erbium-doped fibers to increase the thermal detectivity and spectral purity [156]. Also included in the use of these devices in aircraft structures are sensors treated with deep-learning algorithms to detect parameters through pattern detection [157,158].

In terms of fiber type, there are mainly single-mode silica optical fibers with some doped with gallium or erbium elements to increase spectral transmission, although coated fiber designs have been tested in high-temperature environments (up to 1000 °C) or when exposed to radiation or corrosion as in space-based applications [11,93,154,155].

It has emerged from the literature that FBGs are widely utilized in space-related applications because of their compact size, capability of wavelength-encoded data retrieval, and multiplexing capacity to measure several locations through one fiber. FBGs have already experienced rigorous verification in monitoring strain and temperature in the fuselage skin of aircraft manufactured using composites, solar panels in satellites, and cryogenic fuel components, where the effectiveness of distributed sensing surpasses discrete data obtained from conventional strain gauges or piezoelectric sensors [47,159]. In space missions, FBGs have found application in thermal protection designs in order to detect shock loads and aerodynamic heating experienced in re-entry missions [11,159].

One of the newer applications where OFS can make a significant difference would be in the health monitoring of satellites and space stations. OFS can ensure long-lasting reliability and spatiotemporal distribution at large geographical scales in such applications when compared to conventional electrical strain gauges, facing challenges related to wiring complexity, EMI immunity, and relatively less lifespan of up to five years in space [11,46].

Space exploration missions have much stricter requirements. Lunar and Martian missions require radiation-hardened and vacuum-compatible sensors that can operate in extreme thermal variations. More recent literature highlights the need for radiation-hardened optical fibers and sapphire grating sensors that can operate in ionized radiation environments and above 1000 °C temperatures, beyond which conventional electronic sensors degrade [45]. Space exploration missions using these optical fibers extend the mission lifetime, although it has remained rather costly so far.

Although OFSs offer many benefits, they face some commercial and practical issues. One important factor in the commercial challenges they face is the expense of interrogation units and fiber coatings. These costs contribute significantly to the overall cost associated with OFSs as opposed to conventional sensors [155]. It is further important to note that in-flight OFS recalibration can face challenges such as thermo-mechanical loads, adhesive degradation, and fiber coating fatigue; therefore, experts recommend using redundant fiber topologies, defining in-orbit OFS recalibration strategies, and using OFS deformation analysis algorithms [11,48].

OFSs have highly advantageous capabilities in space exploration technology, ranging from satellite technology to planetary exploration. Their uses go beyond the measurement of strain and temperatures to real-time measurements of vibration, radiation, and deformation. Although the issues concerning cost, calibration, and repairability keep emerging, the latest developments in radiation-hardened fiber, advanced coatings, and multi-functional composites ensure that OFSs will feature prominently in future space crafts and exploratory missions [44,160].

Within aerospace applications, OFSs are increasingly recognized as essential tools for monitoring critical parameters such as strain, vibration, and temperature in aircraft and spacecraft structures. Lightweight and multiplexed FBG networks, along with interferometric and distributed sensing systems, provide reliable performance under the demanding

conditions of high altitudes and propulsion systems. The use of specialized coatings and advanced fibers addresses issues of radiation exposure and thermal stress, though cost and integration into existing aerospace platforms remain significant challenges. Current trends indicate a gradual shift toward embedding OFSs in next-generation aerospace designs, where they will play a key role in ensuring structural safety, optimizing performance, and enabling autonomous health-monitoring capabilities.

Table 10. Intrinsic OFSs in Aerospace Engineering.

Architecture	Application	Fiber Type	Features	Ref.
FBG	Structural monitoring in aircraft, specifically for detection of barely visible impact damage	Silica SMF encapsulated in glass fiber reinforced polymer	- Temperature range: −50 °C to +80 °C - Flight compatibility tests: pressure up to 47,000 ft, relative humidity > 90%, exposure to fluids, vibrations, and fatigue - Temperature sensitivity: 10.2 ± 1.7 pm/°C	[161]
IFPI	Distributed monitoring of high temperatures in aerospace structures within confined spaces	Silica SMF internally modified by laser ablation to form microcavities	- Temperature range: 25 °C to 1000 °C - Spatial resolution: 1 mm - Measurement accuracy: ±0.5 °C - Minimal thermal drift: <0.2 pm/°C at 1000 °C - Response time: <2 s for thermal changes	[162]
FBG sensor network and distributed sensors	Distributed thermal monitoring in simulated space environment testing	- Silica SMF for FBG sensors—Silica MMF for distributed sensors	- Simultaneous monitoring of >100 thermal measurement points - Temperature range: −150 °C to +200 °C - Spatial resolution: up to 0.5 m (DTS) and point-based (FBG) - Thermal resolution: <0.2 °C (FBG) - Validated in thermal vacuum chambers under simulated space conditions	[163]
MZI	Temperature measurement	Erbium-doped silica SMF	- Sensitivity: 571 pm/°C - Temperature range: 5–55 °C - Signal-to-noise ratio (SNR): 50 dB - 3 dB bandwidth: <0.12 nm - High linearity ($R^2 \approx 0.999$)	[156]
FBG	Measurement of mechanical strain on surfaces of aerospace structures	Silica SMF with aerospace-grade encapsulation	- Strain sensitivity: ~1.2 pm/ $\mu\varepsilon$ - Strain range: up to 5000 $\mu\varepsilon$ - Temperature range: −55 °C to 120 °C - Flight-validated: Airbus A350 aircraft - Measured accuracy: ±10 $\mu\varepsilon$	[164]
Specklegram-based interferometer sensor	Fiber curvature detection	Silica MMF with fluorine-doped cladding, gallium-doped core, and boron coating	- Curvature range: 0.96 to 4.30 m^{-1} - Classification accuracy: 100% in stable environments and 98.3% in disturbed environments - Optical signal processing using a convolutional neural network	[157]
Distributed sensor based on optical vector network analysis	Distributed measurement of structural vibrations	Silica SMF	- Vibration frequency range: 10 Hz–40 kHz - Spatial resolution: 1 m - Simultaneous detection of amplitude and phase	[165]
FBG	Detection of temperature, strain, and pressure	Silica SMF	- Temperature range: up to >1000 °C - Long-term thermal resistance: >300 h at 900 °C for type II-IR FBG - Radiation immunity (type II-IR FBG) - Sensitivity: ~10 pm/°C, ~1.2 pm/ $\mu\varepsilon$	[166]
MZI	Temperature measurement in extreme environments	Erbium-doped silica SMF	- Temperature range: 20–80 °C - Sensitivity: 1.27 nm/°C - Laser SNR: >45 dB - Spectral linewidth: ~0.02 nm - High linearity: $R^2 > 0.998$	[167]
FBG	Monitoring of temperature and strain in extreme environments	Silica SMF	- Supported operating temperature: up to 600 °C - Thermal strain accuracy: ±10 $\mu\varepsilon$ - Excellent mechanical and thermal stability after 200 thermal cycles	[168]

Table 11. Extrinsic OFSs in Aerospace Engineering.

Architecture	Application	Fiber Type	Features	Ref.
Sensor based on angular displacement detection between two separated fibers	Angular displacement measurement	Plastic MMF	- Measured angular range: up to 12° - Maximum sensitivity: 5.38 mV/° - Maximum model prediction error: <1% - Sensitivity can be adjusted by varying the separation and size of the receiver	[169]

7. Optical Fiber Sensing Cross-Family Comparative Analysis

The discussion in the previous sections has critically addressed the deployment of different OFS architectures in the main field categories of industry, environmental chemistry, medicine/biomedical applications, structural/civil engineering, and aeronautical/aerospace engineering, with a comparison designed according to applications per discipline, with a view to the specific constraints of each field applying those specific technologies in specific applications of optical fiber sensing. This new section will present a comparison across families.

A comparison shows that FBG sensors have a moderate but very stable sensitivity, such as 1.2 pm/με for strains and 10–11 pm/°C for temperature measurements, functioning within 300 °C and showing high multiplex capabilities with wavelength division methods. This makes FBG sensors particularly favorable within rugged environments

such as aeronautical composite materials monitoring and medical purposes with regard to the importance of cartridge reproducibility and exact calibration. Interferometric sensors, including FPI, MZI, and MI, show significantly better sensitivities, often ranging above tens of pm/°C, with even nanoscale capabilities in terms of refractive wavelength changes per received stimulus (for instance, 60–109 pm/°C with increased temperature for MI sensors and about 2.48 nm/g for aeration sensitivity within an FPI). Yet, these improvements come with refined temperature drift, resonator length errors, and enhanced complexity in calibrations.

Capabilities regarding multiplexing and spatial resolution vary further within the sensing families. FBGs can handle dense quasi-distribution configurations (up to 120 FBGs on four fibers, or seven arrays and five FBGs), in comparison to single-point interferometric probes with restricted multiplexing possibilities only. Conversely, extreme examples related to DOFS technologies, such as Rayleigh, Raman, and Brillouin techniques, capable of full spatially distributed measurements with a resolution of a few millimeters (for instance, ~1 mm resolution with an FPI-based distributed temperature sensor, and 2.6–5 mm resolution with a Rayleigh-based system), up to tens of meters to tens of kilometers' range.

Requirements concerning calibration and compensation may vary greatly among different sets of sensors. For instance, interferometric sensors often include temperature drift correction, cavity length control, and phase tracking, whereas FBGs only involve established methods for decoupling the effects of strain and temperature. DOFS techniques involve calibration models for Stokes and anti-Stokes components and often use reference temperature measurements, two-way measurements, or both for accuracy. It is apparent that complexity increases with increased sensitivity and complexity of the sensors. Collectively, the performance characteristics described in Table 12 above show a specific strength set for each family of architectures, including FBGs, which can produce robust, multiplexed, and repeatable measurements; interferometric sensors, which can be very sensitive but vulnerable to environmental effects; and distributed scattering-based methods, which can offer an unparalleled level of spatial mapping for structural, temperature, and environmental characterization measurements. It is clear that a synthesis among the families emphasizes the importance of considering a series of tradeoffs when choosing an optimal OFS architecture solution.

Table 12. Cross-Family Comparative Summary of OFS Technologies.

Sensor Type	Primary Measurands	Typical Sensitivity/Resolution	Spatial/Temporal Resolution	Multiplexing Capability	Robustness (Temp/EMI/Moisture)	Calibration/Compensation Needs	TRL	Dominant Use Cases	Interrogator Type & Cost Class	Ref
FBG	Strain Measurement	Strain sensitivity ~1.2 pm/$\mu\varepsilon$ and temperature sensitivity ~10–11 pm/°C.	Point sensing; interrogator provides quasi-static to low-Hz dynamic readings; no temporal rate reported	High; multiple FBGs via wavelength-division multiplexing	Withstands ~300 °C; stable when embedded in composite.	Strain–temperature compensation and depolarized interrogation to avoid birefringence effects.	7–8 (validated in composite structural testing)	Strain monitoring in carbon-fiber structures for aerospace and automotive SHM	Depolarized tunable-laser interrogator; medium–high cost	[122]
FBG	Optical transmittance of EC	No quantitative sensitivity values are reported	Point sensing; EC transmittance evolves over multi-minute switching cycles	None; single sensing element	Sensitive to alignment and ambient light	Needs reference LED intensity normalization	5–6 (early-stage industrial proof-of-concept)	In-situ transmittance control in electrochromic smart windows	Simple LED + photodetector; low cost	[110]
FBG	Residual strain (barely visible impact damage)	~10.2 ± 1.7 pm/°C (T); induced wavelength shifts up to ~380 pm	Point sensors spaced 27 mm apart; 2 Hz acquisition during calibration	High; 120 FBGs on 4 fibers	Aerospace-grade; −50 to +80 °C qualified	Cubic T-calibration; threshold $\tau \approx 8$ pm	8–9 (flight-compatible installation)	Impact damage detection & localization in aircraft	FBG interrogator; medium–high cost	[161]
FBG	Temperature measurement	Resolution of 0.1 °C, with thermal sensitivity of 6.5×10^{-6}·°C^{-1}	Thirty-five FBG points with 1 mm spacing; acquisition at 1 Hz	High; 7 arrays × 5 FBGs	Biocompatible	Thermal calibration; strain-free configuration	5–6 (biomedical lab validation)	Thermal monitoring in laser ablation	FBG interrogator; medium–high cost	[127]
FBG	Acceleration & vibration frequency	Strain sensitivity −2.57/−1.6 pm/$\mu\varepsilon$ and acceleration sensitivity up to 38.79/31.43 mV/g	Point sensing with 18 mm suspended length; vibration detection across 100–10,000 Hz	None; single sensing element	Stable structure for general applications	Mode-dependent (TE/TM) spectral calibration	5–6 (advanced lab prototype)	Broadband vibration & acceleration sensing	Broadband Light Source + Optical Tunable Filter + Photodetector; high cost	[114]
FPI	Vibration (acceleration)	Acceleration sensitivity ≈2.48 nm/g at 200 Hz; phase sensitivity 0.04–0.057 rad/g	Point sensor with 500 kHz demodulation speed; operational over 100–2000 Hz vibration range	None; single interferometric sensor	Operates up to 400 °C	Temperature drift & cross-sensitivity compensation	6–7 (advanced Micro-electro-mechanical prototype)	High-temp vibration monitoring (engines/turbines)	Amplified Spontaneous Emission + dual-wavelength demodulation; medium cost	[112]
FPI	Refractive index of biological tissue	Concept-level interferometric sensing; no quantitative sensitivity reported	Point interferometric probe; real-time monitoring concept; no temporal rate reported	None; single interferometric sensor	Diamond coating increases protection and stability	Calibration of phase change relative to refractive-index variations and stabilization of cavity length	1–2 (Technology readiness at concept stage)	Real-time monitoring of tissue response during radiotherapy	Broadband light source and OSA-based; medium cost	[126]
FPI	Distributed temperature along the fiber	Sensitivity of 1.40–2.29 GHz/°C (≈11–18 pm/°C) from 25–1000 °C	Distributed sensing with 1 mm spatial resolution; sweep speed; no temporal rate reported	Very high; more than 15,000 cavities on one fiber	Stable up to 1000 °C	Temperature calibration at different cavity lengths	6–7 (advanced laboratory system with harsh-environment readiness)	Distributed high-temperature monitoring in aerospace, nuclear and industrial furnaces	Optical frequency domain reflectometry interrogator with tunable laser; high cost	[162]
FPI	pH detection of aqueous solutions	Sensitivity of −1.228 μm/pH with wavelength-drift of −0.287 nm/pH across pH 2–12	Point F-P cavity (~270 μm) with single-spot measurement; spectra recorded after stabilization for each pH level	None; single interferometric sensor	Stable at low temperatures	Temperature compensation using an integrated fiber Bragg grating unit	4–5 (laboratory prototype)	Wide-range pH monitoring for chemical and biological fluids	Fiber grating demodulator; medium cost	[146]
MZI	Acetone concentration in gaseous samples	Sensitivity up to 0.0147 ppm^{-1} with a detection limit of 1.5 ppm	Point MZI sensor; spectra acquired once per minute over 10-min cycles	None; single interferometric sensor	Operates at room temperature; compact and portable	Calibration using the full measured spectrum through principal component regression	4–5 (laboratory prototype with analytical validation)	Non-invasive breath analysis for diabetes diagnosis	Super luminescent diode and optical spectrum analyzer; medium cost	[124]
MZI	Acetone concentration in gaseous samples	Sensitivity ~2.6–2.8 × 10^{-3} ppm^{-1} with limits of detection down to 1.7 ppm	Point sensor spaced 1 cm; spectra acquired once per minute over 10-min cycles	None; single interferometric sensor	Operates at room temperature	Calibration using full-spectrum regression through latent structures	4–5 (laboratory prototype with analytical validation)	Non-invasive breath analysis for diabetes diagnosis	Super luminescent laser diode and optical spectrum analyzer; medium cost	[89]
MZI	Temperature measurement	Temperature sensitivity of 571 pm/°C (5–55 °C) with wavelength stability of ~0.1 nm over 2.5 h	Point sensor cavity; laser response governed by ~0.12 nm 3-dB line; no temporal rate reported	None; single interferometric sensor	Stable up to 55 °C; good mechanical strength	Calibration of wavelength drift due to thermo-optic and thermal-expansion effects	5–6 (validated laboratory prototype with practical potential)	Remote temperature monitoring and seawater-temperature calibration	Fiber ring laser cavity with optical spectrum analyzer; medium cost	[156]
MZI	Temperature and refractive index	Temperature sensitivity ≈157–158 pm/°C (−5 to 65 °C) and refractive index sensitivity −19.55 to −24.52 nm/RIU	Point sensor; wavelength stability tested over 60 min with 0.32 nm drift and 1.1 dB power fluctuation	None; single interferometric sensor	Stable laser output for general applications	Calibration of wavelength drift due to thermo-optic and thermal-expansion effects	5–6 (validated laboratory prototype)	High-accuracy temperature and refractive-index monitoring	Fiber ring laser cavity with optical spectrum analyzer; medium cost	[167]

Table 12. *Cont.*

Sensor Type	Primary Measurands	Typical Sensitivity/Resolution	Spatial/Temporal Resolution	Multiplexing Capability	Robustness (Temp/EMI/Moisture)	Calibration/Compensation Needs	TRL	Dominant Use Cases	Interrogator Type & Cost Class	Ref
MI	High-temperature (100–900 °C)	60–80 pm/°C (100–450 °C) and 101–109 pm/°C (450–900 °C)	Point probe 3–8 mm; spectra recorded every 30 min	None; single interferometric sensor	Stable up to 900 °C	Two-slope linear calibration	6–7 (lab prototype with industrial potential)	High-temperature monitoring in industry	Broadband source + OSA; medium cost	[91]
MI	Refractive index and chemical concentration	1039.77 nm per refractive-index unit; 0.288 nm per mg/mL for vitamin C	Point sensor; detection response follows rapid refractive-index changes; no temporal rate reported	None; single interferometric sensor	Stable for microfluidic operation	Calibration of refractive-index changes and cavity-length stability	5–6 (advanced laboratory prototype with biochemical validation)	Low-volume biochemical analysis, vitamin C quantification, DNA hybridization detection	Fiber ring laser cavity with optical spectrum analyzer; medium cost	[95]
MI	Temperature and transverse load	Temperature sensitivity up to 85.1 pm/°C (30–80 °C) and transverse-load sensitivity up to −3.15 nm/N (0–1.96 N)	Point sensing; spectra captured at each temperature and load step using an optical spectrum analyzer; no temporal rate reported	High; two interferometers connected in parallel	Compact and mechanically stable	Calibration of the Vernier envelope and correction of temperature drift	5–6 (laboratory prototype with practical potential)	High-sensitivity temperature and load monitoring in compact environments	Broadband light source and optical spectrum analyzer; medium cost	[92]
MI	Temperature measurement	−164 pm/°C (25–60 °C range)	Point sensor with ~500–1000 µm cavity lengths; no temporal rate reported	None; single interferometric sensor	Stable operation; compact and low cost for general applications	Linear temperature calibration for the polymer-filled cavity	5–6 (laboratory prototype with stable performance)	Temperature monitoring in power systems, structural health monitoring, and biomedical sensing	Broadband light source with optical spectrum analyzer; low to medium cost	[96]
Sagnac (Sagnac + FPI)	Sound pressure and acoustic frequency	Acoustic sensitivity up to 37.1 nm/Pa with resolution of 0.0089–0.037 Pa depending on amplification factor	Single-point FPI–Sagnac sensor; spectra scanned at 64 nm/s with 0.1 nm resolution; no temporal rate reported	None; single sensing cavity	Stable composite-film diaphragm	Cavity-length tuning for sensitivity control and spectral linearization	5–6 (laboratory prototype with performance validation)	High-sensitivity acoustic detection and sound-pressure in general applications	Broadband light source with optical spectrum analyzer; medium cost	[82]
DOFS Rayleigh	Temperature measurement in Li-ion batteries	1.55 GHz/°C with measurement accuracy of ±0.2 °C at 3 mm resolution	3 mm resolution and ~1300 measurement points; no temporal rate reported	Fully distributed sensing along 5 m fiber; ~1300 sensing points	Operates within battery thermal chamber	Temperature calibration due to PTFE encapsulation	7–8 (validated on commercial Li-ion 21,700 cells)	Thermal mapping of Li-ion batteries and battery thermal management	Optical frequency domain reflectometry interrogator with tunable laser; high cost	[121]
DOFS Rayleigh	Magnetic-field measurement	22.85 MHz/mT with a linear range from 3 to 245 mT	20 cm spatial resolution; no temporal rate reported	Fully distributed sensing with 20 cm spatial resolution	Suitable for harsh environments	Strain–temperature decoupling and frequency-shift calibration	5–6 (laboratory prototype with validated performance)	Distributed magnetic-field mapping in harsh environments	Optical time domain reflectometry interrogator with tunable laser; high cost	[115]
DOFS Rayleigh	Strain and optical attenuation	Withstand up to ~70% strain; length-change resolution is ~±7 cm over 10–100 m	Spatial resolution of ~14 cm per sample step; pulses repeated up to 500 kHz	Fully distributed sensing along 100 m plastic optical fiber	Resistant to tension, torsion and prolonged water immersion	Calibration for water absorption effects and attenuation drift	6–7 (validated for offshore mooring-line monitoring)	Structural monitoring of floating wind turbine mooring lines	Optical time domain reflectometry interrogator with pulsed laser and photodetectors; low to medium cost	[140]
DOFS Rayleigh	Horizontal-vertical ground displacement, and pore water pressure	Pressure sensitivity 0.1019 $\mu\varepsilon$/kPa with detection down to 3.62 kPa; displacement resolution 0.2 mm	5 mm spatial sampling; no temporal rate reported	Fully distributed sensing along continuous optical fiber	Suitable for soil, water, and underground environments	Strain–temperature decoupling using reference fiber	6–7 (validated in laboratory and field conditions)	Ground failure monitoring, early warning of landslides, and geotechnical safety	Optical backscatter reflectometer interrogator; high cost	[151]
DOFS Rayleigh	Localized temperature disturbances caused by fouling formation	Temperature resolution ~0.1 °C with ±0.5 °C noise; fouling-induced changes detectable from ~0.8 °C.	2.6 mm spatial resolution; no temporal rate reported	Fully distributed sensing with 2.6 mm spatial resolution	Coating susceptible to chemical and moisture degradation	Calibration for strain–temperature coupling and reactor-specific conditions	6–7 (validated in industrial continuous polymerization reactors)	Real-time tracking of fouling buildup in tubular continuous polymerization reactors	Optical backscatter reflectometer interrogator; high cost	[49]
DOFS Brillouin	Strain measurement in shotcrete tunnel linings	Resolution of ≈1 $\mu\varepsilon$ with reliable detection of localized cracking patterns	5.2 mm spatial resolution and 6.25 Hz sampling	Four distributed fiber channels	Embedded in concrete for harsh tunnel environments	Requires strain–temperature separation; reference cables recommended	6–7 (validated in full-scale laboratory tunnel-lining experiments)	Detection of failure mechanisms in tunnel linings	Optical frequency domain reflectometry interrogator; high cost	[149]
DOFS Brillouin	Strain measurement in immersed tunnels	~0.1 mm accuracy and strain resolution of ~2 $\mu\varepsilon$ from interrogator	0.2–0.5 m spatial resolution depending on fiber length; no temporal rate reported	Fully distributed sensing along continuous fiber with multiple sensor blocks	Protected by steel cover plates inside tunnel	Requires strain–temperature decoupling using adjacent reference fiber segments	7–8 (validated in full-scale laboratory tests and in operational tunnel)	Monitoring joint opening, settlement, and structural safety in immersed tunnels	Brillouin Optical Frequency Domain Analysis interrogator; high cost	[147]

Table 12. *Cont.*

Sensor Type	Primary Measurands	Typical Sensitivity/Resolution	Spatial/Temporal Resolution	Multiplexing Capability	Robustness (Temp/EMI/Moisture)	Calibration/Compensation Needs	TRL	Dominant Use Cases	Interrogator Type & Cost Class	Ref
DOFS Brillouin	Strain and temperature measurement	Strain resolution ~7 $\mu\varepsilon$ and temperature coefficient 1.07 MHz/°C with rail temperature differences up to 12.1 °C detected	50 cm spatial resolution and 60 s of measurement time per scan	Fully distributed sensing along 300 m fiber	Rail-mounted fiber protected under aluminium tape	Requires strain–temperature separation using a reference track	7–8 (validated on operating railway line)	Rail strain monitoring and thermal profiling	Brillouin Optical Frequency Domain Analysis interrogator; high cost	[102]
DOFS Raman	Temperature measurement	Resolution < 0.6 °C at 15 km and typically ~0.3 °C, with accuracy < ±1 °C up to 600 °C	1–5 m spatial resolution (0.5 m sampling); integration time set to 5 s per measurement	Fully distributed sensing along 5–15 km fiber	Gold-coated fiber withstands up to 700 °C	Stokes/anti-Stokes calibration and double-ended configuration for attenuation compensation	7–8 (validated on real loop heater operating at 200–680 °C)	Temperature monitoring in liquid-metal reactors, thermal energy storage, and hydrogen production systems	Raman distributed temperature sensor interrogator (TS-3000); high cost	[138]
DOFS Raman	Temperature measurement for seepage front tracking	Resolution ~0.1–0.2 °C using coil enhancement; reference loggers show ±0.4 °C accuracy	0.63 m spatial resolution and 30 s acquisition time	Fully distributed sensing along 130 m fiber	Stable in saturated and unsaturated sand	Requires Stokes/anti-Stokes calibration and reference thermometers	4–5 (laboratory hydrothermal soil model with validated simulations)	Phreatic-line tracking and hydrothermal behavior analysis in embankments	Raman distributed temperature sensor interrogator (SILIXA XT-DTS); high cost	[152]

8. Recent Trends in OFSs

Figure 15 summarizes the distribution of intrinsic and extrinsic OFS applications based on the literature reviewed from 2019 to 2025. The dataset was compiled by manually examining the selected publications and classifying each study according to the type of sensor documented (intrinsic or extrinsic) and the application area indicated by the authors. This manual count was then organized to produce the final plot.

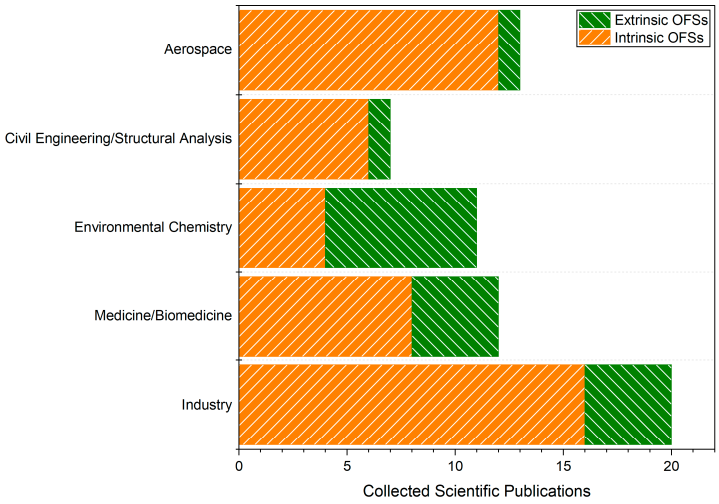

Figure 15. Distribution of collected scientific publications (2019–2025) categorized by application domain, comparing the prevalence of intrinsic and extrinsic OFS implementations across the defined sectors.

The resulting distribution reveals a strong predominance of intrinsic OFSs in sectors such as aerospace, structural analysis, and industry, where these architectures represent approximately 90%, 86%, and 80% of the reviewed publications, respectively. This aligns with the widespread adoption of intrinsic configurations, particularly FBGs and interferometric sensors, in environments demanding high sensitivity and robust performance. Conversely, extrinsic OFSs show a distinct application pattern, with greater representation in environmental chemistry (around 67%), followed by medicine/biomedicine (33%) and industry (20%). These trends reflect the suitability of extrinsic architectures for scenarios requiring direct interaction with external media, functional coatings, or tailored sensing geometries, as commonly found in gas detection, contaminant monitoring, and biomedical interfaces.

In terms of temporal analysis, Figure 16 presents the temporal evolution of intrinsic and extrinsic OFS publications from 2019 to 2025. The dataset was derived from the same set of studies examined before, in which each publication was manually classified according to the type of sensor reported and the year in which the work appeared. This count was then organized to produce the plotted annual distribution.

The results reveal a clear upward trend in intrinsic OFS publications beginning in 2021, reflecting their sustained adoption in structurally demanding and technologically mature applications. This progression is consistent with the increased visibility of FBG- and interferometer-based sensing in structural health monitoring, aerospace components, and biomedical instrumentation. In contrast, extrinsic OFSs show a more recent rise, with their most notable growth occurring toward 2024–2025. This expansion aligns with the emergence of new functional materials, surface-interaction mechanisms, and interdisciplinary applications where direct contact with external media is advantageous. Together, these trends indicate a gradual diversification in the field, with intrinsic OFSs continuing to dominate established engineering sectors while extrinsic OFSs increasingly gain relevance in emerging application domains.

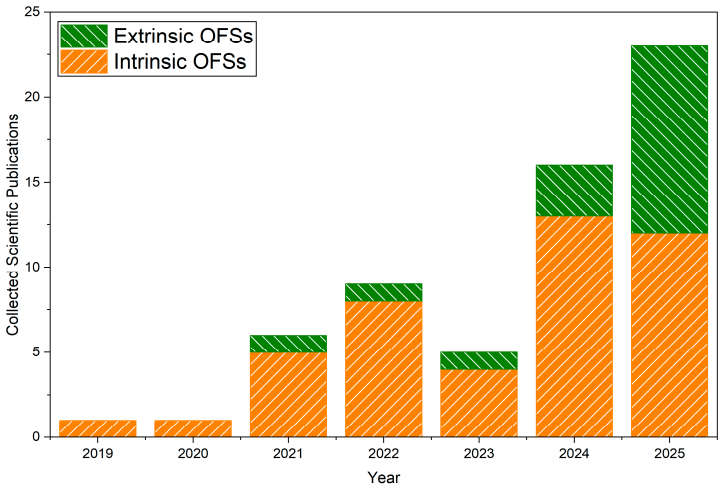

Figure 16. Yearly distribution of collected scientific publications on intrinsic and extrinsic OFSs for the 2019–2025 period, illustrating the progressive increase in research activity for each OFS modality over time.

A comparison of the evolution in publication numbers by year and discipline shows that the industrial sector has remained a dominant and consistent presence throughout the entire study period (Figure 17). The information for this figure was derived from the same body of literature examined throughout this section, where each publication from 2019 to 2025 was manually reviewed and categorized according to its reported application area. The resulting annual counts for each discipline were then organized to construct the temporal evolution shown in the plot.

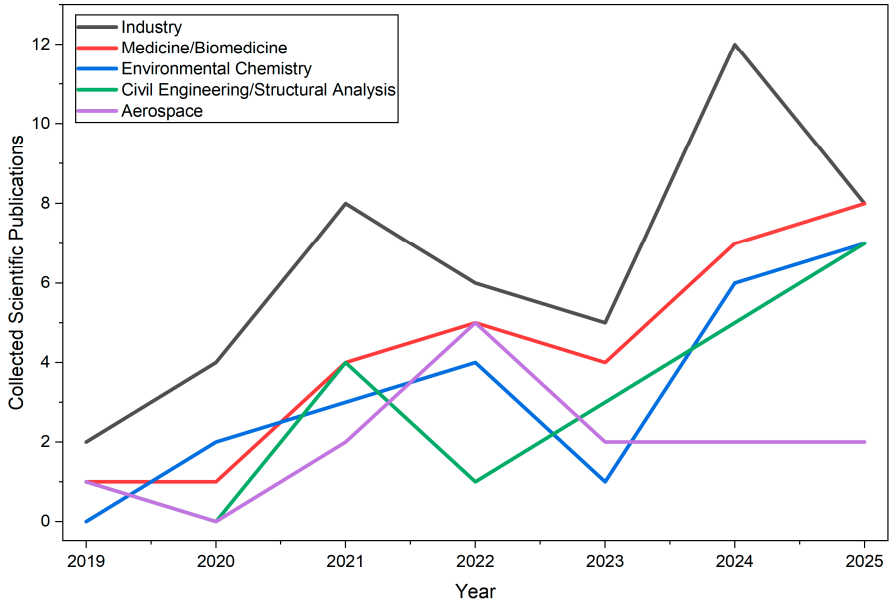

Figure 17. Yearly distribution of collected scientific publications on OFSs across defined application disciplines for the 2019–2025 period, highlighting the progressive increase in research activity and the differing growth patterns among industry, medicine/biomedicine, environmental chemistry, civil engineering/structural analysis, and aerospace.

Across the period examined, the industrial sector appears as the most consistently represented area, reinforcing its role as a principal driver in the development and implementation of OFSs, particularly for process monitoring and equipment diagnostics. The medical and biomedical field shows a steady upward trajectory beginning in 2021, reflecting a growing adoption of optical solutions for diagnostics, physiological monitoring,

and treatment supervision. Environmental chemistry also exhibits a marked rise in the last three years, coinciding with increasing interest in clean, selective, and non-invasive detection tools for pollutants and environmental indicators. Meanwhile, civil engineering and aerospace applications remain actively present, with civil engineering contributing to structural health monitoring initiatives and aerospace continuing to advance embedded sensing solutions for aircraft and spacecraft systems.

Extrinsic sensors are expected to continue gaining prominence in fields such as environmental chemistry and biomedicine, where integration with advanced materials, modular design, and functional customization are key features. Meanwhile, intrinsic sensors will likely remain dominant in areas like structural monitoring, industry, and aerospace. Additionally, some studies suggest a potential convergence of both sensor types, enabling the development of multiparametric applications within more intelligent, autonomous, and compatible frameworks involving emerging technologies.

In the context of emerging research trends, one of the most significant developments in OFSs is their integration with artificial intelligence (AI), machine learning (ML), and Internet of Things (IoT) technologies. As illustrated in Figure 18, the rise in publications addressing these combined approaches reflects a rapidly expanding research front. To obtain the publication counts shown in the plot, the same bibliographic procedure used for earlier figures was applied: the Web of Science search engine was queried under the "All Databases" option using the keyword string "optical fiber sensors applications [discipline]," replacing *discipline* with *machine learning* and *IoT*. Each search was performed under the "All Collections" setting and within the "Topic" field. The annual records retrieved from these searches were exported as Excel files and compiled to produce the final temporal distribution.

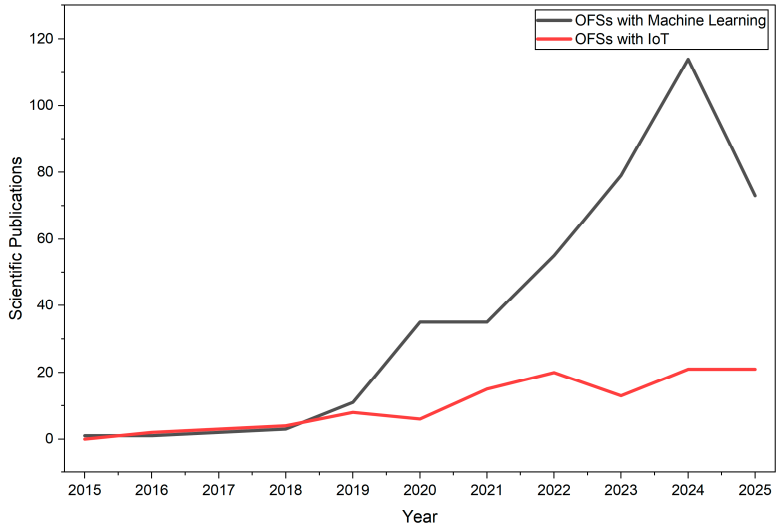

Figure 18. Yearly distribution of scientific publications indexed in the Web of Science database on OFSs incorporating ML and IoT technologies for the 2015–2025 period, illustrating the increasing research activity and the differing growth trajectories of both integration trends.

The resulting trend shows a sharp growth in publications beginning in 2018, reaching a peak in 2024. This trajectory reflects the increasing adoption of ML techniques to enhance optical signal interpretation, improve accuracy, accelerate processing, and enable predictive modeling even under noisy or incomplete measurement conditions [170–173]. Likewise, IoT-based OFS implementations continue to expand, driven by the need for interconnected, autonomous, and remotely accessible sensing platforms in industrial, environmental, and biomedical scenarios.

For example, methods like deep neural networks, support vector machines or linear regression (Figure 19) have been successfully used in distributed OFSs systems to enhance spatial resolution, reduce cross-sensitivity between temperature and strain, and cut measurement times without adding hardware complexity [174–177]. This collaboration between AI and OFSs not only boosts the performance of traditional sensors but also enables the development of intelligent distributed architectures capable of real-time multiparametric monitoring. Notable examples include the use of generative adversarial networks (GANs) for biomedical data restoration, support for obtaining signals for the development of ML models for medical assistance such as heart attacks, LSTM models for analyzing soft actuators, and regression techniques for multivariate estimations under complex environmental conditions [170,178–180].

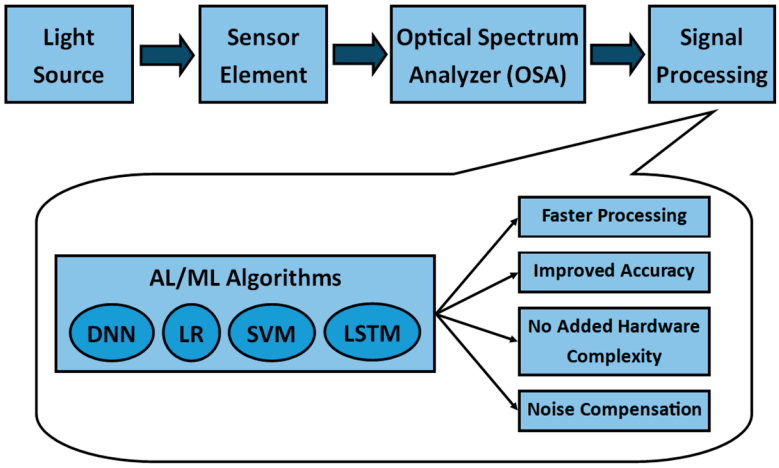

Figure 19. Integration of AI and ML algorithms into the signal-processing stage of an OFS system, illustrating how models such as DNN, LR, SVM, and LSTM enhance performance by enabling faster processing, improved accuracy, noise compensation, and no added hardware complexity.

On the same path, AI/ML techniques are enhancing OFSs in two distinct yet complementary ways: by introducing incremental improvements and by enabling transformative capabilities.

Incremental improvements primarily enhance the precision, speed, and reliability of existing sensing operations. For example, ML signal processing techniques, such as principal component analysis (PCA) and deep-learning-based denoising models, have been used to improve noise robustness and enhance the SNR in OFSs, resulting in higher measurement reliability without altering the sensor's primary function [172]. Similarly, ML algorithms like regression models and artificial neural networks (ANN) calibrate sensor outputs, linearize non-linear responses, and increase resolution, contributing to higher accuracy in strain or temperature sensing tasks [171]. Moreover, automated data processing through real-time ML pipelines allows for more rapid analysis of the massive datasets produced by distributed fiber systems, replacing slower manual or hardware-intensive methods. Improvements, though impactful, do not change the fundamental sensing mechanism but rather refine its performance [181].

In contrast, transformative improvements of AI/ML enable OFSs to perform tasks that were previously impractical. A notable example is the use of ML to resolve cross-sensitivity problems, such as distinguishing temperature from strain in a single Fiber Bragg Grating (FBG). Classical demodulation approaches cannot fully separate these effects without additional hardware, but ML models can decouple both influences, effectively transforming one sensor into a multiparameter device [182]. Likewise, AI allows OFSs to interpret complex patterns and classify events through distributed acoustic sensing

(DAS), where ML models can identify acoustic event categories, such as footsteps, vehicle motion, or leaks, based on the backscattered signals [183]. The same transformation occurs in fiber-based wearable systems, where machine learning has enabled gesture recognition accuracies with very good results, demonstrating that strain-sensitive fibers can classify human movements rather than simply register deformation [184].

This transformation pathway also extends to the integration of IoT technologies with OFSs, where incremental improvements primarily enhance the communication efficiency and operational reach of sensing networks. A key example is improved connectivity and coverage, as IoT links enable real-time remote data acquisition and extend monitoring distances using passive fiber backbones and IoT gateways, allowing continuous observation of structural or environmental conditions over tens of kilometers [185]. Additionally, IoT contributes to higher data throughput, since broadband and multiplexed architectures support the transmission of dense spectral information from multiple OFSs, reducing delays and allowing more frequent updates without altering the sensing mechanism itself [186].

Likewise, transformative improvements also emerge when IoT is tightly integrated with OFSs, enabling qualitatively new operational paradigms. One of the most significant is the rise of edge-enabled real-time decision-making, where data from fiber sensors is processed locally at IoT nodes, allowing immediate anomaly detection and response while eliminating reliance on cloud-level latency [187]. Equally transformative is the integration of OFSs into cyber-physical platforms, where distributed fiber measurements continuously feed virtual replicas of infrastructure, enabling predictive diagnostics, scenario simulation, and autonomous system-level intelligence [188].

Integrating OFSs into IoT infrastructures is one of the most innovative paths in developing distributed, intelligent, and resilient monitoring systems. In these environments, OFSs serve as highly effective sensing nodes within IoT networks, providing unique features such as multiparametric detection, EMI immunity, passive operation without local power, and long-range coverage with high spatial resolution [186,189].

A notable example of effective integration between OFSs and IoT platforms is the design of wavelength-division multiplexed FBG sensor networks, which can operate over existing telecommunications links without disrupting conventional data traffic, demonstrating stable performance even with high-speed data signals [190]. Additionally, the incorporation of new evolutionary strategies has broadened the feasibility of using FBGs in low-power platforms. For example, a deep variational autoencoder (DVAE) model has been used to accurately reconstruct the reflected wavelength from FBG sensors under noisy or low-resolution conditions, significantly improving real-time monitoring accuracy [191]. The convergence of OFSs and IoT has also shown that sensor connectivity can be optimized through Passive Optical Network (PON) configurations, using dense wavelength-division multiplexing (DWDM) techniques and efficient spectrum management. These networks enable the deployment of sensors across vast areas and allow access to their data without the need for electrical links, which represents a crucial advantage in rural [192], underground, or aerospace scenarios [193]. Figure 20 complements this concept by illustrating a representative architecture in which OFSs act as IoT nodes in various application domains.

On another front, configurations based on photonic crystal fibers (PCFs) designed for surface plasmon resonance (SPR) are also being explored [194,195]. Their operating principle is well-suited for IoT environments due to their high sensitivity and compatibility with miniaturized structures [196]. In this context, future research on OFSs could focus not only on improving optical mechanisms or fiber structures but also on exploring new materials, interrogation protocols, and sensor integration strategies within portable embedded platforms incorporating IoT and AI.

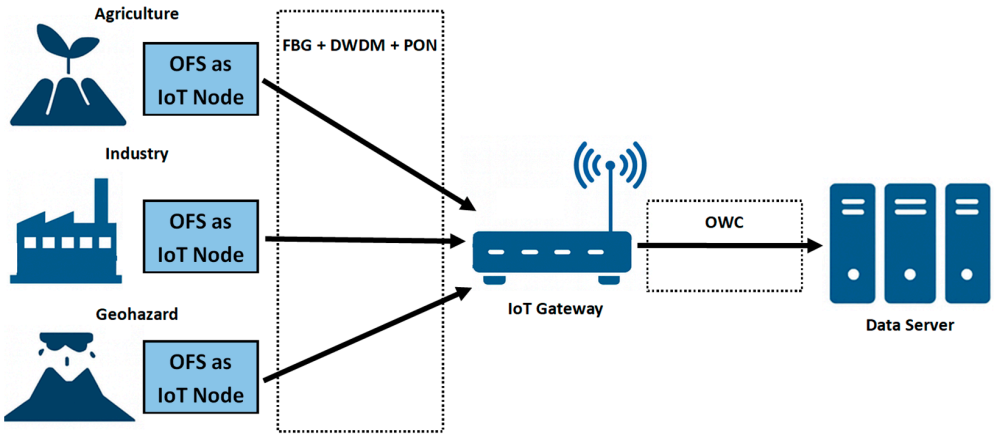

Figure 20. Schematic example architecture of an IoT-based interconnected network of OFS nodes for multipurpose monitoring, showing how OFS nodes deployed in agriculture, industry, and geohazard environments can be integrated through FBG + DWDM + PON transmission schemes, connected to an IoT gateway, and forwarded to a data server via Optical Wireless Communication (OWC).

Although the integration of OFSs with AI, ML, and IoT technologies shows great potential, several technical challenges still need to be addressed for widespread industrial use. Key issues include standardization, interoperability, and industrial scalability.

From a standardization standpoint, the literature consistently highlights the absence of unified frameworks for validating and benchmarking OFS systems improved by AI/ML or integrated into IoT infrastructures. Current research uses a variety of signal processing algorithms, from extreme learning machines to deep variational autoencoders, but depends on locally defined datasets and makeshift evaluation methods, which restrict reproducibility and comparability across different labs and industries [173,176]. Similarly, in IoT-enabled networks, FBG systems integrated into communication infrastructures stress the importance of standardizing channel allocation and interrogation procedures to prevent spectral overlap and ensure reliable coexistence with data channels [193]. Without standard metrics and protocols, expanding OFSs from experimental stages to global IoT networks remains a significant hurdle.

Closely related is the issue of interoperability. OFSs exhibit great versatility, yet integration across different platforms, distributed sensing, FBG arrays, SPR sensors, or optical wireless communication (OWC) remains fragmented. For instance, distributed systems embedded into IoT architectures face trade-offs between processing speed, spatial resolution, and strain measurement range, which prevent seamless integration with other sensing modalities [189]. The combination of free-space OWC channels with FBG sensors has been proposed as a solution to extend monitoring into harsh or inaccessible environments. Still, the lack of common compatibility standards hinders their co-deployment with conventional fiber networks [191]. Similarly, SPR sensors designed for IoT applications highlight the need for cross-platform interoperability to enable joint operation with FBG- or DOFS-based systems [196]. Achieving full interoperability requires not only technical adaptation but also protocol-level agreements among manufacturers and research communities.

Finally, industrial scalability remains a critical factor. Although multiplexing techniques like Dense Wavelength Division Multiplexing (DWDM) and Passive Optical Network (PON) have shown their ability to expand OFS networks over long distances while reducing infrastructure costs [186,193], practical deployment still faces challenges. These include optical power limits, signal degradation in harsh industrial environments, and the need for durable, affordable interrogation units [190]. Emerging solutions, such as passive IoT sensor networks or the use of OWC channels to overcome physical installation barriers, suggest promising pathways for scalability but require signifi-

cant progress in error-correction algorithms and energy efficiency for actual industrial-level deployment [186,191].

9. Future Perspectives and Opportunities of OFSs

9.1. Miniaturization of OFSs

One of the most promising directions in OFS technology has to do with miniaturization. Not only does there appear to be a future direction concerning the actual size of these devices, but there is potentially an expansion of the use of OFS technology in such sectors as the biomedical field, industry, and environmental observation.

Micro- and nano-fabrication technology has spurred the development of highly miniaturized optical probes with dimensions less than one millimeter in size. In fact, there was the introduction of a spatial confocal point distance sensor with a head size of about 600 μm, produced through femtosecond direct laser writing on optical fiber bundles. The development proves that confocal analysis can be performed in small environments, hence facilitating in-situ analysis in additive manufacturing and biomedical analysis in endoscopic applications [197]. In fact, it can be seen that not only can in-situ analysis be facilitated but that precision in measurement can still be ensured at such small sizes.

In the biomedical application area, the relevance of size reduction can be found in implantable and real-time monitoring applications. One such study demonstrated the use of a portable oxygen detection sensor using ruthenium-fluorescent dyes doped in optical fibers. The sensor was portable because it was based on using LEDs as optical sources and phase shift detection circuits, thereby reducing the need for large optical components [198]. The above example highlights how reducing the size of the sensor can expedite the process of using OFS in health monitoring.

At the material level, there exist new directions in the miniaturization of sensing interfaces using plasmonic and nanostructured coatings. Recently, the construction of a glycoprotein detection sensor using discontinuous silver nanostructures formed onto a partially clad polymer optical fiber was reported, where a nanostructure was employed to increase the surface plasmon resonance to enhance sensitivity without scaling up the sensor size [199]. In another study, the idea of optical fiber meta-tips comprising plasmonic metasurfaces fabricated directly onto the fiber end-face was presented, resulting in ultracompact lab-on-tip biosensors that can detect cancer biomarkers [200].

Further support for OFS miniaturization can be derived from the general trend towards multiparameter and multifunctional sensing. It was found in a comprehensive review of the literature that compact FPI, or compact interferometers, make it possible to measure several parameters such as temperature, strain, pressure, and refractive index at the same time in a compact element, and such a level of integration can only be obtained because of the current miniaturization process in OFS [201]. The trend towards multifunctional sensing in small space environments will further increase the range of OFS applications in such environments.

Building upon these successes, it is equally important to reflect upon fundamental technology and economics constraints driving real-world adoption of alternative OFS architectures. By examining across these families of OFS, there appear to be significant trade-offs in performance strengths and weaknesses of the leading sensing technologies. For example, FBGs coupled with miniature sensor technology and Micro-Electro-Mechanical Systems (MEMS) offer superior template-based reproducibility in fabrication, robust long-term reliability, and good compatibility with economical mass fabrication technology domains, giving them significant advantages from an industrial and technology readiness perspective [51,112]. By comparison, there exist fundamental constraints in native sensing capability approaching a technology barrier in FBG technology, in addition to significant

cost constraints due to the cost-intensive nature of interrogator technology [51,112,155,190]. By contrast, FPI, MZI, and MI configurations appear to offer native sensing capability that is several orders of magnitude greater with dramatically less expensive interrogators, thereby offering attractive technology prospects in terms of high-performance OFS adoption [22,24,51]. These superiorities notwithstanding, these OFS technologies appear to confront significant technology challenges in achieving template-based reproducible cavity geometries, good environmental isolation, or economical large-scale fabrication [5,24,86,124]. By these considerations, the selection of advanced OFS architectures appears rather difficult when based upon performance considerations alone.

9.2. Implemented Biosensors

Another area where the OFS technologies can make significant paradigm shifts in medical fields is in the development of implantable biosensors, thereby offering real-time in vivo analysis of critical biochemical parameters in living organisms. Their defining characteristics of miniaturization, biocompatibility, and the capability to offer detection without the need for labels make them prime contenders in this area.

Recently, an analysis was presented that incorporated a graphene oxide-functionalized micro-tapered long-period fiber grating sensor for hemoglobin detection. An exemplary measurement was obtained with a detection limit of 0.02 mg/mL, which is much lower than the cut-off level specified by the World Health Organization for anemia. The fact that these sensors are highly sensitive and can resist interference in complex environments confirms OFSs' applicability in constant blood biomarker measurement, thereby supporting early diagnoses in cases of blood disorders [202].

The other line of exploratory research has centered around the improvement of surface plasmon resonance (SPR) biosensors using hybrid nanostructures. An optical fiber biosensor using $MoSe_2$–Au nanofilms demonstrated enhanced sensitivity by a factor of two compared to standard SPR biosensors, achieving detection sensitivities as low as 0.33 µg/mL in immunoassays of Goat-anti-Rabbit IgG [203]. It can be shown from the above discussion that the combined use of transition metal dichalcogenides with gold nanostructured films can result in extremely selective and ultra-sensitive biosensors suitable for the detection of immune biomarkers at trace concentrations, suitable for use in implantable devices.

More direct, but equally effective designs have also been reported. For example, a bare optical fiber with a thin gold layer was fabricated to detect changes in the refractive index and for real-time protein-binding kinetics measurements. Their detection sensitivities were reported in the order of 10^{-4}–10^{-5} RIU, which was sufficient to detect both antibody and antigen interactions, as well as biomolecular recognition events [204]. One can easily predict that low-cost and minimally invasive OFS devices will soon emerge due to the simplicity of such designs.

In addition, a plasmonic nanocoated tilted fiber Bragg grating (TFBG) in a microfluidic channel was able to detect the variation in urinary protein without any label with an amplitude sensitivity of greater than 8000 dB/RIU and an RI detection limit of 10^{-5} RIU. Using an ultra-thin layer of Ag with a thickness of approximately 20–30 nm to co-excite both the cut-off and plasmonic resonances was able to offer a protein concentration sensitivity of 5.5 dB/(mg mL^{-1}) with an LOD of 1.5×10^{-3} mg mL^{-1}. The researchers further reported that the head of the TFBG could potentially be designed to work in reflection and in the form factor of a hypodermic needle [205].

In medical diagnostics, optical fiber biosensors have found applications in dealing with critical medical issues. For example, an SPR sensor based on plastic optical fiber was developed to measure the level of pancreatic amylase in drained fluid in surgically

implanted drains. It takes about 8 min to measure, having a detection range of about 0.5 U/L. This can lead to the reduction of postoperative complications due to pancreatic fistula by offering early postoperative analysis [206]. These emerging OFS technologies can directly aid in the treatment of patients by offering early detection of critical biomarkers.

Furthermore, advanced designs have expanded the limits of sensitivity and specificity in cancer diagnostics. A black phosphorus–based fiber optic biosensor functionalized with neuron-specific enolase (NSE) antibodies achieved a detection limit of 1.0 pg/mL, four orders of magnitude below the clinical cutoff values for small cell lung cancer. This device harnessed the unique optoelectronic properties of black phosphorus nanosheets combined with a tilted fiber grating, providing unprecedented light–matter interaction within a compact, implantable probe [207].

A recent comprehensive review highlighted the challenges and opportunities of in vivo optical fiber biosensors, focusing on key needs such as biocompatibility, sterilization, packaging, and multiplexing features. The idea of integrating fiber-based probes into catheters, needles, or multi-fiber assemblies has been suggested as a promising way to enable minimally invasive and continuous monitoring of disease biomarkers directly within tissues [208].

9.3. Integration of OFSs with 6G Communications

The integration of OFSs with sixth-generation (6G) networks is becoming a key focus for supporting advanced communication and sensing capabilities. As 6G aims to deliver ultra-low latency, terabit-per-second speeds, and extensive connectivity, OFSs provide the benefits of high-capacity data transmission and distributed sensing within the same fiber network. This combination not only enhances data services but also enables real-time monitoring and control in vital areas like smart cities, transportation, and industrial automation.

A recent review highlighted the importance of combining radio-over-fiber (RoF) and power-over-fiber (PoF) as core elements for 6G architectures. By enabling the simultaneous transmission of radio signals and electrical power through optical fibers, radio- and power-over-fiber (RPoF) systems facilitate simpler fronthaul and backhaul connectivity, as well as efficient powering of dense small-cell networks. The analysis pointed out key challenges such as power transmission efficiency, fiber design, and scalability, but also demonstrated that RPoF can deliver high-capacity links and safe, interference-free power distribution for 6G deployments [209].

Meanwhile, the integration of IoT and RoF technologies has become crucial for supporting the expected massive connectivity of 6G. A detailed study explains how RoF provides broad bandwidth, low attenuation, and EMI immunity making it suitable for environments such as smart homes, hospitals, Industry 5.0, and satellite–terrestrial integrated communications. In this context, OFSs integrated into IoT systems are seen as key enablers of intelligent sensing and control, with RoF offering reliable high-capacity transmission across various devices [210].

The use of DOFSs is considered a key component of 6G networks. Recent studies show that φ-OTDR-based distributed fiber systems can be directly integrated with AI-driven methods like vision transformers to monitor traffic in smart cities. These systems utilize existing buried fiber infrastructure to transmit data and support real-time environmental sensing, aligning with the 6G concept of combined sensing and communication (ISAC) [211].

Complementary to this, the role of plasmonic nanostructures in telecommunications has been widely reviewed, with applications ranging from optical modulators and filters to nanoantennas and THz converters. These devices aim to increase bandwidth and improve the integration density of OFSs, directly supporting ultrafast board-to-board, chip-to-chip, and fiber-to-THz front-ends necessary for 6G infrastructures [212].

An essential aspect of this convergence is ensuring resilience-by-design in 6G networks. A comprehensive framework has been proposed that incorporates resilience principles, protection, self-awareness, and reconfiguration into all network layers. Optical fibers, with their EMI immunity and ability for distributed monitoring, are highlighted as a key technology to ensure robustness against failures, cyberattacks, and natural disasters in 6G-enabled smart infrastructures [213].

Recently, experimental studies have demonstrated the integration of FBG sensors with free-space optical (FSO) multiple-input multiple-output (MIMO) channels. This hybrid approach compensates for environmental effects such as strain, temperature, and atmospheric turbulence while supporting high-capacity 10 Gb/s data transmission. The results show that FBGs embedded in FSO links significantly reduce bit error rates and improve received signal strength, paving the way for last-mile connectivity in 6G IoT applications [214].

9.4. OFSs in Renewable Energy Applications

The shift towards the adoption of renewable energy sources has further accentuated the need for accurate monitoring, predictive maintenance, and efficient energy conversion. In these regards, OFSs have increasingly found application in every area related to the generation, storage, and distribution of renewable energy, with benefits including EMI immunity, small size, and ruggedness in hostile environments.

An important emerging trend is the application of OFSs in the monitoring of energy storage. An experiment demonstrated the first in-situ plasmonic optical fiber sensor measurement of the state of charge in supercapacitors using an FBG coated with gold at the nanoscale to generate surface plasmon resonances. Using such technology, charge-discharge cycles can easily be monitored online without interference from temperatures, hence serving as a low-cost technology in assessing the electrochemical behavior of devices in storing renewable energies [215].

In the hydrogen economy, OFSs have found important applications in hydrogen safety and performance. DOFSs have been incorporated in composite pressure vessels designed for hydrogen storage. Their compactness and ability to be incorporated during manufacturing have facilitated early detection of both strain and damage, hence improving safety and lowering maintenance costs [216]. On the other hand, OFS innovation in hydrogen sensor technology has incorporated interferometry and Fabry-Perot designs, SPR designs with palladium layers, and other technologies. These technologies have combined high sensitivities, rapid detection rates, and robustness, thereby meeting the fundamental need in hydrogen leak prevention for renewable energy technologies [217].

OFSs are also involved in energy transport and distribution. In fact, a conceptual analysis was presented regarding the use of smart ocean transport cables that involve the embedding of optical fibers to detect strain and temperatures in copper wires. In such analysis, it was postulated that there would be no occurrence of overheating beyond critical limits (up to 90 °C) that precipitate failure in undersea power transmission cables, which are critical in maintaining undersea wind or wave power plants [218]. In addition, there has been an assessment of the prospect of using polymeric optical fibers in the condition monitoring of moored marine power devices based on polymers. The assessment presented the effectiveness of PMMA-based fibers, tested with DOFSs, in determining the load characteristics of such devices [219].

In the area of harvesting energy, OFSs have been considered and developed in solar energy utilization and daylighting applications. Experiments have shown the feasibility of a hybrid optical fiber daylighting and LED technology where Fresnel lenses, stepped-index waveguides, and concentrator photovoltaics (CPVs) were combined to split the visible and non-visible parts of the solar spectrum. The visible spectrum was transmitted inside the

building using optical fibers to produce lighting, whereas the other spectrum was converted into electricity to power LEDs in order to attain optical efficiencies in excess of 60% [220]. Finally, advances in computer algorithms have coupled OFS with artificial intelligence in order to optimize renewable energy resources. Recently, an OFS-based AI model was presented using the GAN model in order to optimize the efficiency of fiber-optic-supported renewable resources. By overcoming visibility issues, the characterization of the refractive index, and noise constraints in underground or indoor environments, there have been indications of increased efficiency in using AI-assisted optical fiber technology in renewable resource distribution [221].

9.5. OFSs in Smart Cities

The future of smart cities relies on technologies that offer real-time monitoring, efficient data management, and dynamic infrastructures. One of the emerging technologies in smart cities was OFSs due to their suitability in distributed sensing, EMI immunity, and compatibility with telecommunication infrastructures. OFS technology can offer smart applications in traffic management, seismic detection, structural integrity assessment, and smart buildings.

An innovative use of OFSs regards them as the "fiber-optic auditory nerve of the ground" to harness the capability of distributed vibration sensing (DVS) based on φ-OTDR. Practical experiments have shown that telecom fibers buried in the ground can serve as macrosensors to detect vibrations caused by vehicular traffic, construction works, or environmental events up to 31.8 km. It helped ensure proper monitoring of traffic flow without using cameras or roadside devices, thus highlighting the effectiveness of OFSs as economical tools in smart traffic management in the suburb or in the city [222].

Similarly, expanding ground motion sensing using existing internet fiber infrastructure has been studied as a scalable way to improve urban resilience. By applying distributed acoustic sensing (DAS) on already-installed metropolitan fiber cables, it was demonstrated that the monitored area for seismic events of magnitude > 0.5 could increase from about 1% to over 12–20% of urban areas. This integration significantly lowers the need for expensive dedicated seismic networks, thereby boosting urban safety and hazard preparedness [223].

Health infrastructure is another area where OFSs are making a significant impact. Research on multimode optical fiber strain monitoring has shown that single-mode–multimode–single-mode concatenated structures can surpass FBGs in sensitivity, while also being cheaper and easier to manufacture. These sensors have been effectively used for monitoring the health of pressurized pipelines, highlighting their usefulness in ongoing assessment of civil infrastructure in smart cities [224]. Additional work on mortar–diatom composites has introduced new cement-based materials optimized for embedding OFSs. These materials help reduce heterogeneity, improve sensor stability, and boost CO_2 trapping. This development supports the goal of creating sustainable, sensor-integrated smart buildings [225].

Beyond physical monitoring, OFSs also contribute to next-generation photonic communication systems for smart cities. Research on photonic sensors has proposed integrated solutions for urban applications, including visible light communication, optical wireless networks, and environmental sensing. These photonic methods extend the functions of OFSs beyond sensing, aligning them with the digital infrastructure of smart cities [226].

10. Conclusions

OFSs have progressed from experimental laboratory tools to commercially successful technologies with broad applications in scientific, industrial, biomedical, environmental, and aerospace fields. This evolution begins with the key milestone of the 1967 FS which

started the development of both intrinsic and extrinsic sensing methods. This dual approach has given OFSs exceptional flexibility, allowing their configurations to be tailored for specific needs in sensitivity, selectivity, and durability based on the application.

This comprehensive review, based on the TAK methodology and enhanced with a quantitative graphical analysis, consolidates knowledge that is often scattered across the literature. It shows that intrinsic architectures, especially those utilizing Bragg gratings, interferometry, and scattering, have demonstrated excellent performance in harsh and high-precision environments. At the same time, extrinsic configurations excel at modular integration, making them particularly useful in flexible, non-invasive, or hybrid systems.

The analysis of recent trends shows a clear shift toward smart and autonomous systems, where OFSs are increasingly combined with artificial intelligence (AI), the Internet of Things (IoT), and next-generation communication networks like 6G. These new connections enable the creation of smaller, faster, and more independent sensors capable of distributed sensing and real-time decision-making. At the same time, improvements in chemical coatings, functional materials, and multiplexing techniques are expanding the sensing abilities and scalability of OFS-based systems.

However, challenges remain, especially in lowering fabrication and interrogation costs, improving field calibration procedures, and increasing long-term reliability in harsh environments. Tackling these issues is essential for broader use, particularly in large-scale infrastructure and in vivo biomedical applications.

In summary, the technological path of OFSs shows not only their adaptability and functional variety but also their strategic significance in the age of automation, distributed sensing, and data-driven technologies. This review offers a thorough and comparative base to guide future research and innovation toward more robust, intelligent, and multidisciplinary optical fiber platforms.

Author Contributions: Conceptualization, J.R.M.-A., J.D.F.-R. and J.P.L.-C.; methodology, J.R.M.-A., J.D.F.-R.; software, D.A.R.-R. and D.J.-V.; validation, J.R.M.-A., D.A.R.-R. and V.P.S.-A.; formal analysis, A.D.-M.; investigation, D.A.R.-R.; resources, J.C.E.-L.; data curation, J.D.F.-R.; writing—original draft preparation, D.A.R.-R.; writing—review and editing, D.A.R.-R.; visualization, J.C.E.-L. and D.A.R.-R.; supervision, J.R.M.-A.; project administration, D.J.-V.; funding acquisition, V.P.S.-A. All authors have read and agreed to the published version of the manuscript.

Funding: We are grateful for the Autonomous University of Tamaulipas (UAT), Mexico for the financial support for the publication of the article.

Acknowledgments: Appreciation is extended to the Secretaría de Ciencia, Humanidades, Tecnología e Innovación (SECIHTI) for their support through the National Scholarship for Graduate Studies Number 005642, grant number CBF-2025-G-1233, CBF2023-2024-1089 and the "Estancias Posdoctorales por México 2022" under project No. 2840970. Gratitude is also expressed to the Universidad Autónoma de Tamaulipas (UAT) for granting access to facilities and infrastructure during this review article's development. During the preparation of this manuscript, the author(s) used Grammarly (1.2.211.1787) for the purpose of English editing by generative IA text support. The authors have reviewed and edited the output and take full responsibility for the content of this publication.

Conflicts of Interest: The authors declare no conflicts of interest.

Abbreviations

The following abbreviations are used in this manuscript:

AI	Artificial Intelligence
DOFS	Distributed Optical Fiber Sensor
DVAE	Deep Variational Autoencoder
DWDM	Dense Wavelength-Division Multiplexing
EC	Electrochromic Devices
EFPI	Extrinsic Fabry-Perot Interferometer
FBG	Fiber Bragg Gratings
FPI	Fabry-Perot Interferometer
FSO	Free-Space Optical
GAN	Generative Adversarial Network
IFPI	Intrinsic Fabry-Perot Interferometer
IoT	Internet of Things
ISAC	Integrated Sensing and Communication
LED	Light Emitting Diode
LOD	Limit of Detection
MI	Michelson Interferometer
MIMO	Multiple-Input Multiple-Output
MMF	Multimode Fiber
MZI	Mach-Zehnder Interferometer
NSE	Neuron-Specific Enolase
OFS	Optical Fiber Sensor
OSA	Optical Spectrum Analyzer
OWC	Optical Wireless Communication
PCF	Photonic Crystal Fiber
PoF	Power-Over-Fiber
POF	Polymer Optical Fiber
PON	Passive Optical Network
RPoF	Radio and Power-Over-Fiber
RoF	Radio-Over-Fiber
SI	Sagnac Interferometer
SMF	Single Mode Fiber
SMS	Single-Mode-Multimode-Single-Mode Fiber
SPR	Surface Plasmon Resonance
TAK	Title, Abstract, Keywords
TFBG	Tilted Fiber Bragg Grating
TMDCs	Transition Metal Dichalcogenides

References

1. Bhakta, I.; Phadikar, S.; Majumder, K. State-of-the-art technologies in precision agriculture: A systematic review. *J. Sci. Food Agric.* **2019**, *99*, 4878–4888. [CrossRef]
2. Bec, K.B.; Grabska, J.; Huck, C.W. Miniaturized NIR Spectroscopy in Food Analysis and Quality Control: Promises, Challenges, and Perspectives. *Foods* **2022**, *11*, 1465. [CrossRef]
3. Samadi Pakchin, P.; Fathi, M.; Ghanbari, H.; Saber, R.; Omidi, Y. A novel electrochemical immunosensor for ultrasensitive detection of CA125 in ovarian cancer. *Biosens. Bioelectron.* **2020**, *153*, 112029. [CrossRef]
4. Khani, S.; Rezaei, P. Optical sensors based on plasmonic nano-structures: A review. *Heliyon* **2024**, *10*, e40923. [CrossRef] [PubMed]
5. Pendao, C.; Silva, I. Optical Fiber Sensors and Sensing Networks: Overview of the Main Principles and Applications. *Sensors* **2022**, *22*, 7554. [CrossRef]
6. Ma, S.; Xu, Y.; Pang, Y.; Zhao, X.; Li, Y.; Qin, Z.; Liu, Z.; Lu, P.; Bao, X. Optical Fiber Sensors for High-Temperature Monitoring: A Review. *Sensors* **2022**, *22*, 5722. [CrossRef] [PubMed]

7. Girard, S.; Kuhnhenn, J.; Gusarov, A.; Morana, A.; Paillet, P.; Robin, T.; Weninger, L.; Fricano, F.; Roche, M.; Campanella, C.; et al. Overview of Radiation Effects on Silica-Based Optical Fibers and Fiber Sensors. *IEEE Trans. Nucl. Sci.* **2025**, *72*, 982–1020. [CrossRef]
8. Urrutia, E.; Ayesta, I.; Azkune, M.; Illarramendi, M.A.; Zubia, J. Recent Advances in Sensor Applications of Microstructured Optical Fibers: A Review. *IEEE Sens. J.* **2025**, *25*, 18584–18607. [CrossRef]
9. Pang, F.; Xiang, L.; Liu, H.; Zhang, L.; Wen, J.; Zeng, X.; Wang, T. Review on Fiber-Optic Vortices and Their Sensing Applications. *J. Light. Technol.* **2021**, *39*, 3740–3750. [CrossRef]
10. Zhang, X.; Wang, C.; Zheng, T.; Wu, H.; Wu, Q.; Wang, Y. Wearable Optical Fiber Sensors in Medical Monitoring Applications: A Review. *Sensors* **2023**, *23*, 6671. [CrossRef] [PubMed]
11. Zhu, L.; Sun, G.; Bao, W.; You, Z.; Meng, F.; Dong, M. Structural Deformation Monitoring of Flight Vehicles Based on Optical Fiber Sensing Technology: A Review and Future Perspectives. *Engineering* **2022**, *16*, 39–55. [CrossRef]
12. Chen, S.; Wang, J.; Zhang, C.; Li, M.; Li, N.; Wu, H.; Liu, Y.; Peng, W.; Song, Y. Marine Structural Health Monitoring with Optical Fiber Sensors: A Review. *Sensors* **2023**, *23*, 1877. [CrossRef]
13. Li, J. A review: Development of novel fiber-optic platforms for bulk and surface refractive index sensing applications. *Sens. Actuators Rep.* **2020**, *2*, 100018. [CrossRef]
14. Jean-Ruel, H.; Albert, J. Recent advances and current trends in optical fiber biosensors based on tilted fiber Bragg gratings. *TrAC Trends Anal. Chem.* **2024**, *174*, 117663. [CrossRef]
15. Bado, M.F.; Casas, J.R. A Review of Recent Distributed Optical Fiber Sensors Applications for Civil Engineering Structural Health Monitoring. *Sensors* **2021**, *21*, 1818. [CrossRef]
16. Anjana, K.; Herath, M.; Epaarachchi, J. Optical fibre sensors for geohazard monitoring—A review. *Measurement* **2024**, *235*, 114846. [CrossRef]
17. He, R.; Shen, L.; Wang, Z.; Wang, G.; Qu, H.; Hu, X.; Min, R. Optical fiber sensors for heart rate monitoring: A review of mechanisms and applications. *Results Opt.* **2023**, *11*, 100386. [CrossRef]
18. Gutiérrez, F.; Sevil, J.; Sevillano, P.; Preciado-Garbayo, J.; Martínez, J.J.; Martín-López, S.; González-Herráez, M. The application of distributed optical fiber sensors (BOTDA) to sinkhole monitoring. Review and the case of a damaging sinkhole in the Ebro Valley evaporite karst (NE Spain). *Eng. Geol.* **2023**, *325*, 107289. [CrossRef]
19. Zhang, X.; Zhu, H.; Jiang, X.; Broere, W. Distributed fiber optic sensors for tunnel monitoring: A state-of-the-art review. *J. Rock Mech. Geotech. Eng.* **2024**, *16*, 3841–3863. [CrossRef]
20. Acharya, A.; Kogure, T. Advances in fibre-optic-based slope reinforcement monitoring: A review. *J. Rock Mech. Geotech. Eng.* **2025**, *17*, 1263–1284. [CrossRef]
21. Wang, K.; Dong, X.; Kohler, M.H.; Kienle, P.; Bian, Q.; Jakobi, M.; Koch, A.W. Advances in Optical Fiber Sensors Based on Multimode Interference (MMI): A Review. *IEEE Sens. J.* **2021**, *21*, 132–142. [CrossRef]
22. Bartnik, K.; Koba, M.; Śmietana, M. Advancements in optical fiber sensors for in vivo applications—A review of sensors tested on living organisms. *Measurement* **2024**, *224*, 113818. [CrossRef]
23. Arcadio, F.; Del Prete, D.; Zeni, L.; Cennamo, N.; Seggio, M. Optical Sensor Chips Monitored via Extrinsic Optical Fiber Schemes. *IEEE Sens. Rev.* **2025**, *2*, 179–198. [CrossRef]
24. Zhu, C.; Zheng, H.; Ma, L.; Yao, Z.; Liu, B.; Huang, J.; Rao, Y. Advances in Fiber-Optic Extrinsic Fabry–Perot Interferometric Physical and Mechanical Sensors: A Review. *IEEE Sens. J.* **2023**, *23*, 6406–6426. [CrossRef]
25. Janik, M.; Koba, M.; Śmietana, M. Optical fiber chemo and biosensors operating in the electrochemical domain—A review. *TrAC Trends Anal. Chem.* **2024**, *178*, 117829. [CrossRef]
26. Pottier, P.; Lagisz, M.; Burke, S.; Drobniak, S.M.; Downing, P.A.; Macartney, E.L.; Martinig, A.R.; Mizuno, A.; Morrison, K.; Pollo, P.; et al. Title, abstract and keywords: A practical guide to maximize the visibility and impact of academic papers. *Proc. Biol. Sci.* **2024**, *291*, 20241222. [CrossRef]
27. Barry, E.S.; Merkebu, J.; Varpio, L. State-of-the-art literature review methodology: A six-step approach for knowledge synthesis. *Perspect. Med. Educ.* **2022**, *11*, 281–288. [CrossRef]
28. Booth, A.; Sutton, A.; Clowes, M.; James, M.M.-S. *Systematic Approaches to a Successful Literature Review*, 2nd ed.; SAGE Publications: London, UK, 2012.
29. Snyder, H. Literature review as a research methodology: An overview and guidelines. *J. Bus. Res.* **2019**, *104*, 333–339. [CrossRef]
30. Shah, H.M.; Gardas, B.B.; Narwane, V.S.; Mehta, H.S. The contemporary state of big data analytics and artificial intelligence towards intelligent supply chain risk management: A comprehensive review. *Kybernetes* **2021**, *52*, 1643–1697. [CrossRef]
31. Mtapuri, O. Community-based tourism research in academic journals: A numerical analysis. *Afr. J. Phys. Health Educ. Recreat. Danc.* **2015**, *21*, 688–705.
32. Culshaw, B. Fiber Optics in Sensing and Measurement. *IEEE J. Sel. Top. Quantum Electron.* **2000**, *6*, 1014–1021. [CrossRef]
33. Culshaw, B.; Kersey, A. Fiber-Optic Sensing: A Historical Perspective. *J. Light. Technol.* **2008**, *26*, 1064–1078. [CrossRef]

34. Hall, T.J.; Fiddy, M.A.; Ner, M.S. Detector for an optical-fiber acoustic sensor using dynamic holographic interferometry. *Opt. Lett.* **1980**, *5*, 485–487. [CrossRef]
35. Udd, E. Fiber Optic Smart Structures. *Proc. IEEE* **1996**, *84*, 884–894. [CrossRef]
36. Dandridge, A.; Tveten, A.B.; Sigel, G.H., Jr.; West, E.J.; Giallorenzi, T.G. Optical Fibre Magnetic Field Sensors. *Electron. Lett.* **1980**, *16*, 408–409. [CrossRef]
37. Udd, E. An overview of fiber-optic sensors. *Rev. Sci. Instrum.* **1995**, *66*, 4015–4030. [CrossRef]
38. Ferdinand, P. The Evolution of Optical Fiber Sensors Technologies During the 35 Last Years and Their Applications in Structural Health Monitoring. In Proceedings of the 7th European Workshop on Structural Health Monitoring, Nantes, France, 8–11 July 2014.
39. Ferdinand, P.; Denayrolles, Y.; Mersier, C.; Plantey, J.; Recrosio, N.; Pays, M.; Vielpeau, D. The potential for distributed sensors and optical fibre sensor networks in the electric power industry. *Meas. Sci. Technol.* **1990**, *1*, 908–916. [CrossRef]
40. Al-Raweshidy, H.S.; Uttamchandani, D. Spread spectium technique for passive multiplexing of interferometric optical fiber sensors. *Opt. Commun.* **1990**, *80*, 18–22. [CrossRef]
41. Janani, R.; Majumder, D.; Scrimshire, A.; Stone, A.; Wakelin, E.; Jones, A.H.; Wheeler, N.V.; Brooks, W.; Bingham, P.A. From acrylates to silicones: A review of common optical fibre coatings used for normal to harsh environments. *Prog. Org. Coat.* **2023**, *180*, 107557. [CrossRef]
42. Khan, S.; Le Calvé, S.; Newport, D. A review of optical interferometry techniques for VOC detection. *Sens. Actuators A Phys.* **2020**, *302*, 111782. [CrossRef]
43. Li, X.; Li, Y.; Wei, H.; Wang, C.; Liu, B. A Review of Wearable Optical Fiber Sensors for Rehabilitation Monitoring. *Sensors* **2024**, *24*, 3602. [CrossRef]
44. Marques, C.; Leal-Junior, A.; Kumar, S. Multifunctional Integration of Optical Fibers and Nanomaterials for Aircraft Systems. *Materials* **2023**, *16*, 1433. [CrossRef] [PubMed]
45. Rovera, A.; Tancau, A.; Boetti, N.; Dalla Vedova, M.D.L.; Maggiore, P.; Janner, D. Fiber Optic Sensors for Harsh and High Radiation Environments in Aerospace Applications. *Sensors* **2023**, *23*, 2512. [CrossRef] [PubMed]
46. Lopatin, C. 9-Aerospace Applications of Optical Fiber Mechanical Sensors. In *Opto-Mechanical Fiber Optic Sensors*; Butterworth-Heinemann: Oxford, UK, 2018; pp. 237–262. [CrossRef]
47. Vedova, M.D.L.D.; Berri, P.C.; Maggiore, P.; Quattrocchi, G. Design and development of innovative FBG-based fiber optic sensors for aerospace applications. *J. Phys. Conf. Ser.* **2020**, *1589*, 012012. [CrossRef]
48. Culshaw, B.; Zhang, X.; Wang, A.; Jiang, J.; Liu, T.; Liu, K.; Wang, S.; Yin, J.; Zhao, B.; Zhang, J.; et al. Development of optical fiber sensing instrument for aviation and aerospace application. In Proceedings of the 2013 International Conference on Optical Instruments and Technology: Optical Sensors and Applications, Beijing, China, 20 December 2013. [CrossRef]
49. Klippert, M.; Pauer, W. Distributed optical fiber sensors for real-time tracking of fouling buildup for tubular continuous polymerization reactors. *Chem. Eng. Res. Des.* **2024**, *211*, 168–178. [CrossRef]
50. Mustaffa, S.N.; Rashid, A.R.A.; Jin, T.S.; Menon, P.S.; Razak, M.Z.A.; Markom, A.M.; Haris, H.; Saad, I.; Muhammad, A.R. Metal Oxide Coated Optical Fiber for Humidity Sensing Application: A Review. *IEEE Access* **2023**, *11*, 126568–126600. [CrossRef]
51. Ran, Z.; He, X.; Rao, Y.; Sun, D.; Qin, X.; Zeng, D.; Chu, W.; Li, X.; Wei, Y. Fiber-Optic Microstructure Sensors: A Review. *Photonic Sens.* **2021**, *11*, 227–261. [CrossRef]
52. Hernandez-García, J.C.; Estudillo-A, J.M.; Rojas-Laguna, R.; Chávez, R.I.M.; Martínez-Ríos, A.; Gutiérrez, J.G.; Trejo-Durán, M.; Vargas-Rodríguez, E.; Andrade-Lucio, J.A.; Alvarado-Méndez, E. Instrumentacion y diseño de una fuente de alto voltaje para fabricar rejillas de fibra optica mediante la técnica de arco eléctrico. *Rev. Mex. Física* **2010**, *3*, 255–261.
53. Ramiro, C.R.; Montalvo, E.R.; Mónica, Y.V.R. Estudio y Diseño de una Red de Última Milla, Utilizando la Tecnología G-PON, Para el Sector del Nuevo Aeropuerto de Quito. Bachelor's Thesis, Escuela Politécnica Nacional, Quito, Ecuador, March 2018.
54. Abdhul Rahuman, M.A.; Kahatapitiya, N.S.; Amarakoon, V.N.; Wijenayake, U.; Silva, B.N.; Jeon, M.; Kim, J.; Ravichandran, N.K.; Wijesinghe, R.E. Recent Technological Progress of Fiber-Optical Sensors for Bio-Mechatronics Applications. *Technologies* **2023**, *11*, 157. [CrossRef]
55. Fu, X.; Ran, R.; Li, Q.; Huang, Z.; Li, D.; Zhang, R.; Fu, G.; Jin, W.; Qi, Y.; Bi, W. A Few Mode Fiber Temperature Sensor Filled With PDMS Based on Vernier Effect. *IEEE Photonics J.* **2021**, *13*, 1–5. [CrossRef]
56. Mumtaz, F.; Roman, M.; Zhang, B.; Abbas, L.G.; Ashraf, M.A.; Fiaz, M.A.; Dai, Y.; Huang, J. A Simple Optical Fiber SPR Sensor with Ultra-High Sensitivity for Dual-Parameter Measurement. *IEEE Photonics J.* **2022**, *14*, 1–7. [CrossRef]
57. Dabagh, S.; Singh, R.; Borri, C.; Chiavaioli, F. Functional Nanomaterial Coatings on Optical Fibers: Toward Enhanced Biosensing Performance. *IEEE Sens. Rev.* **2025**, *2*, 157–169. [CrossRef]
58. Roriz, P.; Silva, S.; Frazao, O.; Novais, S. Optical Fiber Temperature Sensors and Their Biomedical Applications. *Sensors* **2020**, *20*, 2113. [CrossRef]
59. Wang, Q.; Farrell, G.; Yan, W. Investigation on Single-Mode–Multimode– Single-Mode Fiber Structure. *J. Light. Technol.* **2008**, *26*, 512–519. [CrossRef]

60. Sokołowski, P.; Łubiński, J.; Wierzba, P.; Czubek, J.; Miluski, P.; Janiak, F.; Guan, S.; Szczerska, M. Polymer Materials for U-Shaped Optic Fiber Sensors: A Review. *Photonics* **2025**, *12*, 56. [CrossRef]
61. Tavares, C.; Silva, J.O.E.; Mendes, A.; Rebolo, L.; Domingues, M.D.F.; Alberto, N.; Lima, M.; Silva, H.P.; Antunes, P.F.D.C. Instrumented Office Chair with Low-Cost Plastic Optical Fiber Sensors for Posture Control and Work Conditions Optimization. *IEEE Access* **2022**, *10*, 69063–69071. [CrossRef]
62. Gao, X.; Xu, J.; Xie, C.; Zhang, W.; Pei, L.; Zheng, J.; Li, J.; Ning, T. Strain-Insensitive Temperature Sensor Based on Few-Mode Fiber and Photonic Crystal Fiber. *IEEE Photonics J.* **2022**, *14*, 1–7. [CrossRef]
63. Nejad, J.Y.; Soroosh, M.; Al-Shammri, F.K.; Alkhayer, A.G. High-sensitive and linear temperature sensor based on liquid-filled photonic crystal fiber. *Opt. Quantum Electron.* **2024**, *57*, 32. [CrossRef]
64. Chen, N.; Guo, W.; Chen, H.; Ding, X.; Yang, F.; Zhu, Y.; Song, M.; Xu, Y. Multifunctional in-fiber polarization beam splitter using liquid crystal infiltrated dual-core photonic crystal fiber with gold layers and its temperature sensing characteristic. *Opt. Laser Technol.* **2025**, *191*, 113350. [CrossRef]
65. Zhang, Y.; Li, Y.; Guo, Z.; Li, J.; Ge, X.; Sun, Q.; Yan, Z.; Li, Z.; Huang, Y. Health monitoring by optical fiber sensing technology for rechargeable batteries. *eScience* **2024**, *4*, 100174. [CrossRef]
66. Halendy, M.; Sielska, A.; Ertman, S. Scalable sensors of refractive index and liquid level based on multimode interference in small-core hollow core fiber. *Measurement* **2025**, *248*, 116977. [CrossRef]
67. Xu, J.; Huang, K.; Zheng, J.; Li, J.; Pei, L.; You, H.; Ning, T. Sensitivity Enhanced Magnetic Field Sensor Based on Hollow Core Fiber Fabry-Perot Interferometer and Vernier Effect. *IEEE Photonics J.* **2022**, *14*, 1–5. [CrossRef]
68. Katrenova, Z.; Alisherov, S.; Abdol, T.; Molardi, C. Status and future development of distributed optical fiber sensors for biomedical applications. *Sens. Bio-Sens. Res.* **2024**, *43*, 100616. [CrossRef]
69. Leffers, L.; Locmelis, J.; Bremer, K.; Roth, B.; Overmeyer, L. Optical Bend Sensor Based on Eccentrically Micro-Structured Multimode Polymer Optical Fibers. *IEEE Photonics J.* **2021**, *13*, 1–7. [CrossRef]
70. Li, C.; Yang, W.; Wang, M.; Yu, X.; Fan, J.; Xiong, Y.; Yang, Y.; Li, L. A Review of Coating Materials Used to Improve the Performance of Optical Fiber Sensors. *Sensors* **2020**, *20*, 4215. [CrossRef]
71. Paul, T.; Roy Choudhury, D.; Ghosh, D.; Saha, C. Advancements in optical sensors for explosive materials Identification: A comprehensive review. *Results Chem.* **2024**, *8*, 101602. [CrossRef]
72. Hengoju, S.; Shvydkiv, O.; Tovar, M.; Roth, M.; Rosenbaum, M.A. Advantages of optical fibers for facile and enhanced detection in droplet microfluidics. *Biosens. Bioelectron.* **2022**, *200*, 113910. [CrossRef] [PubMed]
73. Lin, X.; Li, G.; Wang, Y.; Zeng, K.; Yang, W.; Wang, F. Advances in intelligent identification of fiber-optic vibration signals in oil and gas pipelines. *J. Pipeline Sci. Eng.* **2024**, *4*, 100184. [CrossRef]
74. Poczekajło, P.; Suszyński, R.; Antosz, A. Review of the usage of fiber optic technologies in electrical power engineering and a development outline in Poland. *Energy Rep.* **2024**, *11*, 5227–5234. [CrossRef]
75. Miao, R.; Zhang, X.; Zhang, J.; Li, S.; Wang, P.; Wang, X.-H. Hollow-core anti-resonant optical fibers for chemical and biomedical sensing. *Sens. Bio-Sens. Res.* **2024**, *46*, 100701. [CrossRef]
76. Xu, S.; Kang, P.; Hu, Z.; Chang, W.; Huang, F. Ultrasensitive Optical Fiber Sensors Working at Dispersion Turning Point: Review. *Sensors* **2023**, *23*, 1725. [CrossRef]
77. Aljanabi, M. Resonance frequency analysis of laser optical fiber based on microcantilever. *Int. J. Electr. Comput. Eng. (IJECE)* **2019**, *9*, 3090. [CrossRef]
78. Chi, M.J.; Yang, H.J.; Yang, K.S.; Dong, W.Z.; Wang, X.W.; Zhang, S.; Wang, X.C.; Kong, L.X. High Sensitivity Photon Pressure Sensitive Skin of Piercing Robot Based on Balloon-Shaped Fiber Optic Sensor. *IEEE Access* **2024**, *12*, 54772–54780. [CrossRef]
79. Supe, A.; Zurikovs, D.; Braunfelds, J. Optical Filter-Based FBG Sensor Interrogator Unit for Low-Cost Sensing. *IEEE Sens. J.* **2025**, *25*, 17055–17061. [CrossRef]
80. Huang, B.; Wang, Y.; Liao, C.; Wang, Y. Highly Sensitive Temperature Sensor Based on All-Fiber Polarization Interference Filter with Vernier Effect. *IEEE Access* **2020**, *8*, 207397–207403. [CrossRef]
81. Contreras-Teran, M.A.; Berganza, A.; Lindner, F.; Bierlich, J.; Wondraczek, K.; Villatoro, J. Multipoint Temperature-Independent Vector Bending Sensing with Coupled-Core Fibers. *IEEE Sens. J.* **2024**, *24*, 36784–36790. [CrossRef]
82. Wang, S.; Wang, S.; Jin, R.-B.; Feng, M.; Wu, S.; Zhang, L.; Lu, P. All-Optical Demodulation Fiber Acoustic Sensor with Real-Time Controllable Sensitivity Based on Optical Vernier Effect. *IEEE Photonics J.* **2019**, *11*, 1–11. [CrossRef]
83. Zhang, S.; Lei, Q.; Hu, J.; Zhao, Y.; Gao, H.; Shen, J.; Li, C. An optical Fiber Pressure Sensor with Ultra-Thin Epoxy Film and High Sensitivity Characteristics Based on Blowing Bubble Method. *IEEE Photonics J.* **2021**, *13*, 1–10. [CrossRef]
84. Wang, T.; Liu, B.; Zhao, L.; Mao, Y.; Ren, J.; Zheng, J. High-Sensitivity Liquid Level Sensor Based on the Balloon-Shaped Fiber Optic MZI. *IEEE Photonics J.* **2022**, *14*, 1–7. [CrossRef]
85. Chung, Y.; Jin, W.; Lee, B.; Canning, J.; Nakamura, K.; Yuan, L.; Munendhar, P.; Zhang, L.; Tong, L.; Yu, S. Highly sensitive temperature sensor using intrinsic Mach-Zehnder interferometer formed by bent micro-fiber embedded in polymer. In Proceedings of the 25th International Conference on Optical Fiber Sensors, Jeju, Republic of Korea, 24–28 April 2017. [CrossRef]

86. Miliou, A. In-Fiber Interferometric-Based Sensors: Overview and Recent Advances. *Photonics* **2021**, *8*, 265. [CrossRef]
87. Zhao, Y.; Zhao, H.; Lv, R.-Q.; Zhao, J. Review of optical fiber Mach–Zehnder interferometers with micro-cavity fabricated by femtosecond laser and sensing applications. *Opt. Lasers Eng.* **2019**, *117*, 7–20. [CrossRef]
88. Bhardwaj, V.; Kishor, K.; Sharma, A.C. Tapered optical fiber geometries and sensing applications based on Mach-Zehnder Interferometer: A review. *Opt. Fiber Technol.* **2020**, *58*, 102302. [CrossRef]
89. Hernández-Guerrero, L.D.; Castillo-Mixcóatl, J.; Muñoz-Aguirre, S.; Rodríguez-Torres, M.; Ramírez-Sánchez, E.; Beltrán-Pérez, G. Projection to latent structures regression and its application to Mach–Zehnder interferometer optical fiber sensors for acetone detection. *Opt. Lasers Eng.* **2025**, *184*, 108689. [CrossRef]
90. Caldas, P.; Rego, G. Optical Fiber Interferometers Based on Arc-Induced Long Period Gratings at INESC TEC. *Sensors* **2021**, *21*, 7400. [CrossRef] [PubMed]
91. Guo, J.; Lian, S.; Zhang, Y.; Zhang, Y.; Liang, D.; Yu, Y.; Chen, R.; Du, C.; Ruan, S. High-Temperature Measurement of a Fiber Probe Sensor Based on the Michelson Interferometer. *Sensors* **2021**, *22*, 289. [CrossRef] [PubMed]
92. Wang, T.; Mao, Y.; Liu, B.; Zhao, L.; Ren, J.; Zheng, J.; Wan, Y. Compact Fiber Optic Sensor for Temperature and Transverse Load Measurement Based on the Parallel Vernier Effect. *IEEE Photonics J.* **2022**, *14*, 1–8. [CrossRef]
93. Mikolajek, M.; Martinek, R.; Koziorek, J.; Hejduk, S.; Vitasek, J.; Vanderka, A.; Poboril, R.; Vasinek, V.; Hercik, R.; Wu, Q. Temperature Measurement Using Optical Fiber Methods: Overview and Evaluation. *J. Sens.* **2020**, *2020*, 8831332. [CrossRef]
94. Elsherif, M.; Salih, A.E.; Muñoz, M.G.; Alam, F.; AlQattan, B.; Antonysamy, D.S.; Zaki, M.F.; Yetisen, A.K.; Park, S.; Wilkinson, T.D.; et al. Optical Fiber Sensors: Working Principle, Applications, and Limitations. *Adv. Photonics Res.* **2022**, *3*, 2100371. [CrossRef]
95. Hu, X.-G.; Zhao, Y.; Peng, Y.; Tong, R.-J.; Zheng, H.-K.; Zhao, J.; Hu, S. In-fiber optofluidic michelson interferometer for detecting small volume and low concentration chemicals with a fiber ring cavity laser. *Sens. Actuators B Chem.* **2022**, *370*, 132467. [CrossRef]
96. Wang, S.; Yang, Y.; Niu, P.; Wu, S.; Liu, S.; Jin, R.-B.; Lu, P.; Hu, X.; Dai, N. Fiber tip Michelson interferometer for temperature sensing based on polymer-filled suspended core fiber. *Opt. Laser Technol.* **2021**, *141*, 107147. [CrossRef]
97. Bao, X.; Wang, Y. Recent Advancements in Rayleigh Scattering-Based Distributed Fiber Sensors. *Adv. Devices Instrum.* **2021**, *2021*, 8696571. [CrossRef]
98. Tosi, D.; Molardi, C.; Sypabekova, M.; Blanc, W. Enhanced Backscattering Optical Fiber Distributed Sensors: Tutorial and Review. *IEEE Sens. J.* **2021**, *21*, 12667–12678. [CrossRef]
99. Mizuno, Y.; Theodosiou, A.; Kalli, K.; Liehr, S.; Lee, H.; Nakamura, K. Distributed polymer optical fiber sensors: A review and outlook. *Photonics Res.* **2021**, *9*, 1719–1733. [CrossRef]
100. Zheng, H.; Zhang, J.; Guo, N.; Zhu, T. Distributed Optical Fiber Sensor for Dynamic Measurement. *J. Light. Technol.* **2021**, *39*, 3801–3811. [CrossRef]
101. Lu, P.; Lalam, N.; Badar, M.; Liu, B.; Chorpening, B.T.; Buric, M.P.; Ohodnicki, P.R. Distributed optical fiber sensing: Review and perspective. *Appl. Phys. Rev.* **2019**, *6*, 041302. [CrossRef]
102. Hsu, W.-K.; Lee, Y.-L.; Kuan, T.-T. Brillouin Frequency Shift Sensing Technology Used in Railway Strain and Temperature Measurement. *Appl. Sci.* **2021**, *11*, 7101. [CrossRef]
103. Froggatt, M.; Moore, J. High-spatial-resolution distributed strain measurement in optical fiber with rayleigh scatter. *Appl. Opt.* **1998**, *37*, 1735–1740. [CrossRef]
104. Bao, X.; Chen, L. Recent progress in distributed fiber optic sensors. *Sensors* **2012**, *12*, 8601–8639. [CrossRef] [PubMed]
105. Nilakanta Meitei, S.; Borah, K.; Chatterjee, S. Review on monitoring of transformer insulation oil using optical fiber sensors. *Results Opt.* **2023**, *10*, 100361. [CrossRef]
106. Xu, H.; Wang, J.; Zhu, R.; Strauss, A.; Cao, M.; Wu, Z. Quantitative Identification of Delamination Damage in Composite Structure Based on Distributed Optical Fiber Sensors and Model Updating. *Struct. Durab. Health Monit.* **2024**, *18*, 785–803. [CrossRef]
107. Pouillea, Q.; Ladaci, A.; Cheymol, G.; Girard, S.; Aubry, P. Results on the insertion of optical fiber sensors in components manufactured by Laser Powder Bed Fusion. In Proceedings of the 13th CIRP Conference on Photonic Technologies, Fürth, Germany, 15–19 September 2024. [CrossRef]
108. Matuck, L.; Santos, J.P.; Freitas, F.; Fontes, L.B.; Bierlich, J.; Geniès, S.; Pinto, J.L.; Ferreira, M.S.; Raccurt, O.; Nascimento, M. Towards smart and secure batteries: Linking pressure and temperature profiles with electrochemical behavior through hybrid optical fiber sensors. *Chem. Eng. J.* **2024**, *500*, 156806. [CrossRef]
109. Freitas, A.I.; Pereira, D.; Bierlich, J.; Marques, J.C.; Ferreira, M.S. Simultaneous measurement of refractive index and temperature using a balloon-type optical fiber sensor. *Optik* **2024**, *309*, 171854. [CrossRef]
110. Petermann, I.; Lindblom, M.; Sterner, C.; Gregard, G.; Karlsson, S. Optical fiber sensor solutions for in-situ transmittance control of electrochromic glazing. *Adv. Sens. Energy Mater.* **2025**, *4*, 100134. [CrossRef]
111. Zhang, P.; Wang, S.; Jiang, J.; Li, C.; Xu, T.; Zhiyuan, L.; Yu, X.; Yu, Y.; Liu, K.; Liu, T. Mechanical Filter-Based Differential Pressure Fiber-Optic Fabry-Perot Infrasound Sensor. *IEEE Photonics J.* **2021**, *13*, 1–10. [CrossRef]

112. Qian, J.; Jia, P.; Liu, H.; Ren, Q.; Liu, J.; Qin, L.; Xiong, J. A MEMS Fiber-Optic Fabry-Perot Vibration Sensor for High-Temperature Applications. *IEEE Access* **2022**, *10*, 42908–42915. [CrossRef]
113. López Aveiga, M.G.; Ramos, M.D.F.; Núnez, V.M.; Vallvey, L.F.C.; Casado, A.G.; Medina Castillo, A.L. Portable fiber-optic sensor for simple, fast, cost-effective, and environmentally friendly quantification of total acidity in real-world applications. *Sens. Actuators B Chem.* **2024**, *417*, 136214. [CrossRef]
114. Liu, K.; Luo, B.; Wu, D.; Zou, X.; Zou, X.; Guo, Y.; Fan, J.; Li, Y.; Wang, Z.; Zhao, M. Broadband Vibration Sensor Using Reflected Excessively Tilted Fiber Grating with Clamped Beam. *IEEE Photonics Technol. Lett.* **2021**, *33*, 379–382. [CrossRef]
115. Mahmud, Z.; Ibrahim, S.A.; Azman, M.F.; Mokhtar, M.R.; Abdul Rashid, H.A.; Mad Zahir, M.H. Distributed magnetic field sensor using nickel-acrylate composite coated silica optical fiber. *Optik* **2024**, *305*, 171788. [CrossRef]
116. Guo, K.; He, J.; Xu, G.; Wang, Y. Dual-Polarization Distributed Feedback Fiber Laser Sensor Based on Femtosecond Laser-Inscribed In-Fiber Stressors for Simultaneous Strain and Temperature Measurements. *IEEE Access* **2020**, *8*, 97823–97829. [CrossRef]
117. Zhang, X.; Daw, J.; Payne, C.; Zhong, B.; Fleming, A.; Hua, Z.; Rufner, J. Electric field-assisted embedding of fiber optic sensors in structural materials for structural health monitoring. *J. Mater. Res. Technol.* **2025**, *34*, 15–31. [CrossRef]
118. Ramos, C.C.; Preizal, J.; Hu, X.; Caucheteur, C.; Woyessa, G.; Bang, O.; Rocha, A.M.; Oliveira, R. High resolution liquid level sensor based on Archimedes' law of buoyancy using polymer optical fiber Bragg gratings. *Measurement* **2025**, *252*, 117368. [CrossRef]
119. Krause, F.; Schütte, M.; Nguyen, D.M.; Schweizer, F.; Junker, M.; Sauer, D.U. Novel optical fiber-based method for spatially resolved temperature measurement and thermal anomaly detection in battery modules. *J. Energy Storage* **2025**, *131*, 117347. [CrossRef]
120. Li, T.; Zhao, P.; Wang, P.; Krishnaiah, K.V.; Jin, W.; Zhang, A.P. Miniature optical fiber photoacoustic spectroscopy gas sensor based on a 3D micro-printed planar-spiral spring optomechanical resonator. *Photoacoustics* **2024**, *40*, 100657. [CrossRef]
121. Guo, Z.; Briggs, C.; Vincent, T.A.; Gulsoy, B.; Sansom, J.E.H.; Marco, J. Global thermal image of cylindrical 21700 Li-ion batteries with distributed optical fibre sensor. *J. Power Sources* **2024**, *592*, 233980. [CrossRef]
122. Gabardi, M.; Tozzetti, L.; Faralli, S.; Solazzi, M.; Benedetti, D.; Rajbhandari, S.; Buttaro, G.; Di Pasquale, F. Embedding Fiber Bragg Grating Sensors in Carbon Composite Structures for Accurate Strain Measurement. *IEEE Sens. J.* **2023**, *23*, 16882–16892. [CrossRef]
123. Klippert, M.; Pauer, W. Determination of the clogging time for continuous emulsion copolymerization in a tubular reactor using distributed optical fiber sensors. *Chem. Eng. Res. Des.* **2025**, *215*, 465–475. [CrossRef]
124. Meneses-Mijares, J.; Castillo-Mixcóatl, J.; Muñoz-Aguirre, S.; Beltrán-Pérez, G. Application of principal component regression in Mach–Zehnder interferometer optical fiber sensors in reflection mode for acetone detection as biomarker of diabetes mellitus. *Opt. Laser Technol.* **2024**, *177*, 111196. [CrossRef]
125. Ramírez-Sánchez, E.; Muñoz-Aguirre, S.; Castillo-Mixcóatl, J.; González-León, K.; Rodríguez-Torres, M.; Hernández-Guerrero, L.D.; Beltrán-Pérez, G. A comparative study between PCR and PLSR in a tapered optical fiber sensor for acetone detection. *Opt. Laser Technol.* **2025**, *181*, 111838. [CrossRef]
126. Kosowska, M.; Tuchin, V.V.; Szczerska, M. Concept study on using fiber-optic sensors with nanocrystalline diamond sheet for tissue monitoring in radiotherapy. *Results Opt.* **2025**, *21*, 100837. [CrossRef]
127. De Vita, E.; De Landro, M.; Massaroni, C.; Iadicicco, A.; Saccomandi, P.; Schena, E.; Campopiano, S. Fiber Optic Sensors-Based Thermal Analysis of Perfusion-Mediated Tissue Cooling in Liver Undergoing Laser Ablation. *IEEE Trans. Biomed. Eng.* **2021**, *68*, 1066–1073. [CrossRef]
128. Xu, D.; Gao, H.; Hou, Z.; Zhang, Y.; Tong, X.; Zhang, Y.; Zhang, P.; Shen, J.; Li, C. A High-Sensitivity Fiber-Optic Fabry-Perot Gas Pressure Sensor with Epoxy Resin Adhesive. *IEEE Sens. J.* **2022**, *22*, 10551–10558. [CrossRef]
129. Zhang, Y.; Hu, Y.; Liu, Q.; Lou, K.; Wang, S.; Zhang, N.; Jiang, N.; Yetisen, A.K. Multiplexed optical fiber sensors for dynamic brain monitoring. *Matter* **2022**, *5*, 3947–3976. [CrossRef]
130. Lv, Z.; Niu, P.; Jiang, J.; Wang, S.; Liu, Y.; Liu, T. Reflective SFT-FBG Hybrid Micro-Probe for Simultaneous Measurement of Relative Humidity and Temperature. *IEEE Photonics J.* **2022**, *14*, 1–6. [CrossRef]
131. Pugliese, B.L.; Angelucci, A.; Parisi, F.; Sapienza, S.; Fabara, E.; Corniani, G.; Tenforde, A.S.; Aliverti, A.; Demarchi, D.; Bonato, P. Development of a Wearable Sleeve-Based System Combining Polymer Optical Fiber Sensors and an LSTM Network for Estimating Knee Kinematics. *IEEE Trans. Neural Syst. Rehabil. Eng.* **2025**, *33*, 728–738. [CrossRef]
132. Bartnik, K.; Martychowiec, A.; Kwietniewski, N.; Musolf, P.; Niedziolka-Jonsson, J.; Koba, M.; Smietana, M. Thin-Film-Based Optical Fiber Interferometric Sensor on the Fiber Tip for Endovascular Surgical Procedures. *IEEE Trans. Biomed. Eng.* **2025**, *72*, 930–939. [CrossRef] [PubMed]
133. Martyn, M.; Kam, W.; Woulfe, P.; O'Keeffe, S. Water Phantom Characterization of a Novel Optical Fiber Sensor for LDR Brachytherapy. *IEEE Sens. J.* **2023**, *23*, 1146–1156. [CrossRef]
134. Li, W.; Zhong, X.; Huang, J.; Bai, X.; Liang, Y.; Cheng, L.; Jin, L.; Tang, H.C.; Lai, Y.; Guan, B.O. Wavelength-time-division multiplexed fiber-optic sensor array for wide-field photoacoustic microscopy. *Photoacoustics* **2025**, *43*, 100725. [CrossRef] [PubMed]

135. Cennamo, N.; Pesavento, M.; Arcadio, F.; Marzano, C.; Zeni, L. Advances in plastic optical fiber bio/chemical sensors to realize point-of-care-tests. *TrAC Trends Anal. Chem.* **2024**, *177*, 117797. [CrossRef]
136. Wang, G.; Dai, J.; Yang, M. Fiber-Optic Hydrogen Sensors: A Review. *IEEE Sens. J.* **2021**, *21*, 12706–12718. [CrossRef]
137. Moslemi, A.; Sansone, L.; Esposito, F.; Marques, C.; Campopiano, S.; Giordano, M.; Iadicicco, A. Highly sensitive gold nanostar based optical fiber sensor with tunable plasmonic resonance. *Sens. Actuators Rep.* **2025**, *9*, 100326. [CrossRef]
138. Kim, B.; Kim, Y.; Lee, Y.; Nam, K.-E.; Yoon, J.; Shin, Y.-H.; Kim, H.; Lee, J.; Lee, B. Experimental study on practical application of optical fiber sensor (OFS) for high-temperature system. *Nucl. Eng. Technol.* **2024**, *56*, 5182–5189. [CrossRef]
139. Yi, X.; Zhao, K.; Chen, K.P. Multiplexable Fiber pH Sensors Enabled by Intrinsic Fabry-Peìrot Interferometer Array. *IEEE Sens. J.* **2022**, *22*, 2167–2171. [CrossRef]
140. Grangeat, R.; Girard, M.; Lupi, C.; Leduc, D.; Jacquemin, F. Plastic optical fiber sensors for mooring lines monitoring in floating wind turbines: A reliability study of OTDR measurement. *Appl. Ocean Res.* **2025**, *158*, 104541. [CrossRef]
141. Kokila, K.; Sumathi, T.; Kumaran, S.; Gnanasekar, A.; BoopathiRaja, R. Design and construction of bio carbon derived Bi2Fe4O9 nanocomposites sensor for clad modified optical fiber sensors for detection of ethanol gas. *Chem. Phys. Impact* **2024**, *9*, 100686. [CrossRef]
142. Wang, T.; Zhu, L.; Yue, Y.; Mukai, Y.; Kanda, H.; Yamamoto, T. Fiber-optic sensor modified by electrospun Polymer/Ti(3)C(2) MXene-TiO(2) for dimethyl sulfoxide sensing. *Talanta* **2025**, *287*, 127630. [CrossRef] [PubMed]
143. Wang, N.; Xu, L.; Liu, S.; He, M.; Wang, L. An interferometric optical fiber sensor based on ion-imprinted sodium alginate for Pb(II) detection. *Opt. Fiber Technol.* **2025**, *90*, 104053. [CrossRef]
144. Hosoki, A.; Nishiyama, M.; Kumekawa, N.; Watanabe, K.; Yatabe, R.; Tahara, Y.; Onodera, T.; Sugiyama, A.; Sakurai, N. Lipid-coated hetero-core optical fiber sensor for wide-range chemical detection. *Opt. Laser Technol.* **2024**, *169*, 110045. [CrossRef]
145. Vikas; Caposciutti, G.; Nobili, L.G.; Tellini, B.; Cigada, A.; Saccomandi, P. Nanoparticles-enhanced fiber optic plasmonic sensor for trace-level detection of mercury (Hg^{2+}) ions. *J. Hazard. Mater. Adv.* **2025**, *18*, 100759. [CrossRef]
146. Wang, E.; Niu, H.; Li, P.; Zhai, M.; Zhang, C.; Lyu, G.; Huang, Y. Optical fiber F-P cavity pH sensor based on polyaniline reaction deposition film layer. *Measurement* **2025**, *243*, 116454. [CrossRef]
147. Zhang, X.; Broere, W. Design of a distributed optical fiber sensor system for measuring immersed tunnel joint deformations. *Tunn. Undergr. Space Technol.* **2023**, *131*, 104770. [CrossRef]
148. Zhang, X.; Long, L.; Broere, W.; Bao, X. Smart sensing of concrete crack using distributed fiber optics sensors: Current advances and perspectives. *Case Stud. Constr. Mater.* **2025**, *22*, e04493. [CrossRef]
149. Jansson, A.; Sjölander, A.; Berrocal, C.G.; Rempling, R.; Fernandez, I. Experimental investigation on prevalent local failure mechanisms in hard rock tunnel linings using distributed optical fibre sensors. *Eng. Struct.* **2025**, *333*, 120185. [CrossRef]
150. Pereira, L.; Bourgeois, I.; Rodrigues, H.; Varum, H.; Antunes, P. Fiber Bragg grating based displacement sensors with low visual impact for structural health monitoring applications—Monastery of Batalha case. *Sens. Actuators A Phys.* **2024**, *368*, 115117. [CrossRef]
151. Anjana, K.; Herath, M.; Epaarachchi, J.; Priyankara, N.H. Development of an optical fibre sensor system for ground displacement and pore water pressure monitoring. *Measurement* **2025**, *253*, 117770. [CrossRef]
152. Ghafoori, Y.; Lenart, S.; Bohinc, U.; Kryžanowski, A. Investigating transient seepage flow and heat transfer using optical fiber distributed temperature sensors and hydrothermal modeling. *Int. Commun. Heat Mass Transf.* **2025**, *165*, 108999. [CrossRef]
153. Han, Y.; Tang, J.; Liao, J.; Tan, L. Sensing response of aluminum-side-polished fiber-based surface plasmon resonance sensors to surface roughness. *Phys. Open* **2025**, *24*, 100281. [CrossRef]
154. Nosseir, A.E.S.; Slejko, E.A.; Cervone, A.; Oton, C.J.; Di Pasquale, F. Composite structures with embedded fiber optic sensors: A smart propellant tank for future spacecraft applications. *Acta Astronaut.* **2024**, *223*, 144–158. [CrossRef]
155. Hegde, G.; Asokan, S.; Hegde, G. Fiber Bragg grating sensors for aerospace applications: A review. *ISSS J. Micro Smart Syst.* **2022**, *11*, 257–275. [CrossRef]
156. Lin, W.; Zhao, F.; Shao, L.-Y.; Vai, M.I.; Shum, P.P.; Sun, S. Temperature Sensor Based on Er-Doped Cascaded-Peanut Taper Structure In-Line Interferometer in Fiber Ring Laser. *IEEE Sens. J.* **2021**, *21*, 21594–21599. [CrossRef]
157. Gao, X.; Li, Y.; Wu, J.; Song, B.; Liu, H.; Liu, X.; Sun, H. Deep learning for highly efficient curvature recognition using fiber scattering speckles. *Results Phys.* **2023**, *52*, 106808. [CrossRef]
158. Vanegas-Tenezaca, E.; Galarza, M.; Dauliat, R.; Jamier, R.; Roy, P.; Lopez-Amo, M. Multidirectional Bending Sensor Using Capillary Fibers and Machine Learning for Real-Time Applications. *IEEE Sens. J.* **2025**, *25*, 12734–12741. [CrossRef]
159. Minakuchi, S.; Takeda, N. Recent advancement in optical fiber sensing for aerospace composite structures. *Photonic Sens.* **2013**, *3*, 345–354. [CrossRef]
160. Cutolo, A.; Bernini, R.; Berruti, G.M.; Breglio, G.; Bruno, F.A.; Buontempo, S.; Catalano, E.; Consales, M.; Coscetta, A.; Cusano, A.; et al. Innovative Photonic Sensors for Safety and Security, Part II: Aerospace and Submarine Applications. *Sensors* **2023**, *23*, 2417. [CrossRef] [PubMed]

161. Goossens, S.; Muñoz, K.; Jiménez, M.; Mendíaz, M.M.; Berghmans, F. Barely visible impact damage detection and location on a real scale curved CFRP fuselage panel with optical fibre Bragg grating sensors. *Procedia Struct. Integr.* **2024**, *52*, 647–654. [CrossRef]
162. Du, B.; He, J.; Xu, B.; Xu, X.; Fu, C.; Li, P.; Xiao, X.; Liu, S.; Yang, Y.; Wang, Y. High-Density Weak in-Fiber Micro-Cavity Array for Distributed High-Temperature Sensing with Millimeter Spatial Resolution. *J. Light. Technol.* **2022**, *40*, 7447–7455. [CrossRef]
163. Aimasso, A.; Vedova, M.D.L.D.; Maggiore, P. Innovative sensor networks for massive distributed thermal measurements in space applications under different environmental testing conditions. In Proceedings of the 2022 IEEE 9th International Workshop on Metrology for AeroSpace (MetroAeroSpace), Pisa, Italy, 27–29 June 2022; pp. 503–508. [CrossRef]
164. Goossens, S.; De Pauw, B.; Geernaert, T.; Salmanpour, M.S.; Sharif Khodaei, Z.; Karachalios, E.; Saenz-Castillo, D.; Thienpont, H.; Berghmans, F. Aerospace-grade surface mounted optical fibre strain sensor for structural health monitoring on composite structures evaluated against in-flight conditions. *Smart Mater. Struct.* **2019**, *28*, 065008. [CrossRef]
165. Loayssa, A.; Vallifuoco, R.; Zahoor, R.; Zeni, L.; Sagues, M.; Minardo, A. Distributed Vibration Sensing Based on Optical Vector Network Analysis. *J. Light. Technol.* **2025**, *43*, 2349–2356. [CrossRef]
166. Mihailov, S.J. Femtosecond laser-induced Bragg gratings in silica-based fibers for harsh environment sensing. *APL Photonics* **2023**, *8*, 071102. [CrossRef]
167. Lin, W.; Shao, L.-Y.; Vai, M.I.; Shum, P.P.; Liu, S.; Liu, Y.; Zhao, F.; Xiao, D.; Liu, Y.; Tan, Y.; et al. In-Fiber Mach–Zehnder Interferometer Sensor Based on Er Doped Fiber Peanut Structure in Fiber Ring Laser. *J. Light. Technol.* **2021**, *39*, 3350–3357. [CrossRef]
168. Yang, C.; Tan, Y.; Liu, Y.; Xia, P.; Cui, Y.; Zheng, B. Modeling and Optimization of Laser Cladding Fixation Process for Optical Fiber Sensors in Harsh Environments. *Sensors* **2022**, *22*, 2569. [CrossRef]
169. Zubia, G.; Zubia, J.; Amorebieta, J.; Aldabaldetreku, G.; Durana, G. Exhaustive analysis and simple model of an angular displacement optical fiber sensor. *Sci. Rep.* **2025**, *15*, 19410. [CrossRef] [PubMed]
170. Gao, H.; Wang, Q.; Zhou, J.; Yu, C. Human Vital Signs Signal Monitoring and Repairment with an Optical Fiber Sensor Based on Deep Learning. *Photonics* **2024**, *11*, 707. [CrossRef]
171. Reyes-Vera, E.; Valencia-Arias, A.; Garcia-Pineda, V.; Aurora-Vigo, E.F.; Alvarez Vasquez, H.; Sanchez, G. Machine Learning Applications in Optical Fiber Sensing: A Research Agenda. *Sensors* **2024**, *24*, 2200. [CrossRef]
172. Zhou, Y.; Zhang, Y.-N.; Yu, Q.; Ren, L.; Liu, Q.; Zhao, Y. Application of machine learning in optical fiber sensors. *Measurement* **2024**, *228*, 114391. [CrossRef]
173. Wang, K.; Mizuno, Y.; Dong, X.; Kurz, W.; Köhler, M.; Kienle, P.; Lee, H.; Jakobi, M.; Koch, A.W. Multimode optical fiber sensors: From conventional to machine learning-assisted. *Meas. Sci. Technol.* **2023**, *35*, 022002. [CrossRef]
174. Nordin, N.D.; Zan, M.S.D.; Abdullah, F. Comparative Analysis on the Deployment of Machine Learning Algorithms in the Distributed Brillouin Optical Time Domain Analysis (BOTDA) Fiber Sensor. *Photonics* **2020**, *7*, 79. [CrossRef]
175. Karapanagiotis, C.; Krebber, K. Machine Learning Approaches in Brillouin Distributed Fiber Optic Sensors. *Sensors* **2023**, *23*, 6187. [CrossRef] [PubMed]
176. Wang, J.; Li, Y.; Liao, J. Temperature extraction for Brillouin optical fiber sensing system based on extreme learning machine. *Opt. Commun.* **2019**, *453*, 124418. [CrossRef]
177. Zhu, C.; Zhuang, Y.; Huang, J. Machine Learning Assisted High-Sensitivity and Large-Dynamic-Range Curvature Sensor Based on No-Core Fiber and Hollow-Core Fiber. *J. Light. Technol.* **2022**, *40*, 5762–5767. [CrossRef]
178. Ni, Y.; Wakimoto, S.; Tian, W.; Toda, Y.; Kanda, T.; Yamaguchi, D. Length Estimation of Pneumatic Artificial Muscle with Optical Fiber Sensor Using Machine Learning. *Sensors* **2025**, *25*, 2221. [CrossRef]
179. Madry, M.; Szczupak, B.; Smigielski, M.; Matysiak, B. Simultaneous Temperature and Relative Humidity Measurement Using Machine Learning in Rayleigh-Based Optical Frequency Domain Reflectometry. *Sensors* **2024**, *24*, 7913. [CrossRef]
180. Nava-Martinez, B.N.; Hernandez-Hernandez, S.S.; Rodriguez-Ramirez, D.A.; Martinez-Rodriguez, J.L.; Rios-Alvarado, A.B.; Diaz-Manriquez, A.; Martinez-Angulo, J.R.; Guerrero-Melendez, T.Y. Heart Attack Risk Prediction via Stacked Ensemble Metamodeling: A Machine Learning Framework for Real-Time Clinical Decision Support. *Informatics* **2025**, *12*, 110. [CrossRef]
181. Davarapalli, K.; Kumar, S.; Sabbarapu, G.; Lalam, N.; Vaska, L.; Pasalapudi, U.; Voola, P.; Jenne, H. A Review of Machine Learning Enabled Distributed Fiber Optic Sensors: Principles and Applications. *Sens. Transducers* **2025**, *269*, 8–21.
182. Venketeswaran, A.; Lalam, N.; Wuenschell, J.; Ohodnicki, P.R.; Badar, M.; Chen, K.P.; Lu, P.; Duan, Y.; Chorpening, B.; Buric, M. Recent Advances in Machine Learning for Fiber Optic Sensor Applications. *Adv. Intell. Syst.* **2021**, *4*, 2100067. [CrossRef]
183. Shao, L.; Zhang, J.; Chen, X.; Xu, D.; Gu, H.; Mu, Q.; Yu, F.; Liu, S.; Shi, X.; Sun, J.; et al. Artificial intelligence-driven distributed acoustic sensing technology and engineering application. *PhotoniX* **2025**, *6*, 4. [CrossRef]
184. Luo, Z.; Xu, J.; Zhou, X.; Wang, Z.; Liu, Y.; Wang, S.; Yuan, S.; Zhang, H.; He, B.; Xin, J.; et al. Advances in Fiber-Based Wearable Sensors with Machine Learning. *Adv. Devices Instrum.* **2024**, *5*, 0054. [CrossRef]
185. Herlin, H.S. Applications of Fiber Optic Sensor for Monitoring and Early Warning of Soil Shift on IoT-based System. *Int. J. Inform. Vis.* **2020**, *4*, 117–122. [CrossRef]

186. Lee, H.-K.; Kim, Y.; Park, S.; Kim, J. Passive IoT Optical Fiber Sensor Network for Water Level Monitoring with Signal Processing of Feature Extraction. *Electronics* **2023**, *12*, 1823. [CrossRef]
187. Golovastikov, N.V.; Kazanskiy, N.L.; Khonina, S.N. Optical Fiber-Based Structural Health Monitoring: Advancements, Applications, and Integration with Artificial Intelligence for Civil and Urban Infrastructure. *Photonics* **2025**, *12*, 615. [CrossRef]
188. Lu, L.; Liu, J.; Hu, B.; Gao, Y.; Xu, Q.; Lu, Y.; Huang, G. Application of Digital Twin Platform for Prefabricated Assembled Superimposed Stations Based on SERIC and IoT Integration. *Buildings* **2025**, *15*, 3856. [CrossRef]
189. Qu, S.; Wang, Z.; Qin, Z.; Xu, Y.; Cong, Z.; Liu, Z. Internet of Things Infrastructure Based on Fast, High Spatial Resolution, and Wide Measurement Range Distributed Optic-Fiber Sensors. *IEEE Internet Things J.* **2022**, *9*, 2882–2889. [CrossRef]
190. Kok, S.P.; Go, Y.I.; Wang, X.; Wong, M.L.D. Advances in Fiber Bragg Grating (FBG) Sensing: A Review of Conventional and New Approaches and Novel Sensing Materials in Harsh and Emerging Industrial Sensing. *IEEE Sens. J.* **2024**, *24*, 29485–29505. [CrossRef]
191. Manie, Y.C.; Yao, C.-K.; Yeh, T.-Y.; Teng, Y.-C.; Peng, P.-C. Laser-Based Optical Wireless Communications for Internet of Things (IoT) Application. *IEEE Internet Things J.* **2022**, *9*, 24466–24476. [CrossRef]
192. Qazi, S.; Khawaja, B.A.; Farooq, Q.U. IoT-Equipped and AI-Enabled Next Generation Smart Agriculture: A Critical Review, Current Challenges and Future Trends. *IEEE Access* **2022**, *10*, 21219–21235. [CrossRef]
193. Senkans, U.; Braunfelds, J.; Lyashuk, I.; Porins, J.; Spolitis, S.; Bobrovs, V. Research on FBG-Based Sensor Networks and Their Coexistence with Fiber Optical Transmission Systems. *J. Sensors* **2019**, *2019*, 6459387. [CrossRef]
194. Wang, H.; Liu, S.; Liu, W.; Wang, S. Dual-Parameter Surface Plasmon Resonance Photonic Crystal Fiber Sensor for Simultaneous Magnetic Field and Temperature Detection with Potential SERS Applications. *Photonics* **2025**, *12*, 355. [CrossRef]
195. Oudenani, A.; Sonne, A.; Saleh, C.M.N. Simultaneous Sensing of Temperature and Refractive Index with D-Shaped Photonic Crystal Fiber Infused with Liquid Crystal. *Plasmonics* **2024**, *20*, 4159–4167. [CrossRef]
196. Aktar, M.N.; Basak, N.; Biswas, S.; Abdullah, H.; Uddin, M.S. SPR-Based Fiber Optic Sensor for the Development of Internet of Things (IoT) Technologies. *Plasmonics* **2024**, *20*, 4959–4969. [CrossRef]
197. Prause, K.; Thiele, S.; Herkommer, A.M.; Giessen, H.; Pinzer, B.; Layh, M. Highly miniaturized endoscopic spatial confocal point distance sensor. *Opt. Eng.* **2020**, *59*, 035102. [CrossRef]
198. Fang, H.-M. Miniaturized Real-Time Oxygen Detection Systems Integrated with Optical Fiber by Doping Ru-Based Fluorescence Sensors. *J. Med. Biol. Eng.* **2013**, *33*, 117–123. [CrossRef]
199. Samavati, Z.; Samavati, A.; Ismail, A.F.; Rahman, M.A.; Othman, M.H.D.; Yeganeh, F.N. Optical fiber sensor for glycoprotein detection based on localized surface plasmon resonance of discontinuous Ag-deposited nanostructure. *Opt. Fiber Technol.* **2021**, *62*, 102476. [CrossRef]
200. Principe, M.; Vaiano, P.; Quero, G.; Spaziani, S.; Ucci, S.; Micco, A.; Cutolo, A.; Consales, M.; Cusano, A. Plasmonic optical fiber meta-tip for cancer biomarkers detection. In Proceedings of the Communications: SIF Congress 2022, Milan, Italy, 12–16 September 2023. [CrossRef]
201. Pevec, S.; Donlagić, D. Multiparameter fiber-optic sensors: A review. *Opt. Eng.* **2019**, *58*, 072009. [CrossRef]
202. Wang, R.; Ren, Z.; Kong, D.; Hu, B.; He, Z. Highly sensitive label-free biosensor based on graphene-oxide functionalized micro-tapered long period fiber grating. *Opt. Mater.* **2020**, *109*, 110253. [CrossRef]
203. Liu, K.; Zhang, J.; Jiang, J.; Xu, T.; Wang, S.; Chang, P.; Zhang, Z.; Ma, J.; Liu, T. MoSe2-Au Based Sensitivity Enhanced Optical Fiber Surface Plasmon Resonance Biosensor for Detection of Goat-Anti-Rabbit IgG. *IEEE Access* **2020**, *8*, 660–668. [CrossRef]
204. Zhang, Y.J.; Hsu, J.C.; Tsao, J.H.; Sun, Y.S. Fabrication of a Bare Optical Fiber-Based Biosensor. *Micromachines* **2019**, *10*, 522. [CrossRef]
205. Guo, T.; Liu, F.; Liang, X.; Qiu, X.; Huang, Y.; Xie, C.; Xu, P.; Mao, W.; Guan, B.O.; Albert, J. Highly sensitive detection of urinary protein variations using tilted fiber grating sensors with plasmonic nanocoatings. *Biosens. Bioelectron.* **2016**, *78*, 221–228. [CrossRef]
206. Pasquardini, L.; Cennamo, N.; Malleo, G.; Vanzetti, L.; Zeni, L.; Bonamini, D.; Salvia, R.; Bassi, C.; Bossi, A.M. A Surface Plasmon Resonance Plastic Optical Fiber Biosensor for the Detection of Pancreatic Amylase in Surgically-Placed Drain Effluent. *Sensors* **2021**, *21*, 3443. [CrossRef]
207. Zhou, L.; Liu, C.; Sun, Z.; Mao, H.; Zhang, L.; Yu, X.; Zhao, J.; Chen, X. Black phosphorus based fiber optic biosensor for ultrasensitive cancer diagnosis. *Biosens. Bioelectron.* **2019**, *137*, 140–147. [CrossRef]
208. Bratash, O.; Buhot, A.; Leroy, L.; Engel, E. Optical fiber biosensors toward in vivo detection. *Biosens. Bioelectron.* **2024**, *251*, 116088. [CrossRef]
209. Carneiro de Souza, L.; Dala Pegorara Souto, V.; Cerqueira Sodré, A. Radio- and Power-Over-Fiber Integration for 6G Networks: Challenges and Future Prospects. *IEEE Access* **2025**, *13*, 5321–5341. [CrossRef]
210. Chen, N.; Okada, M. Toward 6G Internet of Things and the Convergence with RoF System. *IEEE Internet Things J.* **2021**, *8*, 8719–8733. [CrossRef]

211. Colares, R.A.; Rittner, L.; Conforti, E.; Mello, D.A.A. Fiber Sensing in the 6G Era: Vision Transformers for ϕ-OTDR-Based Road-Traffic Monitoring. *Appl. Sci.* **2025**, *15*, 3170. [CrossRef]
212. Carvalho, W.O.F.; Mejia-Salazar, J.R. Plasmonics for Telecommunications Applications. *Sensors* **2020**, *20*, 2488. [CrossRef]
213. Khaloopour, L.; Su, Y.; Raskob, F.; Meuser, T.; Bless, R.; Janzen, L.; Abedi, K.; Andjelkovic, M.; Chaari, H.; Chakraborty, P.; et al. Resilience-by-Design in 6G Networks: Literature Review and Novel Enabling Concepts. *IEEE Access* **2024**, *12*, 155666–155695. [CrossRef]
214. Arunachalam, R.; Singh, R.; Vinoth Kumar, M. Towards last-mile connectivity in 6G-IoT: An integrated MIMO-FSO communication system and FBG sensors under atmospheric attenuations, strain and temperature effects. *Eng. Sci. Technol. Int. J.* **2025**, *63*, 101958. [CrossRef]
215. Lao, J.; Sun, P.; Liu, F.; Zhang, X.; Zhao, C.; Mai, W.; Guo, T.; Xiao, G.; Albert, J. In situ plasmonic optical fiber detection of the state of charge of supercapacitors for renewable energy storage. *Light. Sci. Appl.* **2018**, *7*, 34. [CrossRef] [PubMed]
216. Karapanagiotis, C.; Schukar, M.; Krebber, K. Distributed fiber optic sensors for structural health monitoring of composite pressure vessels. *tm-Tech. Mess.* **2024**, *91*, 168–179. [CrossRef]
217. Shen, C.; Xie, Z.; Huang, Z.; Yan, S.; Sui, W.; Zhou, J.; Wang, Z.; Han, W.; Zeng, X. Review of the Status and Prospects of Fiber Optic Hydrogen Sensing Technology. *Chemosensors* **2023**, *11*, 473. [CrossRef]
218. Drissi-Habti, M.; Abhijit, N.; Sriharsha, M.; Carvelli, V.; Bonamy, P.J. Concept of Placement of Fiber-Optic Sensor in Smart Energy Transport Cable under Tensile Loading. *Sensors* **2022**, *22*, 2444. [CrossRef] [PubMed]
219. Gordelier, T.; Thies, P.R.; Rinaldi, G.; Johanning, L. Investigating Polymer Fibre Optics for Condition Monitoring of Synthetic Mooring Lines. *J. Mar. Sci. Eng.* **2020**, *8*, 103. [CrossRef]
220. Vu, N.H.; Shin, S. Optical Fiber Daylighting System Combined with LED Lighting and CPV based on Stepped Thickness Waveguide for Indoor Lighting. *J. Opt. Soc. Korea* **2016**, *20*, 488–499. [CrossRef]
221. Hasanin, T.; Manoharan, H.; Alterazi, H.A.; Srivastava, G.; Selvarajan, S.; Lin, J.C.-W. Mathematical approach of fiber optics for renewable energy sources using general adversarial networks. *Front. Ecol. Evol.* **2023**, *11*, 1132678. [CrossRef]
222. Liang, S.; Zhao, X.; Liu, R.; Zhang, X.; Wang, L.; Zhang, X.; Lv, Y.; Meng, F. Fiber-Optic Auditory Nerve of Ground in the Suburb: For Traffic Flow Monitoring. *IEEE Access* **2019**, *7*, 166704–166710. [CrossRef]
223. Anderson, S.A.; Cunningham, E.; Barford, P.; Fratta, D.; Nissen-Meyer, T.; Wang, H.R. Assessing the Expansion of Ground-Motion Sensing Capability in Smart Cities via Internet Fiber-Optic Infrastructure. *Seism. Res. Lett.* **2024**, *95*, 3633–3651. [CrossRef]
224. Morshed, A.H.E.; Atta, R.M. Multimode optical fiber strain monitoring for smart infrastructures. *Ain Shams Eng. J.* **2023**, *14*, 102181. [CrossRef]
225. Canning, J. Mortar-diatom composites for smart sensors and buildings. *Opt. Mater. Express* **2021**, *11*, 418119. [CrossRef]
226. Saadi, M.; Chaudhary, S.; Kumar, S. Editorial: Applications of photonic sensors in smart cities. *Front. Commun. Netw.* **2023**, *4*. [CrossRef]

Disclaimer/Publisher's Note: The statements, opinions and data contained in all publications are solely those of the individual author(s) and contributor(s) and not of MDPI and/or the editor(s). MDPI and/or the editor(s) disclaim responsibility for any injury to people or property resulting from any ideas, methods, instructions or products referred to in the content.